Technical Document 2868
October 1995

IR 1995 Annual Report

CONTENTS

INTRODUCTION

INTRODUCTION

New and innovative ideas proposed by the scientists and engineers of the Naval Command, Control and Ocean Surveillance Center (NCCOSC) RDT&E Division (NRaD) are supported and encouraged by the Executive Director through the Independent Research (IR) program. This program supports initial research in several areas of interest to the Navy, including command and control, communications, ocean surveillance, and navigation.

The FY 95 IR program was administered by Dr. Alan Gordon. The program began with the Executive Director's February 1994 call for proposals that emphasized Information Understanding, Ocean Surveillance, Communications, High-Performance Computing, Human/Computer Interfaces, Navigation, Solid-State Materials and Devices, and Environmental/Propagation Effects. Scientists and engineers responded with 79 written proposals. Of those, 19 were withdrawn or disqualified, and the remaining 60 were each heard in hour-long proposal meetings held throughout the summer of 1994. Each proposal was presented orally before a different *ad hoc* committee chosen for its specific expertise. Members of these committees included Dr. Gordon, Dr. George Dillard, line management, NRaD technical experts, faculty members from local universities, and visiting professors on the ONR–ASEE Summer Faculty Research Program. Based on administrative and peer review, 29 projects were selected for funding that constituted the $2,463K FY 95 Independent Research Program.

This report contains tables that provide information on active and multisponsored projects and lists of publications and patents. Although the Independent Exploratory Development (IED) program was terminated at the end of FY 93, this report includes information on patents that resulted from the IED program after the FY 94 IR report. The bulk of this report contains short descriptions of FY 95 IR projects that highlight their objectives and accomplishments. In addition, three IR projects have been selected for more in-depth treatment.

The featured projects are

"Blind Equalizers for High-Data-Rate Digital Communications" by R. A. Axford, Jr. The author describes blind equalization as an important technique for the mitigation of channel impairments in bandwidth-efficient, high-data-rate digital communications systems that employ phase-shift keyed (PSK) and quadrature-amplitude-modulated (QAM) signals. This research investigated some performance issues with, and developed some refinements to, the widely used constant modulus algorithm (CMA) for blind equalization.

"A Discretely Tunable Ultraviolet Laser for Multichannel Covert Communications" by P. Poirier and F. Hanson. The authors describe the development of laser sources in the ultraviolet region from 260 to 280 nm, considered a promising approach for an intentionally range-limited, covert communication link. A discretely tunable source coupled with variable wavelength filters would be desirable for multiple channel or bidirectional operation. The moderate to high repetition rate, Q-switched laser performance of a quadrupled diode-pumped Nd:YALO laser discretely tunable between 266 and 275 nm is reported. The transmitted power ratio of custom interference separation filters is presented.

"Cell Loss Evaluation of ATM Statistical Multiplexing" by A. Shum. The author describes a discrete model of an Asynchronous Transfer Mode (ATM) statistical multiplexer subject to heterogeneous

groups of on-off traffic sources. Algorithms to compute the exact steady-state and transient cell loss probabilities of the multiplexer have been formulated. Unfortunately, the computational complexity of the exact algorithms is exponential in the sizes of the multiplexer parameters. To circumvent this difficulty, an asymptotic approximation algorithm is designed to estimate the steady-state cell loss probability. Although the approximation algorithm is more efficient than the exact algorithm, its time complexity remains exponential. Two polynomial-time approximation algorithms to the asymptotic approximation procedure are proposed to further reduce the computational burden. Simulation studies were conducted to assess the validity of the algorithms. For all multiplexing scenarios examined, the algorithmic results and simulation outputs showed perfect agreement.

	Independent Research					Independent Exploratory Development				
Fiscal Year	91	92	93	94	95	91	92	93	94	95
Funding ($K)	3,118	1,745	2,278	2,312	2,463	1,820	888	834	—	—
Number of projects	35	21	27	28	29	23	13	12	—	—
Professional work-years	23	13	15	14	15.3	14	7	7	—	—
Refereed journals, books, and dissertations (published/accepted)	28	21	26	13	26	10	1	2	—	—
Refereed journals, books, and dissertations (submitted)	N/A	N/A	N/A	10	9	N/A	N/A	N/A	—	—
NRaD publications	13	11	5	5	3	14	10	3	1	—
Presentations to professional meetings (invited)	16	23	12	6	27	12	7	—	—	—
Presentations to professional meetings (contributed)	38	16	54	19	33	7	8	6	—	—
Patents/SIR issued	5	5	4	7	5	4	8	6	3	2
Claims allowed, pending issue	1	—	—	2	2	2	3	4	—	—
Patent applications filed	10	11	14	6	6	14	10	7	5	4
Invention disclosures authorized	5	6	4	—	5	4	3	2	1	1
Invention disclosures submitted				7	7				1	—
Percent of completed projects transitioned	39	54	36	25	54	56	56	10	—	—

TRANSITIONED PROJECTS

Near Vertical Incidence Skywave Antenna

This project developed a novel concept for broadband, compact antennas and built and tested reduced-scale prototypes manufactured on PC-board stock. The concept is to have spiral antennas with sinusoidal wire arms. Some prototypes were tested, and initial results are that some size reduction can be achieved in narrowband applications, though this may not be true in broadband applications. The transition sponsor is funding the completion of the testing of existing prototypes and the design, fabrication, and testing of three full-scale UHF/VHF prototypes using the IR design concept. If successful, the application would be the replacement, and possible reduction in number, of existing shipboard UHF/VHF antennas.

NRaD IR Project: ZU05
NRaD POC: Dr. Willard Cronyn
Transition Project: SCN, NRaD Project Identifier not yet assigned
Transition Sponsor: Thomas Giaudrone

Measurement and Prediction of Sediment Assimilation Capacity

This project investigated biochemical and sorption processes that determine the bioavailability of toxins in harbors, estuaries, etc. Both theoretical modeling and laboratory verification experiments were pursued. This work is important since the Navy must be knowledgeable about contaminants it may introduce into these waters and must comply with various water-quality regulations. Also, the need for remediation efforts requires a knowledge of the fate of contaminants. Development of the laboratory test system, model validation, and experiments to measure assimilation capacity are continuing in the FY 96 transition project. The results of this work are planned to be used in site assessments at Navy sites located in Narragansett Bay, RI.

NRaD IR Project: ZU08
NRaD POC: Robert Johnston
Transition Project: OPN DERA, NRaD ME83
Transition Sponsor: LT Jim Conway

Elimination of the Mechanical Dither of a Ring Laser Gyroscope by the Implementation of a Quantum Well Mirror

The goal of this IR project was, via theoretical modeling and experimental investigations, to see whether quantum well (QW) active mirrors could replace electromechanical mirrors for biasing ring laser gyroscopes (RLG) out of the dead-band region. The IR project fabricated a quantum well device and demonstrated that cost and performance benefits are possible for RLGs used in naval ships, aircraft, and missiles, in addition to the higher reliability expected from an all solid-state QW device. The transition project will examine a number of issues related to QW mirrors, including additional performance improvements obtainable from nonsinusoidal waveforms. The project should result in a demonstration RLG using a QW mirror.

NRaD IR Project: ZW90
NRaD POC: Dr. Fran Karwacki
Transition Project: 6.2N, NRaD NB13
Transition Sponsor: Dr. Sherman Gee

Photonic Frequency Converting Feed Network for Broadband Transmit/Receive Antennas

This IR project investigated two different photonic techniques for up/down conversion of signals in the gigahertz range. The project demonstrated conversion efficiencies superior to all-electronic approaches for signals being converted between 1 gigahertz and the range of a few tens of gigahertz. In the transition project, a breadboard system will be constructed and tested with real RF signals being received by an antenna. The significance of this work to the Navy is that it will, if successful, eventually allow multiband sharing of a single shipboard antenna through a single fiber-optic feed.

NRaD IR Project: ZU10
NRaD POC: Dr. Steve Pappert
Transition Project: 6.2N, NRaD CH75
Transition Sponsor: William Miceli

Acoustic Bottom Interaction Using the Parabolic Equation

This project developed a new 2.5-dimensional parabolic acoustic propagation code that includes bottom shear waves and detailed consideration of the liquid/bottom interaction. Thus, this is an especially suitable code for analyzing shallow water propagation. In FY 96, the work transitioned to two projects. One project has analyzed the optimal placement of array elements with respect to the bottom for project Spinnaker, which is deploying a lightweight, low-power acoustic array in the Arctic Ocean. In the second transition, the code is being used to evaluate the effects of mismatched bottom properties on matched-field processing and matched-field tracking for the Shallow Water Environmental Cell Experiment 1996 (SWELLEX96).

NRaD IR Project: ZW94
NRaD POC: Dr. Dave Rees
First Transition Project (Spinnaker): 6.2N and 6.3N, NRaD MA10
Transition Sponsor: 6.2N: Dr. Thomas Curtain and
Tommy Goldberry,
Greg Dreyer
Second Transition Project (SWELLEX96): 6.2N, NRaD SUB6
Transition Sponsor: Dr. John Tague

Bioluminescent Signatures of Underwater Bodies

The IR project determined that wall shear stress, on the order of 1 dyne/cm^2, appears to be the dominant trigger for bioluminescence. Furthermore, luminescent plankton were shown to be a viable method for flow visualization. The transition project will expand the types of organisms and fluid flows studied, to further characterize the relationship between bioluminescence and fluid flow. This will allow better understanding of conditions in which objects of interest to the Navy may be detected through flow-induced bioluminescence.

NRaD IR Project: ZW77
NRaD POC: Dr. Jim Rohr
Transition Project: 6.1N, NRaD HM38
Transition Sponsor: Dr. Eric Shulenberger

The Effects of Benthic Characteristics on Water-Column Optical Properties

This IR project examined the relationship between benthic processes and optical properties. The project demonstrated, through field measurements and modeling, that benthic properties such as grain size, organic content, and mineralogy can be used to gain information about the sea bottom's optical properties, such as albedo. The transitional sponsor is employing the IR principal investigator to apply these measurement and modeling techniques to a specific site. The naval application of this work is to airborne optical surveillance sensors.

NRaD IR Project: ZU15
NRaD POC: Jon Schoonmaker
Transition Project: 6.1F, NRaD SX08
Transition Sponsor: Mark Anderson

SELECTED INDEPENDENT RESEARCH PROJECTS

Blind Equalizers for High-Data-Rate Digital Communications

R. A. Axford, Jr.

Blind equalization is an important technique for the mitigation of channel impairments in bandwidth-efficient, high-data-rate digital communications systems that employ phase-shift keyed (PSK) and quadrature-amplitude-modulated (QAM) signals. This research investigated some performance issues with, and developed some refinements to, the widely used constant modulus algorithm (CMA) for blind equalization. A stochastic gradient lattice implementation of CMA (LCMA) was developed. It was shown that the convergence performance of LCMA is less sensitive than that of the standard transversal CMA to variations in channel-induced amplitude distortion. Because the CMA cost function is better matched to PSK than to QAM signals, both the transversal and lattice implementations of CMA exhibit significantly more misadjustment for QAM signals than for PSK signals. Two alternative blind equalization algorithms were developed. These algorithms are based on cost functions that are similar to the CMA cost function, yet exactly matched to specific QAM constellations. These alternative algorithms, the Multiple Modulus Algorithm (MMA) and the CMA-Assisted Decision Adjusted Modulus Algorithm (CADAMA), exhibited misadjustment levels for QAM comparable to those exhibited by CMA for PSK. However, CADAMA is applicable to higher order QAM constellations than MMA. Finally, a problem that has been reported in which CMA fails to satisfactorily converge in response to certain scrambled signals was investigated. The manners in which this widely used method of data scrambling can cause PSK and QAM signals to violate the CMA convergence conditions were precisely identified. It was also shown that these scrambled signals can alter the stationary points of the CMA algorithm. Guidance was developed regarding the selection of data scrambler parameters, given the order of the PSK or QAM constellation, such that the transmitted signal does not violate the CMA convergence conditions.

INTRODUCTION

In a digital communications system, the two most valuable resources are bandwidth and power. This research focused on situations in which bandwidth is the more precious of these two resources. In applications such as line-of-sight microwave links and telephone voiceband data communications, modulation techniques that conserve bandwidth at the expense of power are often employed to increase the bandwidth efficiency, measured in bits per second per Hertz of occupied bandwidth (bits/sec/Hz). In addition to requiring increased signal-to-noise ratios to maintain acceptable bit error rates, bandwidth-efficient modulation techniques such as phase-shift keyed (PSK) and quadrature amplitude modulation (QAM) also exhibit increased sensitivity to channel impairments such as multipath propagation and distorted amplitude responses. As the bandwidth efficiency of a particular PSK or QAM signal is increased, both its sensitivity to channel impairments and the need to employ compensation techniques to mitigate their effects increase.

One of the most widely used techniques for compensating for channel impairments when bandwidth-efficient modulations are employed is adaptive equalization. In traditional adaptive channel equalization schemes, training sequences of known data are periodically sent by the transmitter to allow adjustment of the receiver's equalizer coefficients. Training requires cooperation between the

transmitter and receiver(s) that is often undesirable. For example, in a multipoint data network, many receivers may be listening to a single transmitter and may desire to enter and leave the network at random times. Also, on a line-of-sight microwave link, recovery from outages due to multipath fading must be accomplished at times that are impossible to predict. Furthermore, the periodic transmission of training sequences reduces the overall bandwidth efficiency of the communications system because useful data cannot be sent during the training periods. As an alternative, blind equalization techniques accomplish the adjustment of adaptive equalizer coefficients without the use of training sequences.

The majority of blind equalization schemes can be categorized as either Bussgang or polyspectra-based techniques [1], [2]. Polyspectra-based techniques generally require more data than Bussgang techniques to achieve equivalent performance, and thus, they are not well-suited for online processing of digital communications signals. They were not considered in this project. Members of the Bussgang family are similar to the least-mean-square (LMS) algorithm in that stochastic gradient descent techniques are used to minimize a cost function in an iterative fashion. In trained LMS equalization, the cost function is the mean-square error between the training sequence and the equalizer output $\hat{a}(n)$. In Bussgang blind equalization, the cost function depends on a statistical description of the transmitted signal and on a memoryless nonlinear function of $\hat{a}(n)$. In this context, the term "memoryless" implies that the value of the nonlinear function at time n depends only on $\hat{a}(n)$ and not on any previous values of the equalizer output.

This research investigated some performance issues with, and developed some refinements to, the most widely used Bussgang algorithm for blind equalization of digital communications signals, namely the constant modulus algorithm CMA [3], [4]. CMA is based on the recognition that multipath distortion and additive interference cause amplitude fluctuations in a signal that, in the absence of these impairments, would otherwise exhibit a constant modulus (at the symbol sampling instants). In this sense, CMA is referred to as a "property restoral" algorithm [5]. By restoring the constant modulus property, CMA indirectly compensates for multipath distortion and reduces intersymbol interference (ISI). In [3], and subsequently in [6], it was shown that the CMA cost function reaches its global minimum for zero ISI. Therefore, the CMA equalizer may also be viewed as a "zero forcing" equalizer akin to that pioneered by Lucky in [7].

The initial focus of this project was on the acceleration of the convergence of CMA using a lattice filter structure (LCMA). It was shown that the convergence performance of LCMA is less sensitive to increasing amounts of channel-induced amplitude distortion than that of the transversal implementation (TCMA) for both PSK and QAM signals. However, for practical ranges of step-size parameters and moderate amplitude distortion, LCMA exhibits more misadjustment (excess mean-square error in the converged adaptive filter compared to the mean-square error achieved by the optimum Weiner filter) than does TCMA for PSK signals. The reasons for this extra misadjustment were explained in detail in [8] and stem from the jittering of the additional adaptive coefficients in the lattice portion of the LCMA equalizer. In the case of QAM signals, the extra misadjustment caused by the lattice coefficients is dominated by another misadjustment term, namely that caused by the QAM constellation—CMA cost-function mismatch. In other words, for QAM signals, the converged misadjustment levels of LCMA and TCMA are essentially equal (and LCMA converges more quickly). The results of the research on LCMA in blind equalization were reported in [8]–[11].

CMA's excessive misadjustment for QAM signals was directly addressed in this project. Two alternative blind equalization algorithms based on cost functions similar to the CMA cost function, but exactly matched to the QAM constellations, were developed. These new algorithms are the Multiple Modulus Algorithm (MMA) and CMA-Assisted Decision Adjusted Modulus Algorithm (CADAMA). The misadjustment performance of these new algorithms for QAM signals is comparable to that achieved with CMA for PSK signals, and they do not require a great deal of additional calculations. Consequently, MMA and CADAMA were demonstrated as viable alternatives to CMA for QAM signals. A lattice version of MMA was also introduced. The results of the research on QAM-specific alternative blind equalization algorithms were reported in [8] and [12]–[14].

The successful convergence of CMA depends critically on the statistical properties of the transmitted signal. This research examined the potential misconvergence situation that has been reported [15] when a transmitter that is used with a CMA-based receiver employs a data scrambler. Guidance was developed regarding the selection of scrambler parameters, given the order of the PSK or QAM constellation, such that the transmitted signal does not violate the CMA convergence conditions given in [3]. This is an important issue because, if proper care is not taken in selecting the scrambler parameters, the statistical properties of the scrambled signal can sufficiently violate the necessary conditions for CMA convergence such that the algorithm will fail to converge to a solution that equalizes the channel. The results of the research on CMA misconvergence were reported in [8] and [16]–[18].

CMA-STYLE BLIND EQUALIZERS FOR QAM SIGNALS

CMA is based on the minimization of the phase-blind cost function [3]

$$J_{CMA} \triangleq \frac{1}{4}E\left[\left(|\hat{a}(n)|^2 - R_2\right)^2\right], \quad R_2 \triangleq E\left[|a_m|^4\right]/E\left[|a_m|^2\right], \tag{1}$$

where $\hat{a}(n)$ is the equalizer output. The expected values in the definition of the modulus constant, R_2, are taken over the constellation points $\{a_m\}_{m=0}^{M-1}$ under the assumption that all M points are equally probable. If, as in PSK, all of the constellation points lie on a single radius, $r \triangleq |a_m|$, then $R_2 = r^2$. In QAM, R_2 is related to an average squared amplitude of the symbols. In general, however, $R_2 \neq E|a_m|^2$ for the standard QAM constellations. Furthermore, if the QAM constellation points lie on the multiple radii $\{r_i\}_{i=1}^{\rho}$, then, typically, $R_2 \neq r_i^2, \forall i, 1 \leq i \leq \rho$. That is, equation (1) does not go to zero at any of the points of most standard QAM constellations. For example, in figure 1 (a and b), circles are drawn at the radius, $\sqrt{R_2}$, for the 8-QAM and 16-QAM constellations shown, respectively. Equation (1) only goes to zero on the radius, $|\hat{a}(n)| = \sqrt{R_2}$. While CMA can be successfully applied to QAM signals [3], [19], its cost function, as shown in equation (1), is better matched to PSK in the sense that it goes to zero at all the signal points of a PSK constellation. For QAM, the mismatch between the constellation and the CMA cost function causes the adaptive tap-weights to jitter about their optimum settings even in the ideal case of perfect equalization in a noise-free setting.

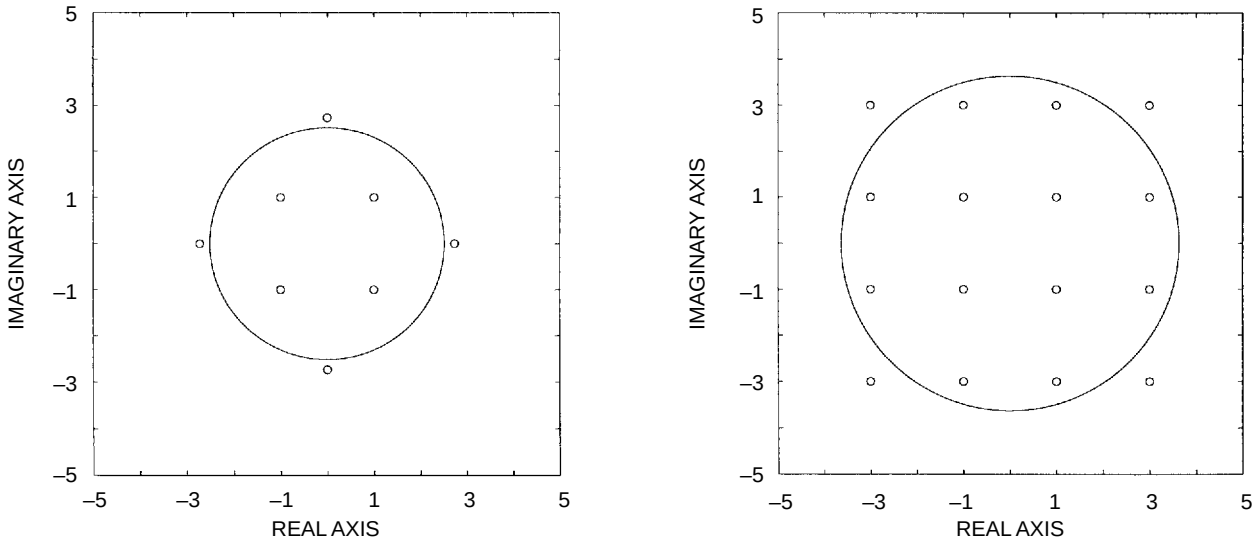

(a) 8-QAM *(b) 16-QAM*

Figure 1. Circles with radius equal to the square root of the modulus constant, R_2, given by equation (1) drawn in the complex plane of the constellation.

The two variants of CMA developed in [8], [12]–[13] are specifically tailored for QAM constellations in that they are based on cost functions that go to zero at all of the signal point radii. Each resulting algorithm has the advantage of significantly reducing the misadjustment in the converged solution. Misadjustment $\mathcal{M}$ is defined as $\mathcal{M} \triangleq \left(\epsilon_\infty^2 - \epsilon_{\min}^2\right)/\epsilon_{\min}^2$, where ϵ_∞^2 is the asymptotic mean-square error (MSE) achieved by the converged adaptive filter (with tap-weights jittering about the optimum settings), and $\epsilon_{\min}^2$ is the MSE achieved by the optimum Weiner filter (with tap-weights fixed at the optimum settings). Both approaches, namely MMA and the Decision-Adjusted Modulus Algorithm (DAMA), were originally proposed for real-value pulse amplitude modulation (PAM) signals in [20]. Significant refinements of MMA introduced in [8] and [12] extended the applicability of the algorithm well beyond the expectations indicated in [20]. In [21], DAMA is reintroduced as Radius Directed Equalization (RDE). The main problem with DAMA discussed in [21], namely the failure of the algorithm to converge in the face of moderate-to-severe amplitude distortion, was addressed in [8] and [13] with a new hybrid algorithm.

MMA is based on stochastic gradient descent minimization of a cost function that penalizes all equalizer outputs that do not lie on the radii $\{r_i\}_{i=1}^{\rho}$ of the QAM constellation. The MMA cost function, generalized from [20] for complex-valued signals, is

$$J_{MMA} \triangleq \frac{1}{4} E\left[\prod_{i=1}^{\rho}\left(|\hat{a}(n)|^2 - r_i^2\right)^2\right]. \tag{2}$$

Note that equation (2) is identical to equation (1) for PSK, for which $\rho = 1$. Clearly, MMA requires *a priori* knowledge of the QAM constellation. DAMA is based on stochastic gradient descent minimization of the cost function

$$J_{DAMA} \triangleq \frac{1}{4} E\left[\min_i \left(\left|\hat{a}(n)\right|^2 - r_i^2 \right)^2 \right], \quad 1 \le i \le \rho. \tag{3}$$

Equation (3) is also identical to equation (1) for PSK, and clearly DAMA also requires *a priori* knowledge of the QAM constellation. Furthermore, with each symbol estimate produced by the DAMA equalizer, a decision must be made as to which radius of the constellation is the closest to the estimate. The corresponding term of the DAMA cost function then applies to the next cycle of the equalizer's tap-weight update. DAMA can only be applied if the amplitude distortion has been sufficiently equalized. DAMA will not converge if the number of incorrect radius decisions is large, and therefore, it cannot be used reliably for the initial phase of blind equalization of the amplitude distortion. Consequently, the DAMA algorithm needs to be assisted by another algorithm to perform the initial adjustment of the blind equalizer. This research developed a new hybrid algorithm, the CMA-Assisted Decision Adjusted Modulus Algorithm (CADAMA), that employs the CMA algorithm to perform initial adjustment of the equalizer. CADAMA switches from CMA mode to DAMA mode when the amplitude equalization has been sufficiently accomplished to achieve the significantly reduced misadjustment that results from using a cost function that goes to zero at all of the signal point radii. The criterion for switching between the modes is based on comparing either the empirical density or distribution function of radius decisions (calculated over an observation interval) to the known discrete probability density or distribution function, respectively, of radii in the constellation as determined by the number of signal points on each radius. The comparison can be made using either Pearson's chi-square or the Kolmogorov–Smirnov goodness-of-fit test. The number ρ of radii to which CADAMA can be applied is greater than the number of radii to which MMA can be applied.

Figure 2 plots four CMA and four MMA learning curves (MSE vs. iteration) for the 8-QAM constellation shown in figure 1(a). Although $\epsilon^2_{\min}$ ranges over a factor of 3.77 for the four values of eigenvalue disparity, $\chi(\boldsymbol{R})$, the asymptotic MSE achieved by CMA, ϵ^2_∞ (CMA), ranges only over a factor of 1.23. This indicates that the CMA cost function—QAM constellation mismatch, rather than $\epsilon^2_{\min}$, is the dominant factor in determining ϵ^2_∞ (CMA). In contrast, the asymptotic MSE achieved by MMA, ϵ^2_∞ (MMA), ranges over a factor of 3.80, roughly the same as $\epsilon^2_{\min}$. The achieved value of ϵ^2_∞ (MMA) more closely tracks the channel conditions than does ϵ^2_∞ (CMA). Accordingly, the misadjustment achieved by MMA, $\mathcal{M}$(MMA), is roughly constant at a level of 0.18 for the four values of $\chi(\boldsymbol{R})$. In contrast, $\mathcal{M}$(CMA) actually decreases for 8-QAM as $\chi(\boldsymbol{R})$ rises since the value of $\epsilon^2_{\min}$ rises much more quickly than does ϵ^2_∞ (CMA). Nonetheless, $\mathcal{M}$(CMA) > $\mathcal{M}$(MMA) by factors ranging from 19.8 to 76, i.e., roughly 13 to 19 dB. Finally, note that, within about 5%, the convergence times τ_∞ (MMA) $\approx \tau_\infty$ (CMA) for all four values of $\chi(\boldsymbol{R})$.

Clearly MMA's convergence performance for a two-amplitude QAM constellation (e.g., 8-QAM) represents a compelling improvement over CMA. However, it was shown in [8] and [12] that for a three-amplitude constellation (e.g., 16-QAM) the convergence time of MMA exhibits exaggerated sensitivity to increasing $\chi(\boldsymbol{R})$ with increases in convergence time approaching 300% for an eigenvalue disparity of 17 dB. Furthermore, for yet higher order standard QAM constellations (with greater than three amplitudes), MMA is not applicable at all. In contrast, the convergence time of CADAMA does not exhibit exaggerated sensitivity to increasing $\chi(\boldsymbol{R})$, and it can be applied to higher order QAM constellations.

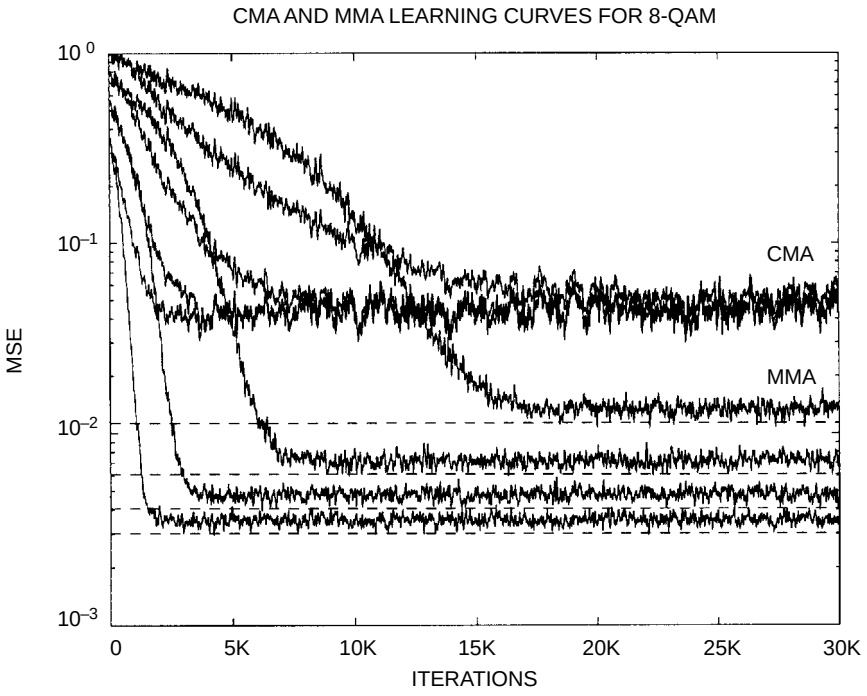

Figure 2. CMA and MMA learning curves for 8-QAM, step-size $\mu = 2 \times 10^{-4}$, and channel eigenvalue disparities of 7.8, 10.5, 13.4, and 16.7 dB. The Wiener MSEs ($\epsilon^2_{\min}$) for the four eigenvalue disparities are indicated by the horizontal dashed lines. For either algorithm, the four learning curves correspond to eigenvalue disparities of 7.8, 10.5, 13.4, and 16.7 dB, respectively, moving from left to right.

Figure 3 plots four CMA and CADAMA learning curves for the 16-QAM constellation shown in figure 1(b). The switching between the CMA and DAMA modes in CADAMA was accomplished with the chi-square test conducted at the 0.5% level of significance. The reductions in $\mathcal{M}$ achieved by CADAMA compared to CMA for 16-QAM ranged from 18.7 to 25.7 dB. These dramatic reductions in misadjustment came at the expense of 48 to 60% increases in convergence time. If the reduction in misadjustment substantially reduces the convergence time of a subsequent carrier recovery algorithm as suggested in [21], then the overall convergence time of the combined equalization and carrier recovery operation could be reduced by using CADAMA instead of CMA.

Figure 4 plots CADAMA and CMA learning curves for the standard 128-QAM cross constellation (e.g., figure 5.22 of [22]). The switching between the CMA and DAMA modes in CADAMA was accomplished with the Kolmogorov–Smirnov goodness-of-fit test conducted at the 0.05% level of significance. The misadjustment achieved by CADAMA is $\mathcal{M} \approx 0.10$ whereas for CMA, it is $\mathcal{M} \approx 21.37$. The reduction in $\mathcal{M}$ is, therefore, roughly 23.3 dB.

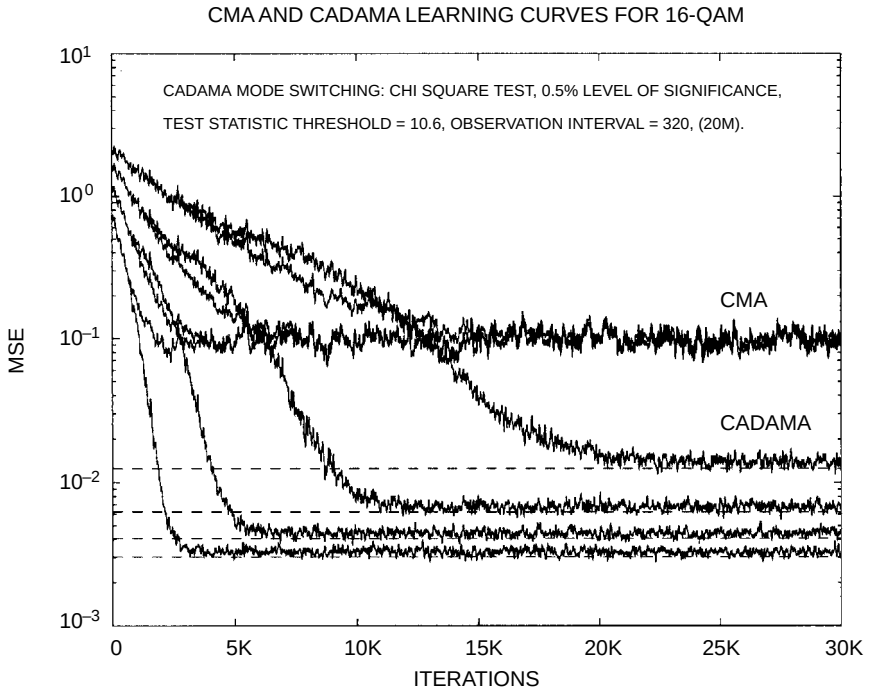

Figure 3. CMA and CADAMA learning curves for 16-QAM, step-size $\mu = 5 \times 10^{-5}$*, and channel eigenvalue disparities of 7.8, 10.5, 13.4, and 16.7 dB. The Wiener MSEs (*$\epsilon^2_{\min}$*) for the four eigenvalue disparities are indicated by the horizontal dashed lines.*

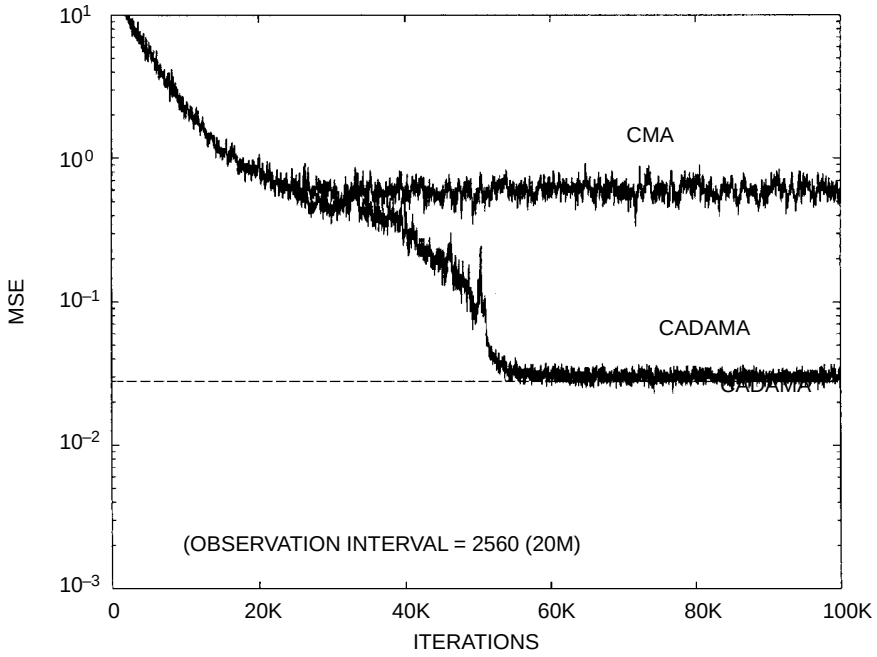

Figure 4. CMA and CADAMA learning curves for 128-QAM, step-size $\mu = 5 \times 10^{-7}$*. χ(**R**) = 16.8 dB. The Wiener MSE* $\epsilon^2_{\min}$ *= 0.0281 is indicated by the horizontal dashed line.*

CONCLUSIONS

This project conducted investigations into some of the performance issues that arise when CMA is used for blind equalization of both PSK and QAM digital communications signals. Two new blind equalization algorithms, closely related to CMA but specifically tailored for QAM signals, were also developed to address the excessive misadjustment that CMA exhibits when it is applied to QAM signals.

A detailed derivation of a stochastic gradient lattice (SGL) version of CMA, LCMA was presented in [8]. It was shown that because the error-function component of the CMA tap-weight update is non-linear in the equalizer output, the LCMA tap-weight updates must all use the final order error. In contrast, since the trained SGL equalizer error-function component is linear in the equalizer output, its tap-weight updates can use the individual stage errors instead of the final order error. The use of the individual stage errors over the final order error is preferred in the trained SGL equalizer because it results in significantly improved mean-square-error performance [23].

The convergence performance of LCMA was compared to the more standard transversal implementation of CMA, TCMA, in equalizing progressively more severe channel-induced amplitude distortion. It was found that the convergence performance of LCMA was degraded to a lesser degree than that of TCMA as the amplitude distortion increased for both PSK and QAM signals. However, for practical ranges of step-size parameters and moderate amplitude distortion, LCMA displays greater misadjustment after convergence than does TCMA for PSK signals when the step-size parameters are selected to give equal convergence times. This additional misadjustment is caused by the jittering of the adaptive partial correlation (PARCOR) coefficients in the lattice portion [8]. For QAM signals, the mismatch between the CMA cost function and the QAM constellation contributes a much larger component to the misadjustment than that due to the PARCOR jittering. Thus, for QAM signals, LCMA offers improved convergence performance compared to TCMA over the entire range of amplitude distortion and step-size parameters that were examined.

The CMA cost function goes to zero at only a single ring in the complex plane of the signal constellation. In the case of PSK, this ring is at the (single) radius of the signal points and the cost function is well-matched to the constellation. Since QAM constellations consist of signal points on multiple radii, the nature of the mismatch with the CMA cost function is that the cost function does not go to zero at all of the signal points of the QAM constellation. (For most of the standard QAM constellations, the standard CMA cost function does not go to zero at *any* of the QAM signal points.) The excessive misadjustment exhibited by CMA for QAM is thus caused by the fact that, if the equalizer was preset with the optimum coefficients, the CMA tap-weight update algorithm would still jitter the adaptive tap-weights about the optimum values, even in the absence of any thermal noise. An expression was derived that quantifies the portion of the CMA asymptotic tap-weight variance that is due to the mismatch between the CMA cost function and various QAM constellations [8], [12].

The two alternative blind equalization algorithms that were developed in this project are each based on cost functions that go to zero at every signal point radius of the QAM constellation [8], [12]–[13]. This results in significantly improved misadjustment performance for QAM signals, as predicted by the fact that the asymptotic tap-weight variance equals zero for these two algorithms under the assumptions of perfect equalization and no thermal noise [8], [12], [13]. MMA is based on a cost

function that is a product of terms, each term equal to the original Godard cost function for one of the QAM constellation's signal point radii [8], [12]. DAMA is a dual-mode (CMA/DAMA) algorithm that employs CMA for the initial phase of equalization [8], [13]. The DAMA mode is based on a cost function that is the minimum term of the set of terms whose product comprises the MMA cost function. It was shown that MMA can only be applied to standard QAM signals with up to three radii. CADAMA, on the other hand, was successfully applied to 128-QAM, a constellation with signal points on 16 radii. The switching between modes in CADAMA was accomplished via the application of standard statistical goodness-of-fit tests.

The dependence of successful CMA convergence on the statistical properties of scrambled signals was also addressed in this project [8], [16], [17]. It was shown that, given the order of the PSK or QAM signal, unless the parameters of the data scrambler are chosen properly, the probabilistic symmetry of the transmitted constellation can be highly distorted. This asymmetry causes certain moments of the constellation to deviate from zero, which is their value for uniformly distributed constellations. It was demonstrated that sufficiently distorted scrambled signals can alter the stationary points of the CMA tap-weight algorithm to the extent that a CMA equalizer that has already converged in response to a uniformly random symbol sequence can be caused to move away from settings that equalize the channel. It was shown that if the scrambler is implemented by adding modulo-2, a pseudo-noise (PN) sequence, to the data bits before they are encoded $\log_2(M)$ bits at a time into M-ary PSK or QAM symbols, then any negative impacts of the scrambler on the convergence performance of CMA will be minimized by ensuring that the period of the PN sequence is relatively prime to $\log_2(M)$.

REFERENCES

1. J. G. Proakis and C. L. Nikias. 1991. "Blind Equalization," *Adaptive Signal Processing*. *Proceedings of the International Society for Optical Engineering (SPIE)*, vol. 1565, pp. 76–87.

2. S. Bellini and F. Rocca. 1986. "Blind Deconvolution: Polyspectra or Bussgang Techniques," *Digital Communications.* Elsevier Science Publishers B.V.

3. D. N. Godard. 1980. "Self-Recovering Equalization and Carrier Tracking in Two-Dimensional Data Communications Systems," *IEEE Transactions on Communications*, vol. COM-25, no. 11, pp. 1867–1875.

4. J. R. Treichler and B. G. Agee. 1983. "A New Approach to Multipath Correction of Constant Modulus Signals," *IEEE Transactions on Acoustics, Speech and Signal Processing*, vol. ASSP-31, no. 2, pp. 459–472.

5. B. G. Agee. 1989. "The Property Restoral Approach to Blind Signal Extraction," Ph.D. Dissertation, University of California, Davis, CA.

6. G. J. Foschini. 1985. "Equalizing Without Altering or Detecting Data," *AT&T Technical Journal*, vol. 64, no. 8, pp. 1885–1911.

7. R. W. Lucky. 1965. "Automatic Equalization for Digital Communication," *Bell System Technical Journal*, vol. 44, pp. 547–588.

8. R. A. Axford. 1995. “Refined Techniques for Blind Equalization of Phase Shift Keyed (PSK) and Quadrature Amplitude Modulated (QAM) Digital Communications Signals,” Ph.D. Dissertation, University of California, San Diego, CA.

9. R. A. Axford. 1993. “Lattice Blind Equalizers,” presentation at the 4th Navy R&D Information Exchange Conference, 13–15 April, San Diego, CA.

10. R. A. Axford. 1993. “Blind Equalization with the Lattice Constant Modulus Algorithm,” *Proceedings of the IEEE Military Communications Conference* (*MILCOM*), pp. 268–272.

11. R. A. Axford. 1993, 1994. “Improved CMA Blind Equalizer Convergence Performance for QAM Signals Using a Lattice Filter Structure,” presented at École Nationale Supérieure des Télécommunications (ENST), 16 December 1993, Paris, France, and at NSF ICAS Annual Review, University of California, San Diego, 20 January 1994, San Diego, CA.

12. R. A. Axford, L. B. Milstein, and J. R. Zeidler. 1995. “The Transversal and Lattice Multiple Modulus Algorithms for Blind Equalization of QAM Signals,” *Proceedings of the IEEE Military Communications Conference* (*MILCOM*), pp. 586–591.

13. R. A. Axford, L. B. Milstein, and J. R. Zeidler. 1995. “A Dual-Mode Algorithm for Blind Equalization of QAM Signals: CADAMA,” *Proceedings of the 29th Asilomar Conference on Signals, Systems and Computers*.

14. R. A. Axford. 1995. “Blind Equalizers Based on Godard-Style Cost Functions Tailored for Quadrature Amplitude Modulated (QAM) Signals,” presented at École Nationale Supérieure de L’Électronique et de ses Applications (ENSEA), 28 June, Cergy-Pontoise, France, and at the Institut de Recherche et d’Enseignement Supérieur aux Techniques de L’Électronique (IRESTE), Université de Nantes, 29 June, Nantes, France.

15. J. R. Treichler, V. Wolff, and C. R. Johnson. 1991. “Observed Misconvergence in the Constant Modulus Adaptive Algorithm,” *Proceedings of the 25th Asilomar Conference on Signals, Systems and Computers*, pp. 663–667.

16. R. A. Axford, L. B. Milstein, and J. R. Zeidler. 1994. “On the Misconvergence of CMA Blind Equalizers in the Reception of PN Sequences,” *Proceedings of the IEEE Military Communications Conference* (*MILCOM*), pp. 281–286.

17. R. A. Axford, L. B. Milstein, and J. R. Zeidler. “On the Misconvergence of the Constant Modulus Algorithm (CMA) for Blind Equalization in the Reception of PN Sequences,” *IEEE Transactions on Signal Processing* (in process).

18. R. A. Axford, L. B. Milstein, and J. R. Zeidler. 1994. “On the Misconvergence of the Constant Modulus Algorithm (CMA) for Blind Equalization in the Reception of PN Sequences,” presented at École Nationale Supérieure des Télécommunications (ENST), 20 October, Paris, France, and at the NSF ICAS Annual Review, University of California, San Diego, 7 November, San Diego, CA.

19. N. K. Jablon. 1992. “Joint Blind Equalization, Carrier Recovery, and Timing Recovery for Higher-Order QAM Signal Constellations,” *IEEE Transactions on Signal Processing*, vol. 40, no. 6, pp. 1383–1398.

20. W. A. Sethares, G. A. Rey, and C. R. Johnson, Jr. 1990. “Approaches to Blind Equalization of Signals with Multiple Modulus,” *Proceedings of the IEEE International Conference on Acoustics, Speech and Signal Processing* (*ICASSP*), pp. 972–975.

21. M. J. Ready and R. P. Gooch. 1990. “Blind Equalization Based on Radius Directed Adaptation,” *Proceedings of the IEEE International Conference on Acoustics, Speech and Signal Processing* (*ICASSP*), pp. 1699–1702.

22. S. Benedetto, E. Biglieri, and V. Castellani. 1987. *Digital Transmission Theory*, Prentice-Hall, Upper Saddle River, NJ.

23. E. H. Satorius and S. T. Alexander. 1978. “Rapid Equalization of Highly Dispersive Channels Using Adaptive Lattice Algorithms,” NOSC TR 249 (Apr), Naval Ocean Systems Center, San Diego, CA.

Principal Investigator: 0601152N
Roy Axford NRaD ZW80

A Discretely Tunable Ultraviolet Laser for Multichannel Covert Communications

P. Poirier and F. Hanson

The development of laser sources in the ultraviolet region from 260 to 280 nm is considered a promising approach for an intentionally range-limited, covert communication link. A discretely tunable source coupled with variable wavelength filters would be desirable for multiple channel or bidirectional operation. The moderate to high repetition rate, Q-switched laser performance of a quadrupled diode-pumped Nd:YALO laser discretely tunable between 266 and 275 nm is reported. The transmitted power ratio of custom interference separation filters is presented.

INTRODUCTION

Solid-state laser sources in the ultraviolet (UV) region from 260 to 280 nm are an attractive approach for an intentionally short-range communication system through the atmosphere [1]. Optical absorption at low altitudes due to trace ozone content physically limits the range to a few hundred meters. Further, scattering at these wavelengths allows the propagation to be non-line-of-sight. These characteristics would be useful for a variety of military and civilian applications that require covertness with added flexibility for certain geometric scenarios where line-of-sight alignment is not possible. Modulation at repetition rates of a few kHz is usually required for voice communication. However, a pulse position modulation scheme could be used to achieve the necessary data rates with moderate average repetition frequencies between 100 and 1000 Hz. A compact and efficient system is essential for most field-environment applications. Further, a tunable multiwavelength source coupled with variable wavelength separation filters would be desirable for multiple channel or bidirectional operation. The selection of filtering schemes becomes more difficult as the wavelength separation decreases. A minimum 5-nm separation would probably be a limit for any useful system.

One method of obtaining multiple wavelengths in the desired UV region could utilize efficient frequency quadrupled neodymium-doped lasers that operate at several lines. Although these lasers typically do not have lines with comparable gains or are not at optimal wavelength separations [2,3], one material that appears to have optimal characteristics is neodymium-doped $YAlO_3$ (Nd:YALO). In this paper, we investigate the feasibility of using a Nd:YALO laser that could be tuned between two widely spaced and comparable gain lines in the $^4F_{3/2} \rightarrow {}^4I_{11/2}$ infrared (1-micron) band and frequency quadrupled to the UV. The goal of this work was to provide a minimum of 0.2 millijoules of energy per pulse at both ultraviolet wavelengths at the highest repetition rate at an electrical input power less than 1 kW. These values were based on the requirements for the previously funded Intentionally Short-Range Communication (ISRC) project. Using an appropriate modulating scheme, a laser operating at several hundred pulses per second could provide 2.4 kbps or higher data rates for communication applications. A system operating at 600 Hz had earlier been designed and built for the ISRC project using a quadrupled Nd:YAG laser with the energy and power requirements specified above. However, this system operated at a single wavelength and could only allow multichannel operation using various modulation techniques that decrease available bandwidth.

LASER PERFORMANCE

Nd:YALO is a crystal that has properties generally comparable with the commonly used Nd:YAG. It is, however, a biaxial material with an emission spectrum known to consist of several sharp lines spread over 50 nm for emission polarized along all three axes. The effective cross section of the strongest component is comparable with that for Nd:YAG and occurs at 1079.5 nm for light polarized along the b-axis. The substantial body of research that has been published on the laser performance of Nd:YALO has dealt primarily with operation at this wavelength [4–6]. For polarization along the a- and c-axes, the emission is not dominated by a single line and consists, instead, of a series of well-spaced lines with comparable intensities as shown in figure 1 for emission along the

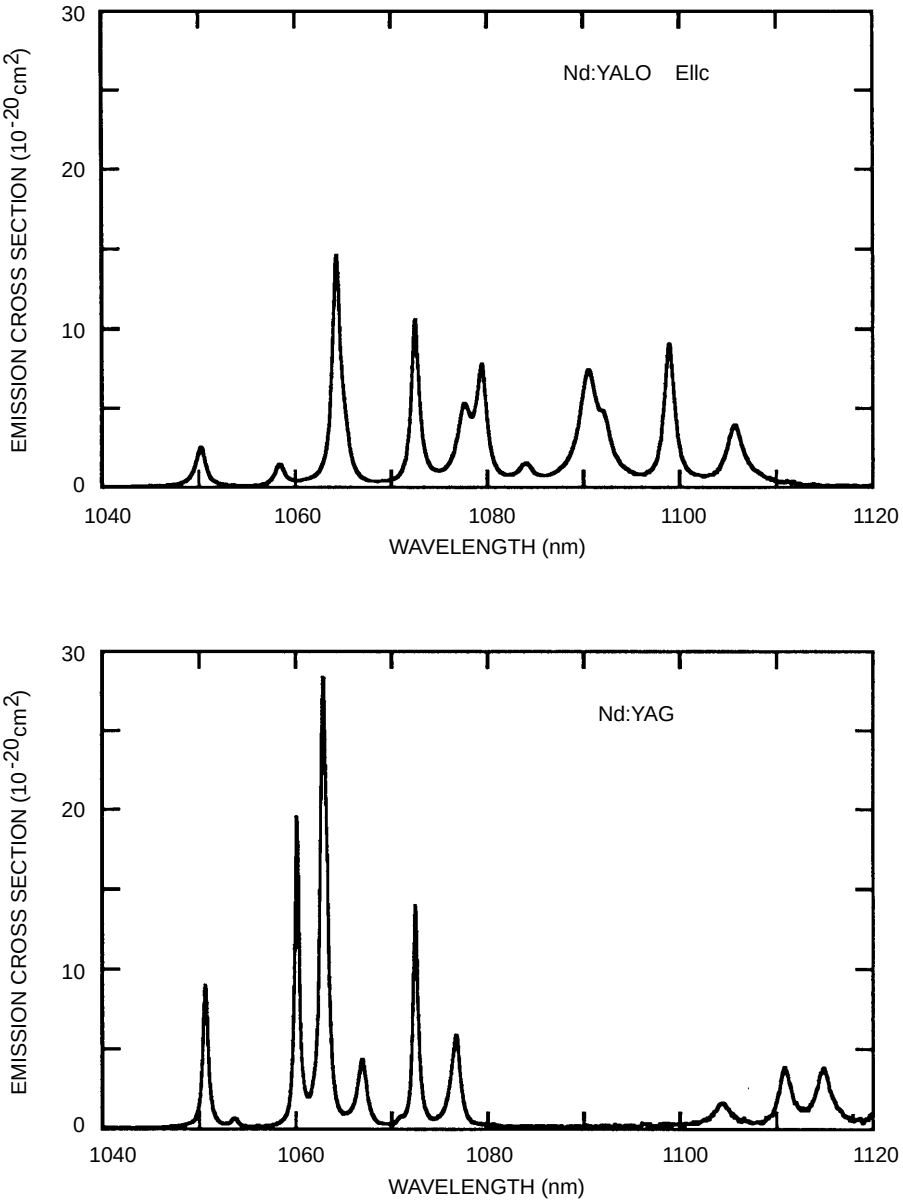

Figure 1. Emission cross sections of Nd:YAG and Nd:YALO.

c-axis. The emission cross section of the high-gain, 1064-nm line of Nd:YAG is greater than the widely separated 1064- and 1099-nm Nd:YALO lines by a factor of two and is shown here for comparison.

Nd:YALO has a complex absorption spectrum with several peaks unlike Nd:YAG, which has a predominant peak at 808 nm. Many high-power pulsed diode arrays are designed to operate at this wavelength at the maximum average power so that they can be used as pump sources for Nd:YAG. The optimal absorption peak for Nd:YALO along the a-axis is at approximately 803 nm. The most efficient coupling design for side-pumping with the laser-diode arrays incorporated two five-bar arrays [7]. The output in the high-divergence plane from each of the 10 individual bars was collimated with a short-focal-length cylindrical lens, and the combined output was focused with a large cylindrical lens into the 3-mm-diameter rod. The spectrum of the pump sources shifts to longer wavelengths as the average power increases. These collimated arrays have a spectrum range of 803 to 808 nm. This range resulted in efficient laser output only at lower repetition rates with minimum spectral shift. Other available arrays with a larger spectrum range (796 to 808 nm) but without the incorporated lenses (uncollimated) were used at higher repetition rates at the cost of reduced overall efficiency.

Nd:YALO also has stronger thermal induced focusing and astigmatism compared with Nd:YAG. Operating at higher repetition rates increases the heat load within the laser rod and shifts the pump laser spectrum as well. It is therefore difficult to determine whether a decrease in efficiency at higher repetition rates is due to absorption mismatch or thermal lensing problems without obtaining direct experimental data.

Therefore, we designed a water-cooled laser head for side-pumping with two collimated or four uncollimated high-power diode array stacks. We characterized the Q-switched laser performance at the two green lines using the cavity shown in figure 2. Here all three mirrors were high reflectors at the infrared wavelengths. Mirror M3 was a high reflector at the green lines, and the folding mirror, M2, was transmissive at these wavelengths. Q switching was obtained with a standard acousto-optic quartz cell designed for 1064 nm. A special birefringent filter consisting of a crystal quartz wave plate and linear polarizer was fabricated to permit tuning between the desired lines. The wave plate was designed to give a retardation of exactly seven full waves at 1099 nm and approximately 7.25 waves at 1064 nm. The wave plate could be oriented so that, at 1064 nm or the nearby 1072.5-nm line, two passes would result in a significant transfer of intensity into the orthogonal polarization and rejection by the polarizer. When the wave plate axis was aligned parallel to the polarizer axis, oscillation occurred on the stronger 1064-nm line. A LiB_3O_5 (LBO) crystal, 3.5 mm by 3.5 mm by 8.6 mm and oriented for type I second-harmonic generation (infrared to green conversion), was placed at the waist of the cavity between mirrors M2 and M3. We accomplished tuning from 532 to 550 nm by rotating the wave plate and tilting the LBO crystal.

The results at 100 Hz and at 600 Hz are shown in figure 3 with the collimated and uncollimated arrays, respectively. For an optimal 150-μsec pulse width, the associated duty cycle for the arrays produces a spectral center peak of approximately 803 nm at these repetition rates. Pump energy indicates the average energy incident on the rod. The green output from the laser cavity was further

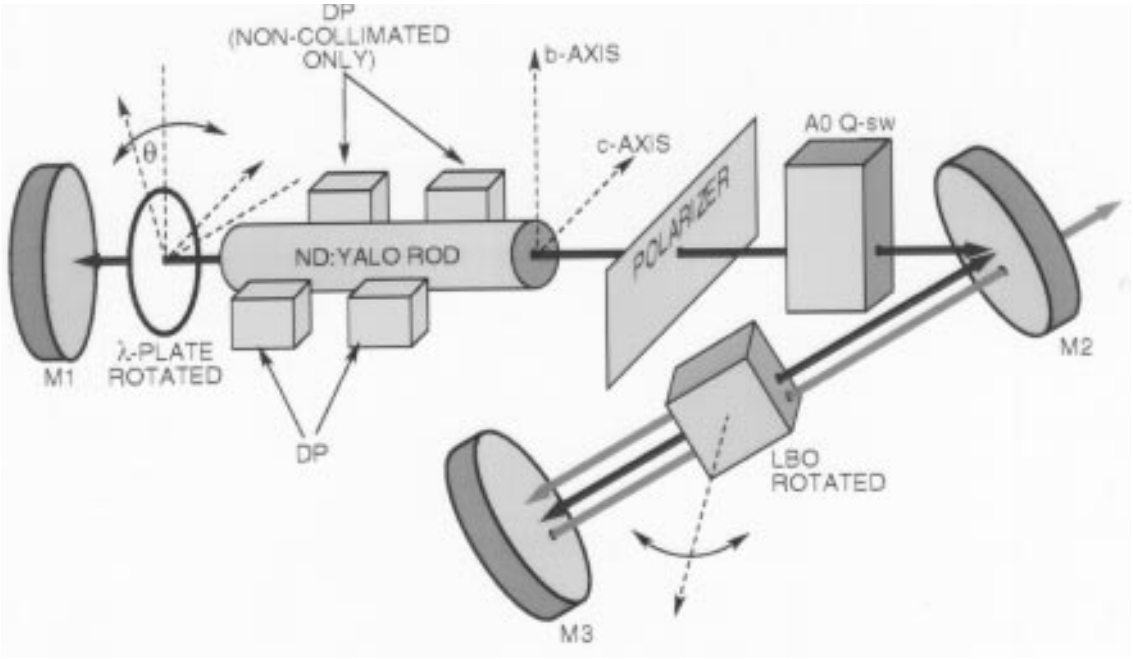

Figure 2. Nd:YALO cavity layout: DP, diode pump arrays; M1, M2, and M3, mirrors; AO Q-sw, acousto-optic quartz cell; λ-Plate, wave plate; LBO, lithium triborate crystal.

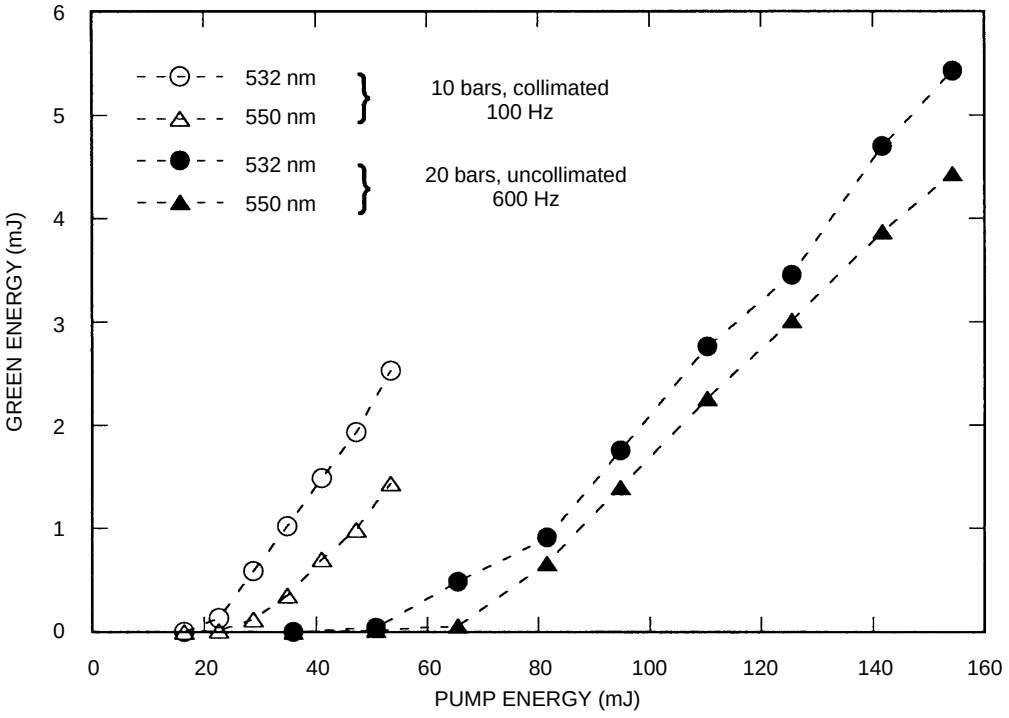

Figure 3. Pulsed energies at 532 and 550 nm from the Q-switched Nd:YALO laser at 100 and 600 Hz.

frequency-doubled externally in a 7-mm-long, uncoated BaB_2O_4 (BBO) crystal to obtain UV light at 266 and 275 nm. The green beam was collimated and focused into the BBO crystal. These results are given in figure 4, in which the incident green energy, either at 532 or 550 nm, was measured before the uncoated focusing lens, and the UV output was measured after separation from the residual unconverted green with a Pellin–Broca prism.

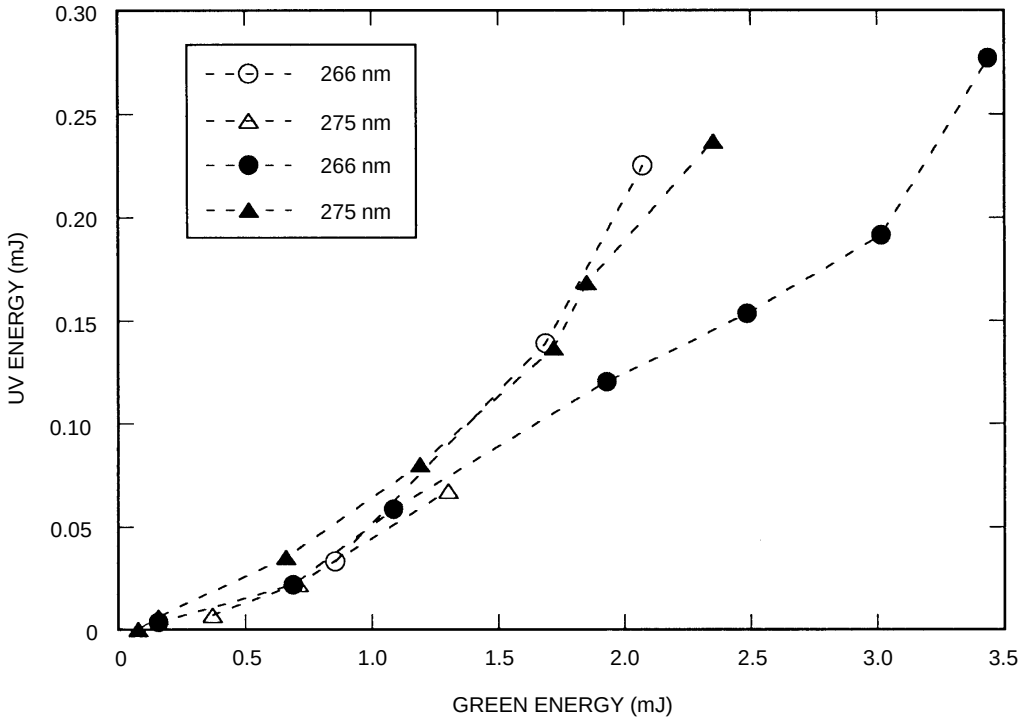

Figure 4. Pulsed energies at 266 and 275 nm obtained by frequency doubling in BBO at 100 and 600 Hz.

The peak performance with the uncollimated arrays occurred at 600 Hz with a UV lasing output exceeding 0.2 millijoules per pulse for both 266- and 275-nm laser wavelengths. The results at 1 kHz were slightly lower than the optimal performance shown in figures 3 and 4 (0.16 to 0.18 millijoules) due to diode wavelength and, perhaps, thermal lensing effects in the Nd:YALO rod. Careful measurements were made of the astigmatic focal lengths of the rod with the current side-pumping geometry. The focal-length measurements taken in the lab were used to calculate the transverse mode spot sizes within the cavity. The calculations indicated that the cavity could be redesigned to accommodate the stronger lensing effects at repetition rates greater than 1 kHz.

SEPARATION FILTER PERFORMANCE

In order to separate the two wavelengths at the receiver of a communications link based on the laser design, appropriate filters must be designed to provide a 10:1 ratio or greater of separation with a full acceptance angle of ≥ 40 degrees. A custom interference filter was obtained from Barr Associates that gave an approximately 4-nm shift of the cutoff wavelength across the specified angular range. The normalized transmitted power through the filters is shown in figures 5 and 6 for the 266- and 275-nm pass filters, respectively, as a function of incident angle. The average values for the

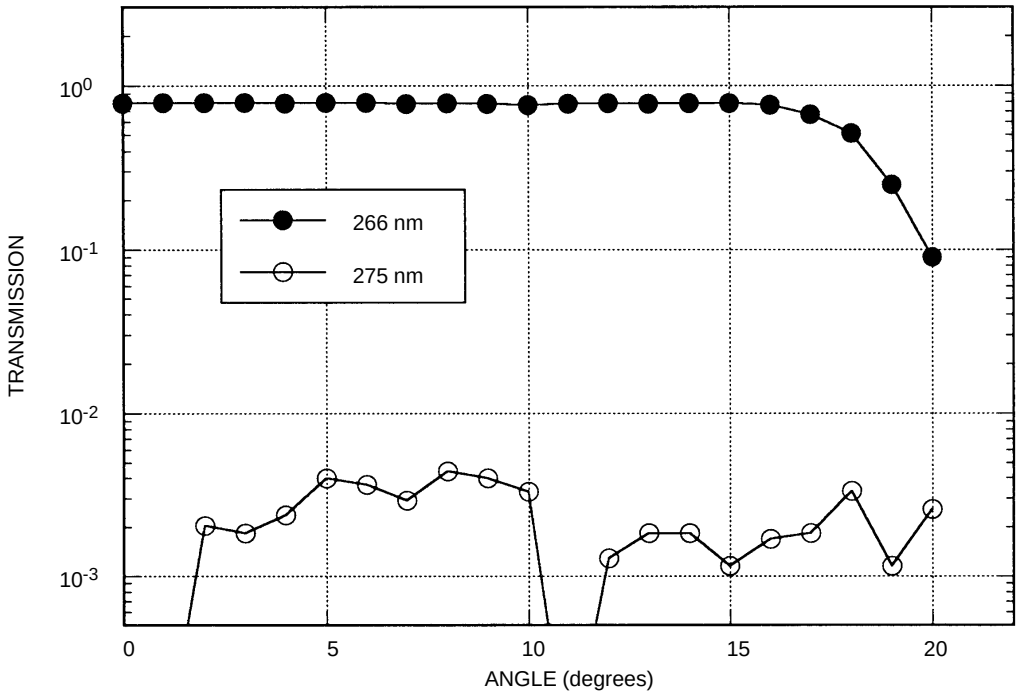

Figure 5. Normalized transmission through 266-nm passing filter for S and P polarization average.

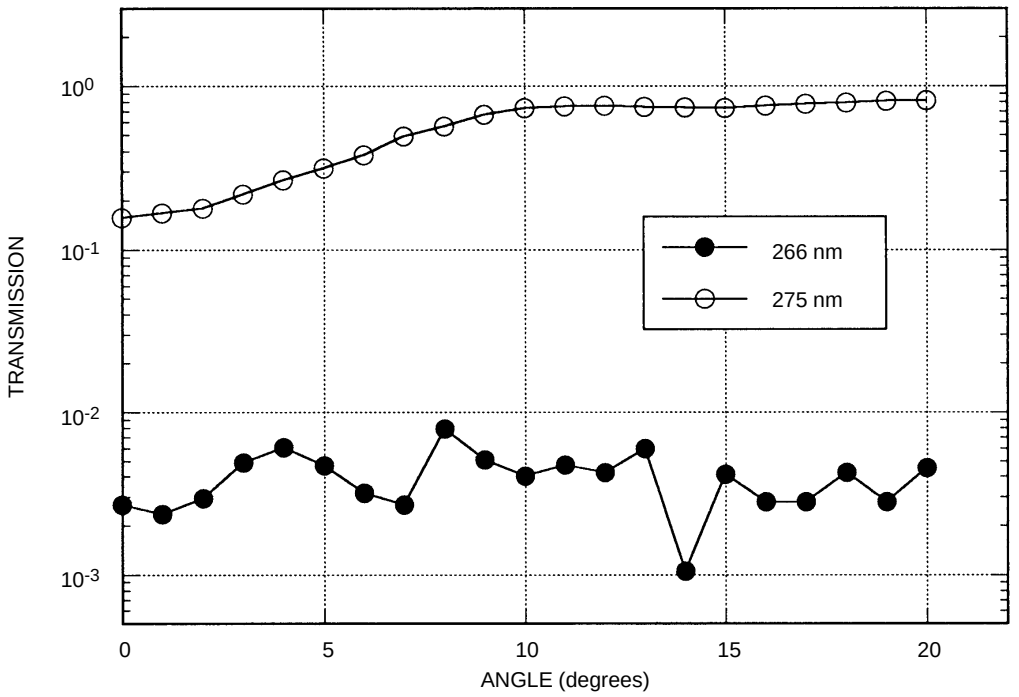

Figure 6. Normalized transmission through 275-nm passing filter for S and P polarization average.

measured S and P polarized inputs were calculated to simulate an unpolarized input from a multiple scattering scenario. The calculated integrated power ratios from a light source with a scattering input cone angle of 40 degrees was greater than 100:1 for both the 266- and 275-nm filters.

Another promising filter technology might involve an angularly insensitive absorption cutoff filter. A filter could be made based on the $Al_xGa_{1-x}N$ system [8]. For the correct Al/Ga ratio, a cutoff filter at 270 nm could potentially be made. We have, at this date, had no success in obtaining a sample with our specifications.

CONCLUSIONS

We have demonstrated a high-repetition rate, diode-pumped Nd:YALO laser that can be used as a discretely tunable transmitter source at 266 and 275 nm. The laser was efficiently operated at 600 Hz and showed a minor decrease in performance at the higher repetition rates due to a combination of pump-diode wavelength shift away from the absorption peak range and thermal lensing effects. The simplicity of the cavity configuration is comparable with a typical quadrupled Nd:YAG laser with the addition of a single quartz plate, and allows for more than one wavelength operation. The overall efficiency at the higher repetition rates could be improved in future designs with optimal pumping wavelength and coupling. Two interference filters were shown to provide the necessary separation between the two ultraviolet wavelengths with a power ratio of greater than 100:1 over the required field-of-view angles for a potential receiver.

REFERENCES

1. J. Yen. 1992. “Intentionally Short-Range Communications (ISRC) Exploratory Development Plan,” NRaD TD 2286 (Jun), Naval Command, Control and Ocean Surveillance Center RDT&E Division, San Diego, CA.

2. J. Marling. 1978. “1.05 – 1.44 μm Tunability and Performance of the CW Nd^{3+}:YAG Laser,” *IEEE Journal of Quantum Electronics*, vol. 14, pp. 56–62.

3. M. B. Danilov and I. Y. Milev. 1992. “Simultaneous Multiwavelength Operation of Nd:YAG Laser,” *Applied Physics Letters*, vol. 61, pp. 746–748.

4. G. A. Massey. 1972. “Measurements of Device Parameters for Nd:YAlO3 Lasers,” *IEEE Journal of Quantum Electronics*, vol. 8, pp. 669–674.

5. H. Shen, Y. Zhou, G. Yu, X. Huang, C. Wu, and Y. Ni. 1983. “Influences of Thermal Effects on High Power CW Outputs of B-axis Nd:YAP Lasers,” *Chin. Phys*, vol. 3, pp. 45–53.

6. F. Hanson. 1989. “Laser-Diode Side-Pumped Nd:$YAlO_3$ Laser at 1.08 and 1.34 μm,” *Optics Letters*, vol. 14, pp. 674–676.

7. F. Hanson and P. Poirier. 1995. “Multiple-Wavelength Operation of a Diode-Pumped Nd:$YAlO_3$ Laser,” *Journal of the Optical Society of America*, vol. 12, pp. 1311–1315.

8. M. Asif Khan, J. N. Kuzina, D. T. Olson, J. M. Van Hove, M. Blasingame, and L. F. Reitz. 1992. “High-Responsivity Photoconductive Ultraviolet Sensors Based On Insulating Single-Crystal GaN Epilayers,” *Applied Physics Letters*, vol. 60, pp. 2917–2919.

Principal Investigator: 0601152N
Pete Poirier NRaD ZW89

Cell Loss Evaluation of Asynchronous Transfer Mode (ATM) Statistical Multiplexing

A. Shum

A discrete-time model of an Asynchronous Transfer Mode (ATM) statistical multiplexer subject to heterogeneous groups of on-off traffic sources is proposed. Algorithms to compute the exact steady-state and transient cell loss probabilities of the multiplexer have been formulated. Unfortunately, the computational complexity of the exact algorithms is exponential in the sizes of the multiplexer parameters. To circumvent this difficulty, an asymptotic approximation algorithm is designed to estimate the steady-state cell loss probability. Although the approximation algorithm is more efficient than the exact algorithm, its time complexity remains exponential. Two polynomial-time approximation algorithms to the asymptotic approximation procedure are proposed to further reduce the computational burden. Simulation studies were conducted to assess the validity of the algorithms. For all multiplexing scenarios examined, the algorithmic results and simulation outputs showed perfect agreement.

INTRODUCTION

Asynchronous Transfer Mode (ATM) networks will be the backbone of future information superhighways. Because of their ability to efficiently transport multiple traffic types, such as voice, data, and imagery, they are destined to revolutionize the global telecommunications industries. The driving principle behind ATM is statistical multiplexing. Statistical multiplexing is so crucial to an ATM network that, in fact, the term Asynchronous Transfer Mode is essentially an alias for statistical multiplexing. To be more precise, statistical multiplexing is a means of sharing a communication channel by many traffic sources simultaneously. A statistical multiplexer (figure 1) consists of three basic components: a communication channel, a buffer and a set of traffic sources sharing the channel. Traffic is generated by the traffic sources and removed by the channel. As long as the aggregate traffic rate of the traffic sources is below the capacity of the channel, the amount of traffic in the buffer does not accumulate; however, when the aggregate rate exceeds the channel capacity, the excess traffic is stored in the buffer, and when the buffer is full, the excess traffic will be lost. Many of the issues encountered during the design of an ATM network involve the determination of how big the buffer size and channel capacity should be, or whether an additional traffic source could be supported by a multiplexer. To resolve these issues, one should have an understanding of the effect of statistically multiplexing different types of traffic onto a single communication channel. Providing a theoretical understanding of the cell loss behavior of ATM statistical multiplexing is the primary objective of this research.

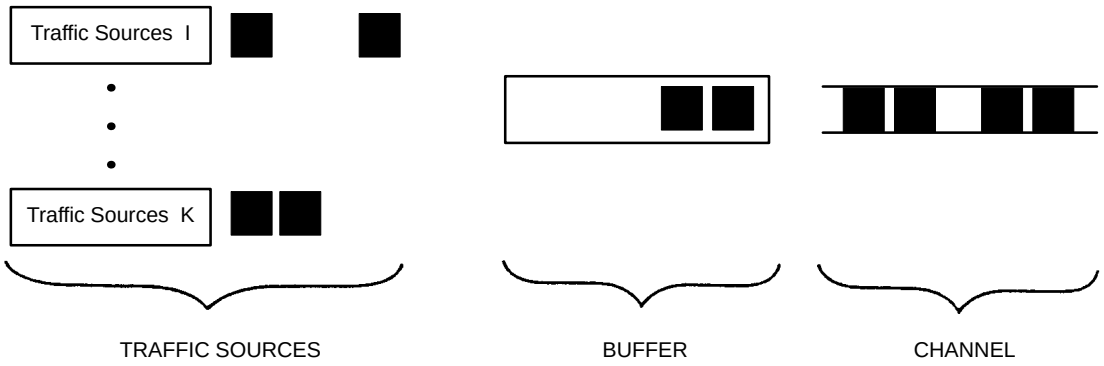

Figure 1. A statistical multiplexer.

ATM STATISTICAL MULTIPLEXER MODEL

The statistical multiplexer model with heterogeneous groups of on-off traffic sources is selected as the object of our evaluation. Although it has simple structures, the model captures many of the salient features of a real ATM statistical multiplexer. The model and its parameters are described as follows:

The buffer may store up to B cells. The channel may transmit up to C cells per time slot. The duration of a time slot is τ. There are M types of traffic sources sharing the channel. There are N_i traffic sources of the *i-th* type for $i = 1, 2, ..., M$. A traffic source of the *i-th* type alternates between *on* and *off* periods. During its on period, the source generates R_i cells per time slot, and during its off period, it generates nothing. The duration of its on period is X_i; its off period, Y_i. A schematic of an *i-th* type traffic source is shown in figure 2.

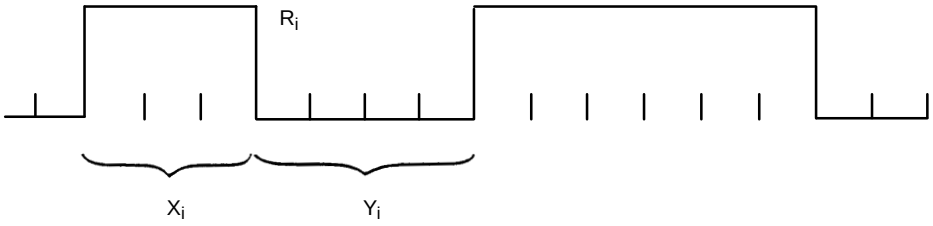

Figure 2. An i-th type traffic source.

We make the following simplifying assumptions:

(i) $Pr(X_i = j) = \alpha_i^{\,j-1}(1-\alpha_i)\ \ 0 < \alpha_i < 1 \quad i = 1, 2, ..., M$

(ii) $Pr(Y_i = j) = \beta_i^{\,j-1}(1-\beta_i)\ \ 0 < \beta_i < 1 \quad i = 1, 2, ..., M$

(iii) (Evolutionary Equation) The number of cells at the buffer at a time k+1 is computed as $\max(\min(i + \underline{R} \cdot \underline{J} - C, B), 0)$, where i is the number of cells in the buffer at time k; $\underline{J}$ is the state of the traffic sources at the start of time k.

(iv) (Stationary Condition) $\sum_{i=1}^{M} R_i N_i \frac{\frac{1}{1-\alpha_i}}{\frac{1}{1-\alpha_i} + \frac{1}{1-\beta_i}} < C$

(v) $\sum_{i=1}^{M} N_i R_i > C$

Assumptions (i) and (ii) permit us to obtain a solution to estimate the expected cell loss rate of model. The problem is completely intractable if any other distribution assumptions were made for X_i and Y_i. Assumption (iii) states that the number of cells at the beginning of the (k+1)-th time slot is equal to i, the number of cells at the buffer at the beginning of the k-th time slot, plus the number of cells generated during the k-th slot, $\underline{R} \cdot \underline{J}$, subtracted by the number of cells removed by the channel during the time slot, C; however, the number of cells in the buffer will never exceed the buffer size B, and it will never drop below 0. Assumption (iv) states that the mean aggregate traffic rate of all sources is less than the capacity of the channel; this allows the states of the multiplexer to have a stationary distribution. Assumption (v) ensures that we do not have a trivial problem, as $\sum_{i=1}^{M} N_i R_i \leq C$ implies that cell loss would never occur. Notice that the parameters C, B, M and $(\alpha_i, \beta_i, R_i, N_i)$ $i = 1, 2, \ldots, M$ completely specify an ATM multiplexing scenario.

ANALYSIS

The objective of this section is to formulate a procedure to compute the exact steady-state and transient cell loss probabilities for the above model. We introduce the following variables:

- L_k the number of cells in the buffer at the beginning of the k-th time slot
- $L = \lim_{k \to \infty} L_k$ the number of cells in the buffer at the beginning of a time slot in steady state
- J_{ik} the number of the i-th type traffic sources that are on at the beginning of k-th time slot
- $S(M, \underline{N}) = \left\{ (j_1, j_2, \ldots, j_M) \middle| 0 \leq j_i \leq N_i \ i=1,2,\ldots,M \right\}$
- $S(B, M, \underline{N}) = \left\{ (i, \underline{j}) \middle| 0 \leq i \leq B \ , \underline{j} \in S(M, \underline{N}) \right\}$
- $\underline{J_k} = (J_{1k}, J_{2k}, \ldots, J_{Mk}) \in S(M, \underline{N})$
- $Pr(\underline{J_{k+1}} = \underline{l_{k+1}} \middle| \underline{J_k} = \underline{l_k})$ $0 \leq k$, $\underline{l_{k+1}}$ and $\underline{l_k} \in S(M, \underline{N})$ the probability that $\underline{J_{k+1}} = \underline{l_{k+1}}$ given that $\underline{J_k} = \underline{l_k}$
- $(L_k = j \ , \underline{J_k} = \underline{l})$ the joint event of $L_k = j$ and $J_k = \underline{l})$

- $Pr(L_{k+1} = j\,,\, \underline{J}_{k+1} = \underline{l} \mid L_k = i,\, \underline{J}_k = \underline{m})$ the probability that the state at time k+1 is $(j,\, \underline{l})$ given that the state at time k is $(i,\, \underline{m})$
- $\xi(A)$ the *indicator function* of the event A, i.e., $\xi\{A\} = \begin{cases} 1 & A \text{ is true} \\ 0 & A \text{ is not true} \end{cases}$

If the 2-tuple $(i,\, \underline{j}) \in S(B,\, M,\, \underline{N})$ were used to denote a *state* of the multiplexer, then the set of states $S(B,\, M,\, \underline{N})$ forms a Markov chain. The *transition probability* from state $(i,\, \underline{m})$ at time k to state $(j,\, \underline{l})$ at time k+1 for the Markov chain is:

$$Pr(L_{k+1} = j\,,\, \underline{J}_{k+1} = \underline{l} \mid L_k = i\,,\, \underline{J}_k = \underline{m}) = \xi\{j = \max(\min(i + \underline{R}\cdot\underline{m} - C\,,\, B),\, 0)\} Pr\{\underline{J}_{k+1} = \underline{l} \mid \underline{J}_k = \underline{m}\}\,, \tag{1}$$

where

$$Pr(\underline{J}_{k+1} = \underline{l} \mid \underline{J}_k = \underline{m}) = \prod_{i=1}^{M} Pr(J_{i,\,k+1} = l_i \mid J_{i,\,k} = m_i) \tag{2}$$

and

$$Pr(J_{h,k+1} = j \mid J_{h,k} = i) = \sum_{m=1}^{i} \sum_{\{l\,:\,l = m - j\}} \binom{i}{m} (\alpha_h)^m (1 - \alpha_h)^{i-m} \binom{N - i}{l} (\beta_h)^{N_h - i - l} (1 - \beta_h)^l \tag{3}$$

$$\binom{x}{y} = \frac{x!}{y!(y - x)!} \text{ if } y \le x \text{ and } \binom{x}{y} = 0 \text{ otherwise.}$$

The state evolution equation of the multiplexer is

$$Pr(L_{k+1} = j,\, \underline{J}_{k+1} = \underline{l}) = \sum_{(i,\underline{m}) \in S(B,M,\underline{N})} Pr(L_{k+1} = j,\, \underline{J}_{k+1} = \underline{l} \mid L_k = i,\, \underline{J}_k = \underline{m}) Pr(L_k = i,\, \underline{J}_k = \underline{m})\,, \tag{4}$$

where L_k and $\underline{J}_k$ denote the number of cells in the buffer and the state of the traffic sources at time k, respectively.

Notice that once $Pr(L_k = j,\, \underline{J}_k = \underline{l})$ is known for each $(j,\, \underline{l}) \in S(B,M,\underline{N})$ and $k > 0$, the steady-state and the transient cell loss probabilities of the model may be determined. We first formulate a procedure to obtain $Pr(L_k = j,\, \underline{J}_k = \underline{l})$.

Given that the multiplexer is at state $(i,\, \underline{m}) \in S(B,M,\underline{N})$ at time 0, the probability that the state of the multiplexer at time k is $(j,\, \underline{l})$, that is, the transient probability that the multiplexer is at $(j,\, \underline{l})$, may be *recursively* determined according to equation (4), if one sets $Pr(L_0 = i,\, \underline{J}_0 = m) = 1$ and $Pr(L_0 = x,\, J_0 = y) = 0$ for $(x,\, \underline{y}) \neq (i,\, \underline{m})$. The time complexity of obtaining $Pr(L_k = j,\, \underline{J}_k = \underline{l})$ is $O(k(B \prod_{i=1}^{M} N_i)^2)$. The probability that the state of the multiplexer is at $(j,\, \underline{l})$ at a *random epoch* sufficiently far away from

time 0 (the steady-state probability that the multiplexer is at (j, $\underline{l}$)) satisfies the following fixed-point equation:

$$Pr(L = j, \underline{J} = \underline{l}) = \sum_{(i,\underline{m}) \in S(B, M, \underline{N})} Pr(L = j, \underline{J} = \underline{l} \mid L = i, \underline{J} = \underline{m}) Pr(L = i, \underline{J} = \underline{m}) \cdot \quad (5)$$

Although the steady-state probabilities $Pr(L = j, \underline{J} = \underline{l})$ may be computed recursively using equation (4) by letting $k \rightarrow \infty$, doing so would take prohibitively large number of iterations. The $Pr(L = j, \underline{J} = \underline{l})$'s may be obtained via the following iterative procedure (the *Exact Algorithm*):

Exact Algorithm to Compute $Pr(L = i, \underline{J} = \underline{j})$

$k = 0$;
for $((i, \underline{j}) \in S(B, M, \underline{N}))$
{
$(p^k)_{(i,\underline{j})} = \dfrac{1}{\mid S(B, M, \underline{N}) \mid}$;
};

for $((i, \underline{j}) \in S(B, M, \underline{N}))$
{
$(p^{k+1})_{(i,\underline{j})} = 0$;
};

While ($\left| p^{k+1}{}_{(i,\underline{j})} - p^k{}_{(i,\underline{j})} \right| \geq \delta$ for any $(i, \underline{j}) \in S(B, M, \underline{N})$)
{
$k = k+1$;
for $((i, \underline{j}) \in S(B, M, \underline{N}))$
{
pick any ε_k such that $0 < \varepsilon_k < 1$;

$$p^k{}_{(i,\underline{j})} = (1 - \varepsilon_k) p^{k-1}{}_{(i,\underline{j})} + \varepsilon_k \sum_{(l,\underline{m}) \in S(B, M, \underline{N})} \xi \left\{ i = max(min(l + \underline{R} \cdot \underline{m} - C, B), 0) \right\} \prod_{i=1}^{M} Pr(J_i = j_i \mid J_i = m_i) p^{k-1}{}_{(l,\underline{m})};$$

};

$$S = \sum_{(i,\underline{j}) \in S(B, M, \underline{N})} p^k{}_{(i,\underline{j})};$$

for $((i, \underline{j}) \in S(B, M, \underline{N}))$

{
$$p^k{}_{(i,\underline{j})} = \frac{p^k{}_{(i,\underline{j})}}{S};$$
};
};

The procedure terminates whenever it has found a consistent set of $p_{(i, \underline{j})}$'s ($Pr(L = i, \underline{J} = \underline{j})$'s) that satisfy equation (5).

The condition $\sum_{i=1}^{M} R_i N_i \frac{\frac{1}{1-\alpha_i}}{\frac{1}{1-\alpha_i}+\frac{1}{1-\beta_i}} < C$ ensures that the Markov chain is ergodic. The ergodicity in turn ensures that a unique steady-state distribution solution exists. This implies that, if the procedure converges, it would converge to a unique solution. In general, the existence of a solution does not imply convergence. Our computational experiences suggest that the procedure always converges, however. The *space* complexity of the procedure is $O(B\prod_{i=1}^{M} N_i)$; the *time* complexity is $O(B^2\prod_{i=1}^{M} N_i^2)$.

Once the state probability distribution of the multiplexer is determined, the cell loss rate at the multiplexer may be found as follows:

We define the variables

- NL(l = i, $\underline{J}$ = $\underline{l}$) the number of cells that are lost at the end of a time slot, given that, at the start of the time slot, the number of cells in the buffer is *i*, and the state of the traffic sources is $\underline{l}$.
- NA(L = i, $\underline{J}$ = $\underline{l}$) the number of cells that arrive during a time slot k, given that, at the start of the time slot, the number of cells in the buffer is *i*, and the state of the traffic sources is $\underline{l}$.
- LR(L = i, $\underline{J}$ = $\underline{l}$) the cell loss rate during a time slot, given that the number of cells in the buffer is *i*, and the state of the traffic sources is $\underline{l}$ at the start of the time slot.

We find that

$$NL(L = i, \underline{J} = \underline{l}) = \max(\sum_{j=1}^{M} R_j l_j - (B - i + C),\ 0)\,, \tag{6}$$

$$NA(L = i, \underline{J} = \underline{l}) = \sum_{j=1}^{M} R_j\, l_j\,, \text{ and} \tag{7}$$

$$LR(L = i, \underline{J} = \underline{l}) = \frac{NL(L = i, J = 1)}{NA(L = i, \underline{J} = \underline{l})}\,. \tag{8}$$

The cell loss rate during a time slot is:

$$\sum_{(i,\underline{j}) \in S(B, M, \underline{N})} LR(L = i, \underline{J} = \underline{j}) Pr(L = i, \underline{J} = \underline{j})\,. \tag{9}$$

Equations (6) to (9) outline the steps to compute the steady-state cell loss probability of the multiplexer once the stationary probability of the multiplexer at each state $(i,\ \underline{m}) \in S(B,\ M,\ \underline{N})$ is found. Equations analogous to (6) to (9) may be developed to compute the transient cell loss probability of the multiplexer once the transient state probability of the multiplexer at each state $(i,\ \underline{m}) \in S(B,\ M,\ \underline{N})$ is known. The cell loss rate predicted by the Exact Algorithm has been compared to simulation output and showed excellent agreement. We will provide an example of the comparison.

APPROXIMATION ALGORITHMS

The number of computations required by the Exact Algorithm is prohibitively excessive when the parameters N_i's are large. To circumvent this difficulty, we formulated three approximation algorithms to estimate the steady-state cell loss rate of the model when N_i is large. The detail of the formulation of those algorithms is omitted here; however, the approximation algorithms are based on the observation that, when N_i is large, the influence of the parameters α_i and β_i on the cell loss rate of the multiplexer is effected through the function $\gamma_i(\alpha_i, \beta_i) \equiv \gamma_i = \frac{\frac{1}{1-\alpha_i}}{\frac{1}{1-\alpha_i} + \frac{1}{1-\beta_i}}$. The three algorithms are referred to as the *Asymptotic Approximation Algorithm*, the *Diffusion Approximation Algorithm*, and the *Approximate Diffusion Approximation Algorithm*. We evaluated the accuracy of the approximation algorithms by comparing their results to those obtained from simulation, and found that the algorithmic results and simulation outputs are in perfect agreement (within noise level). One example of the comparisons is included in the next section. The salient features of the four algorithms are summarized in table 1.

Table 1. Steady-state cell loss estimation algorithms.

	Exact	Asym. Approx.	Diffusion Approx.	Appr. Diffusion Approx.
Time Complexity	$O((B\prod_{i=1}^{M} N_i)^2)$	$O(B^2\prod_{i=1}^{M} N_i)$	$O(B^2\sum_{i=1}^{M} N_iR_i)$	$O(B^2)$
Space Complexity	$O(B\prod_{i=1}^{M} N_i)$	$O(B)$	$O(B)$	$O(B)$
Accuracy	Noise Level	Noise Level	Noise Level	Noise Level

NUMERICAL EXAMPLES

We checked the validity of the algorithms by comparing their results to the outputs of simulation studies. Two of the comparisons are as follows:

Example 1

We selected the following multiplexing scenario to test the validity of the *Exact Algorithm*. The multiplexer parameters are as follows:

- $B = 20$ $C = 27$ $M = 2$
- $N_1 = 2$ $\alpha_1 = 0.2$ $\beta_1 = 0.5$ $R_1 = 20$
- $N_2 = 3$ $\alpha_2 = 0.1$ $\beta_2 = 0.8$ $R_2 = 15$

We constructed a simulation for the same scenario. The simulation estimated the cell loss rate to be 0.082366904, whereas the Algorithm projected the loss rate to be 0.080323504. The relative difference is less than 2.5 percent.

Example 2

We selected the following scenario to test the *Diffusion Approximation Algorithm*.

- B = 20 C = 3556 M = 5
- N_1 = 50 R_1 = 10 γ_1 = 0.6
- N_2 = 50 R_2 = 30 γ_2 = 0.7
- N_3 = 20 R_3 = 20 γ_3 = 0.5
- N_4 = 50 R_4 = 50 γ_4 = 0.3
- N_5 = 3 R_5 = 60 γ_5 = 0.2

Notice that the parameters N_i's are chosen to be large so that certain asymptotic conditions are met. We constructed a simulation of the same scenario. The simulation estimated the cell loss rate to be 0.003015543; the Diffusion Approximation Algorithm predicted the loss rate to be 0.002997045. The relative difference is 0.61 percent, a noise level difference. These comparisons strongly support the validity of the algorithms.

APPLICATION: ATM BUFFER DIMENSIONING

Now we demonstrate how this research may be used to address perhaps the most fundamental problem in designing an ATM network: *buffer dimensioning*. In an ATM statistical multiplexer, a buffer is provided so that cells arriving during a congestion period may be retained. Assuming that cells are transmitted on a first in, first out (FIFO) basis, the queuing delay experienced by a cell ranges from 0 to approximately $\frac{B}{C}$; therefore, the expected delay and delay variation increase as B increases. Since ATM is expected to transport cells that have stringent delay requirements (e.g., short end-to-end delay and small delay variation), it is preferable that the buffer size at a multiplexer of the network is as small as possible. On the other hand, the buffer size must be large enough to smooth out the stochastics of the arriving cells to prevent excessive cell losses. Clearly, the proper choice of B is a tradeoff between the minimizing of the delay variation and the cell loss rate at the multiplexer. A reasonable tradeoff is to select the smallest buffer size, B*, such that the resulting cell loss rate is below an acceptable threshold, μ. This is the buffer dimensioning problem.

Suppose that one wishes to design a multiplexer that is used to transport 200 packetized voice connections. Further, assume that the voice encoder of each connection samples an incoming signal at 8000 samples/sec and that each sample is encoded into an 8-bit unit. A cell is packed with 48 samples. The encoder has a silence detector and therefore would not generate samples during the period that the talker is silent. The expected burst period, the interval during which a talker speaks, is 0.96 seconds; the expected silence period is 1.60 seconds. We assume that the channel may transmit up 15,000 cells/sec. Further assume that a cell loss rate of 10^{-4} at the *multiplexer* suffices to satisfy the cell loss requirement of each connection. What should B* be? Mapping this problem to our multiplexer model, we determine the parameters to be as follows:

- $M = 1 \quad C = 1500 \quad N_1 = 200 \quad R_1 = 17 \quad \alpha_1 = 0.9 \quad \beta_1 = 0.94$.

The smallest value for the parameter B such that the expected loss rate at the multiplexer is less than 10^{-4} is found to be 525.

CONCLUSION

The multiplexer subject to heterogeneous groups of on-off traffic sources (or a close variation of it) is considered to be one of the most general models ever proposed, and is widely regarded as one of the best models for evaluating ATM multiplexing. As far as we were able to determine, there were no closed-form solutions for estimating the expected loss rate of the model. In fact, not even a numerically stable algorithmic solution existed to compute the loss rate. Lacking a satisfactory solution to this problem is one reason why so many basic ATM design issues still have not been resolved. The contribution of this research is the development of numerically stable and accurate algorithms to estimate the transient and steady-state cell loss rates of a faithful ATM statistical multiplexer model. The key drawback of this work is that the solution is algorithmic rather than in closed form. Obtaining a closed-form solution for the expected loss rate of this model appears to be an extraordinarily formidable task.

BIBLIOGRAPHY

Anick, D., D. Mitra, and M. Sondhi. October 1982. “Stochastic Theory of a Data-Handling System with Multiple Sources,” *Bell System Technical Journal*, pp. 1871–1894.

Baiocchi, A. and N. Blefari–Melazzi. December 1993. “An Error-Controlled Approximate Analysis of a Stochastic Fluid Flow Model Applied to an ATM Multiplexer with Heterogeneous ON-OFF Sources,” *IEEE/ACM Transactions on Networking*, vol. 1, no. 6, pp. 628–637.

Cox, D. and H. Miller. 1968. *The Theory of Stochastic Processes*. John Wiley & Sons, Inc.

Elwalid, A. and D. Mitra. June 1993. “Effective Bandwidth of General Markovian Traffic Sources and Admission Control of High-Speed Networks,” *IEEE/ACM Transactions on Networking*, vol. 1, no. 3, pp. 329–343.

Kobayashi, H. and Q. Ren. December 1992. “A Mathematical Theory for Transient Analysis of Communication Networks,” *IEICE Transactions on Communications*, vol. E75–B, no. 12, pp. 1266–1276.

Kosten, L. 1984. “Stochastic Theory of Data Handling Systems with Groups of Multiple Sources,” *Performance of Computer-Communication Systems*, pp. 321–331.

Mitra, D. 1988. “Stochastic Theory of a Fluid Model of Producers and Consumers Coupled by a Buffer,” *Advanced Applied Probability*, vol. 20, pp. 646–676.

Papoulis, A. 1965. *Probability, Random Variables and Stochastic Processes*, McGraw–Hill.

Shum, A. 1994. “Quantitative Performance Evaluation of an ATM-Based Multiplexer.” NRaD TR 1670 (Sep). Naval Command, Control and Ocean Surveillance Center RDT&E Division, San Diego, CA.

Shum, A. 1995. “Discrete-Time Analysis of an ATM Multiplexer.” NRaD TR 1704 (Sep). Naval Command, Control and Ocean Surveillance Center RDT&E Division, San Diego, CA.

Principal Investigator: 0601152N
Allen Shum NRaD ZW96

APPLICATIONS FROM PAST IR/IED PROJECTS

Improvements in Surveillance: IR to the Fleet

In FY 77, a Naval Ocean System Center (NOSC) IR project, Advanced Research in Surveillance (NOSC IR 714009, DTIC 788 518) was undertaken to find ways to improve the product delivered by surveillance information-processing systems. This program provided the initial impetus for NOSC and others to examine the benefits to the ocean surveillance product (OSP) that could be obtained through multisource integration. Mainly through analysis of the Church Pedal experiment, the IR project found that improvements to the OSP could be obtained through cross-sensor correlation of data, through use of currently discarded data, and through cueing of sensors. This IR project transitioned to the Naval Electronics Systems Command (NAVELEX)-sponsored Multisensor Interaction 6.2 project where further algorithmic work was pursued by NOSC and which resulted in the development of the Ocean Surveillance Tracker Correlator (OSTC). OSTC was a testbed for various surveillance multisource integration concepts and algorithms. OSTC led to bringing multisensor integration to the Ocean Surveillance Information System (OSIS) Centers in the mid 1980s via the OSIS Baseline Upgrade (OBU) Program, with TRW as the prime developer. This resulted in VAX-based systems, which were followed in the early 1990s by the Space and Naval Warfare Systems Command (SPAWAR)-sponsored OSIS Evolutionary Development (OED) Program to move the system to a workstation architecture. Currently, INRI, Inc., is involved in further OED work that will result in improved software for the Joint Maritime Command Information System (JMCIS).

Another result of the IR project's analysis of the Church Pedal exercise was the realization that improved usage of electronic intelligence (ELINT) data could contribute to the quality of the OSP. Additional exercises were held in the FY 77–79 time period, including Church Calm and Post Oak, which featured collection and analysis of ELINT data. Also, in FY 79, NOSC initiated an Independent Exploratory Development (IED) project, Ocean Surveillance Information Processing and Modeling (NOSC ZD49, DTIC ICZD 4900), which examined the way sensor data were being processed by OSIS and identified areas in which algorithmic approaches could improve the timeliness and accuracy of the OSP. ELINT was one of the areas identified. Based on these results, the IR project principal investigator developed and tested a statistical ELINT correlation algorithm that became Target Recognition by Extraction of Statistical Attributes (TERESA) under NAVELEX sponsorship in 1981. TERESA has impacted many fleet systems. It was directly incorporated into OBU and later became the basis for ELINT correlation approaches in the Advanced Tactical Workstation (ATW), in the Tomahawk Weapon Control System, in the Naval Tactical Command System–Afloat (NTCS–A), in the Joint Maritime Command Information System (JMCIS), and ultimately in the joint services' Global Command Control System (GCCS).

Contact:
G. Fred Kramer

Lightweight Arrays and Optical Multiplexers: Contributions to Naval Acoustic Sensor Developments

Two separate IR projects, each initiated in the mid-1980s, continue to contribute to various ongoing naval acoustic system developments. One project, which began in FY 85 as “Research for Acoustic Conversion Module” (NOSC ZT27, DTIC DN305016) was motivated by the Principal Investigator’s realization that achievement of higher gains in underwater acoustic arrays could only be obtained if the arrays were made much less expensive and, consequently, lightweight and flexible. This would allow a larger number of hydrophones to achieve higher array gain without incurring unacceptable weight and cost penalties. The IR program demonstrated that array gain could be maintained for flexible arrays through a combination of matched-field processing and innovative self-cohering methods. Weight, cost, and power objectives for this type of array were met by NRaD-developed, low-power analog time-division multiplexing (TDM) techniques, which allowed acoustic information from many sensors to use a single wire. The resulting lightweight, flexible, inexpensive type of array has become known as Slack Line Array technology, and its early applications have been documented previously in NOSC TD 2212.

A second technology impacting current acoustic sensor developments began in the FY 85 IR project, “Optical Properties of Single-Mode, Fiber-Fused, Biconically Tapered Couplers” (NOSC ZT24, DTIC DN305007). This project developed the theoretical modeling and the experimental techniques needed to fabricate reliable and reproducible fused, tapered, single-mode fiber couplers suitable for optical power division and wavelength division multiplexers (WDM). Initial applications of this project have been reported in NOSC TD 1957 and NRaD TD 2723. Work at NRaD on WDM technology continues under the ONR 6.2 Distributed Surveillance Program (NRaD SUBD), where the goal is to decrease the optical channel separation of the PINC WDMs and increase the total number of wavelengths that may be used, thereby increasing the capacity of current fiber-optical links. Additionally, under the ONR 6.3 Common All Optical Towed Array (CAOTA) Manufacturing Science and Technology program, NRaD is developing methods for more economic, automatic, and higher yield manufacture of polarization-independent WDM couplers (PINC WDM).

Both Slack Line Array Technology and WDM are contributing to the development of the Spinnaker Arctic Acoustic System. Spinnaker involves installing an acoustic research system in the Arctic Ocean (under ice) off the coast of northern Canada. It will demonstrate lightweight, low-power, easily deployable, and rugged array components and systems, including a 200-km unrepeatered, fiber-optic telemetry link. This effort is expected to exploit the harsh shallow waters of a unique regional environment and is also targeted for application in other areas. Spinnaker has been developed since the late 1980s by this laboratory under ONR/SPAWAR 6.2/6.3 sponsorship and the Esquimalt Defence Research Detachment (EDRD) under Canadian Chief of Research and Development (CRAD) sponsorship and is scheduled for full system deployment in FY 96. The Spinnaker system deployment will consist of two multi-aperture, distributed, coherent arrays, each connected to shore by a fiber-optic cable deployed by an autonomous underwater vehicle, and recorded and processed in real time. Slack Line Technology is used in the arrays, and PINC WDM couplers are used to create the bidirectional optical link to shore.

Slack Line Technology is also being used in various other projects. The Autonomous Buoyed Environmental (ABE) Sensor System, starting development at NRaD under ONR 6.1/6.2 sponsorship, will use Slack Line developed TDM techniques to minimize weight and power associated with gathering sensor data. ABE will be capable of supporting a customizable suite of sensors, such as conductivity, temperature, depth (CTD), suspended sediment measurements, ambient noise, wave height measurements, etc. ABE will autonomously make measurements for periods up to 1 month, then release a buoy that will radio the data back to shore. Finally, the current ONR-sponsored NRaD 6.2 ULITE development program is extending Slack Line TDM techniques to wider acoustic bandwidth and even lower power electronic-to-optical conversion.

Contacts:

Acoustics
Dr. Newell O. Booth

WDM Technology
Matt McLandrich

Spinnaker
Dr. Barbara J. Sotirin

Slack Line/ULITE
Mark Stevenson

Target Detection and Classification Using Multispectral Infrared Imagery

In FY 91, the Naval Ocean Systems Center (NOSC) initiated the Independent Research (IR) project "Adaptive Image Processing for Target Detection" (NOSC ZW51, DTIC 300155). The object of this project was to develop adaptive algorithms for detecting targets present against natural backgrounds in multispectral infrared imagery. Prior to this project, this problem was generally approached in a nonadaptive fashion, where first, prior estimates were made of target and background statistics, and then detection algorithms were applied to those statistical distributions. The IR project developed adaptive filtering techniques using two-dimensional least mean-square (LMS) noise-canceling to exploit the differences in signatures between the natural background and man-made objects. The signature of natural objects tends to have a higher correlation between spectral bands than man-made objects, thus allowing detections. The adaptive process allowed this type of processing to be effective even when the natural background was nonstationary, as is generally the case.

In FY 93, the IR project transitioned to the Defense Advanced Research Projects Agency (DARPA) Warbreaker Project (NRaD CD36), which applied the algorithms developed in the IR program to infrared and radar imagery. In FY 94, the IR principal investigator continued his studies under the sponsorship of the ONR 6.2 Ocean Surveillance Block Program. In this program, the emphasis shifted from detection to classification by incorporating prior knowledge of the target's and background's infrared multispectral emissivity into the classification process, which heretofore had relied mainly on geometric clues, such as texture, shapes, and edges. This work was pursued through FY 95.

Work is presently continuing under prospective Advanced Research Projects Agency (ARPA) sponsorship. One research direction involves buried target detection through the exploitation of emissivity differences between surface and subsurface constituents. Due to weathering action, the surface emissivity can be quite different for an undisturbed surface than for a surface that has been turned over in the recent past, bringing previously buried material to the surface. Another proposed direction is to examine the tradeoff between processing in the emissivity or the radiance domain. Imagery is collected as spatial multispectral radiance distributions, but differences between target and background are based on differences between their emissivity versus wavelength curves. Further research is needed to clarify whether the adaptive processing is most optimally undertaken in the emissivity or radiance domain.

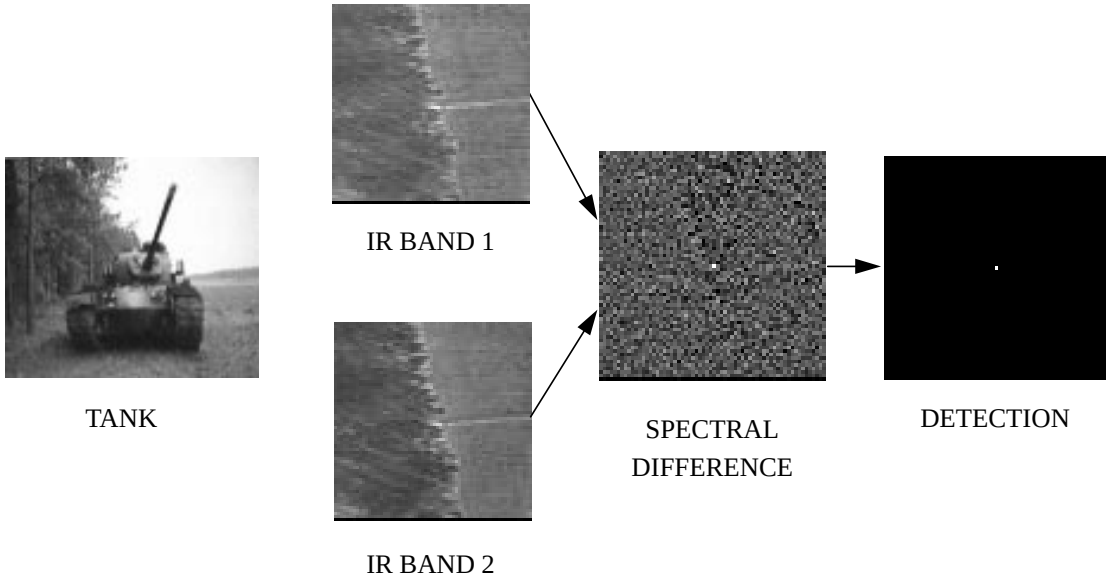

Figure 1. NRaD multispectral processing.

Contact:
L. E. (Skip) Hoff

PROJECT SUMMARIES

COMMAND AND CONTROL

Task Profiling for Heterogeneous Computing

Objective(s). Establish task profiling (code, data, and algorithms) as a methodology of predicting affinities of tasks to various machines and, by extension, to a meta-computer.

Accomplishment(s). Developed methodology, based on the task profiling approach, to predict expected compute times of a heterogeneous queue of tasks on a heterogeneous suite.

A basic probabilistic model was developed that provides a generic multimodal distribution as the expected outcome of executing a code or portion of a code. In this model, it is assumed that flow distribution and branch points can be provided at compile time, e.g., via standard code analysis tools. In addition, at compile time, information can be provided by standard tools, such as FORGE, to give estimates of various machines' behavior on various code portions. At run-time, we derive data size and information on branch point distribution to construct the desired multimodal distribution.

The following experiments were conducted:

a. Analysis of code/machine estimates using FORGE and comparisons with actual results.
b. Comparisons of actual results, on a whole code, by changing branch point probabilities, data size, etc., with expected results, using our model.

Finally, in order to integrate the results of this study into SmartNet, we have derived the concept of a 'rogue' job, which gives the probability of an actual result conforming to a distribution. We use this to estimate both the likelihood that actual results correspond to the expected distribution, or portions thereof, as well as estimates of which branch points were actually taken.

Principal Investigator: 0601152N
Richard Freund NRaD ZU06

Deductive Inference in a Nonmonotonic Logic

Objective(s). Two prerequisites for computers to have "common sense" are (a) relevant knowledge, and (b) sophisticated logic. The goal of this project is to develop a logic that will enable computers to have the "common sense" to recognize when generalizations have exceptions and, thereby, avoid applying those generalizations "blindly."

Accomplishment(s). For the logic under development, it was shown in FY 95 that one can ascertain whether a specified set of premises implies a specified conclusion by solving a collection of linear programming problems. This result will be used in FY 96 to find a deductive calculus for the logic.

In classical logic, the conclusions inferred from premises are guaranteed to be correct. This means that it is impossible for the premises to be true and the conclusions false. However, in many situations where a human being would draw tentative conclusions that have high probability of being correct, classical logic concludes nothing, because none of the potential conclusions are 100-percent certain. What is needed for use in computers is a new logic whereby conclusions need not be certain but do have a high probability of being correct. Because such a logic would occasionally infer incorrect conclusions, it should have the property of "nonmonotonocity." This means that the logic should have the capability of retracting old conclusions when new information casts doubt on them. To accomplish this, the logic would need to be able to recognize exceptions to general rules.

A Bayesian approach is being used to develop the logic. A *possible world* was defined to be a probability distribution over a finite set of events. Each possible world may be represented by a point in *n*-dimensional Euclidean space. A prior distribution, uniform over all possible worlds, was adopted. The statement " If *A* then *B* " was defined to mean that the conditional probability of *B* given *A* is at least $1 - \varepsilon$, where ε is variable. Given any such statement, there is a subset of possible worlds in which the statement is true. Roughly speaking, a set of premise statements was defined to *imply* a conclusion statement if the conclusion statement is true in nearly all possible worlds (as measured by the uniform pair) in which the premise statements are true. It was shown that one can ascertain whether a hypothesized implication is valid by solving a collection of linear programming problems. This result will be used to develop a deductive calculus for the logic. (A candidate deductive calculus has already been formulated but has not yet been shown to be valid.)

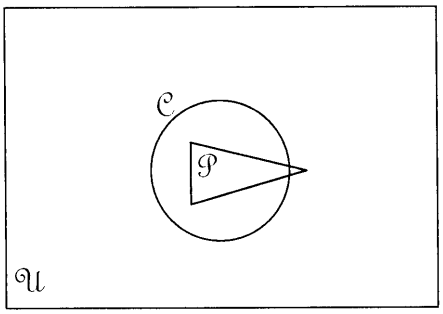

Figure 1. An L. Venn diagram illustrating what it means for a set of premises to imply a conclusion. The rectangle, U*, is the set of all possible worlds. The triangle,* P*, is the set of possible worlds in which the premises are true. The circle,* C*, is the set of possible worlds in which the conclusion is true. Because the conclusion is true in nearly every possible world in which the premises are true, the conclusion is implied by the premises. Thus, in a valid implication, the conclusion has a high probability of being correct but is typically not certain to be correct.*

Principal Investigator: 0601152N
Donald Bamber NRaD ZW84

Generating Software Objects from a Functional Model

Objective(s). Derive a technical method for finding software objects from a functional model.

Accomplishment(s). A technical method, called "Software Object Abstraction (SOA)," has been derived by which one can find software objects by using the information provided by a functional model. This method is derived based on object-oriented theories and the Structured Analysis with Real-Time Extension (SART) method by Hartley and Pirbhai (1988).

This research began when a large program required transition from functional analysis to object-oriented design. Literature searches and discussions with experts in the software engineering field revealed that software objects could not be found from a functional model. After an extensive study, the principal investigator derived the following approach for finding software objects from a functional model.

One must thoroughly understand what information is provided by the functional model, what information is required to build the object model, and how to use the information (from the functional model) to build the object model. Also, one must have an in-depth knowledge of the problem domain. Based on object-oriented theories and functional analysis methods, the principal investigator derived a method, "Software Object Abstraction (SOA)," to find the software objects. An NRaD technical report titled "Abstracting Software Objects from a Functional Model" is being written.

In this technical report, the principal investigator defines a functional model, an object model, what information one may extract from a functional model, and how to use the information to construct an object model. A technical approach is also established to find the attributes, operations, and state models of the software objects. The objects that are found using the SOA method conform to the object-oriented modeling and design approach as advocated by Rumbaugh et al. (1991). In this report, the principal investigator also illustrates the application of the method by finding the software objects from a sample functional software requirements specification given by Shumate and Keller (1992).

At present, the majority of existing embedded defense software systems were developed using structured analysis and design methods. As the systems evolve, there is a need to enhance and rebuild the systems for the purpose of removing uncovered program defects, satisfying the demand of new requirements, improving system capability, and most importantly, utilizing state-of-the-art and more powerful hardware and software. Hence, the Department of the Navy (DoN) advocates the migration from military proprietary hardware to open system architecture.* Yet with the notorious high cost of software development and the long-lead software developmental schedule, redeveloping all existing systems is not feasible. Therefore, we must research ways to reengineer and rebuild our existing

---

*An open system is defined as one that consists of modular, multivendor interoperable, building blocks that are assembled into functional units (Mr. Rex Buddenberg, Chair of Open System Working Group, Government Computing Meeting, 16 February 1991).

software systems that can be hosted in open systems. The first step in this direction is to abstract software objects from the existing functional software system and rebuild the system in reusable component form. This is indeed a difficult task and is the topic of research in software architecture that deals with a family of systems. The research result from this project provides a means of abstracting software objects from an existing functional software specification. This lays the foundation for further research of software reengineering from lower lever artifacts, i.e., existing undesirable design or source codes.

REFERENCES

Hartley, Derek J. and Imtaz A. Pirbhai. 1988. *Strategies for Real-Time System Specification*. Dorset House, New York, NY.

Rumbaugh, J., M. Blaha, W. Premerlani, F. Eddy, and W. Lorensen. 1991. *Object-Oriented Modeling and Design*. Prentice Hall, Englewood Cliffs, NJ.

Shumate, Ken and Marilyn Keller. 1992. *Software Specification and Design: A Disciplined Approach*. John Wiley & Sons, New York, NY.

Principal Investigator: 0601152N
Lydia C. Shen NRaD ZU16

Development and Applications of Relational Event Algebra

Objective(s). (1) Develop a mathematically sound and feasible-to-implement construction technique for the establishment of an event algebra/sample space underlying any of a large class of numerically based input-output probability models—called relational event algebra—extending the previously developed special case of conditional event algebra that treated arithmetic divisions of probabilities as conditional probabilities. (2) Show how this procedure can be used in combining information in a data fusion context to improve present approaches to combining probabilities representing complex system outputs, especially the large-scale ones used to model parts of, or entire, command, control, and communications (C^3) systems.

Accomplishment(s). Extending previous work on conditional event algebra, progress was made in developing the fundamentals of relational event algebra (REA), resulting in an extensive tabulation of explicit formulas for algebraic counterparts for several classes or functions of probabilities, including linear multiple argument forms with possible overlapping events, various polynomial and series forms, and certain nonlinear functions.

The predecessor of relational event algebra (REA), conditional event algebra (CEA), was developed in response to the need for a consistent, rigorous, and sound basis for combining logically conditional expressions compatible with conditional probability evaluations [1]. Unfortunately, at first, there appeared many choices of CEA, but later it was demonstrated that, in general, only one natural choice of CEA exists (figure 1) [2]. This CEA—corresponding to a legitimate probability space—is based upon a countable product probability space construction from the given sample space of unconditional events, as justified through two fundamental characterization theorems improved to a significant extent during FY 95 ([3], section 3.6). In turn, the product-form CEA (denoted for convenience as PS) was shown to provide direct applications to data fusion and C^3 decision-making problems [4, 5].

It was pointed out that CEA addressed actually only a special case of a much larger class of problems: the establishment of a consistent and mathematically sound basis for events that are compatible with given numerical functions of probabilities (CEA corresponding to arithmetic divisions only). This motivated the initial development of an REA based upon PS [6], the main thrust of the FY 95 work. Specifically, an extensive tabulation of explicit formulas for algebraic counterparts for several classes or functions of probabilities was obtained, including linear multiple argument forms with possible overlapping events, various polynomial and series forms, and certain nonlinear functions. A number of preliminary applications of these results was provided for data fusion and combination of evidence problems [7]. Since REA, as developed here, depends upon PS, further determination of properties of the latter impacts directly upon REA. To this end, several additional desirable properties of PS were derived or improved upon during FY 95, including definitive connections with McGee's rational betting scheme approach to CEA, non-monotonic logic and deduction, conditional probability density functions, and previously proposed CEA. All of this is summarized in [3] (see also the special CEA issue of *IEEE Transactions on Systems,* "Man & Cybernetics," for other viewpoints [8] and [9 through 12] for new extensions to conditional fuzzy sets—and hence applications to

conditioning in natural language. Finally, the related topic of determining the measures of central tendency of fuzzy sets was considered in [13].

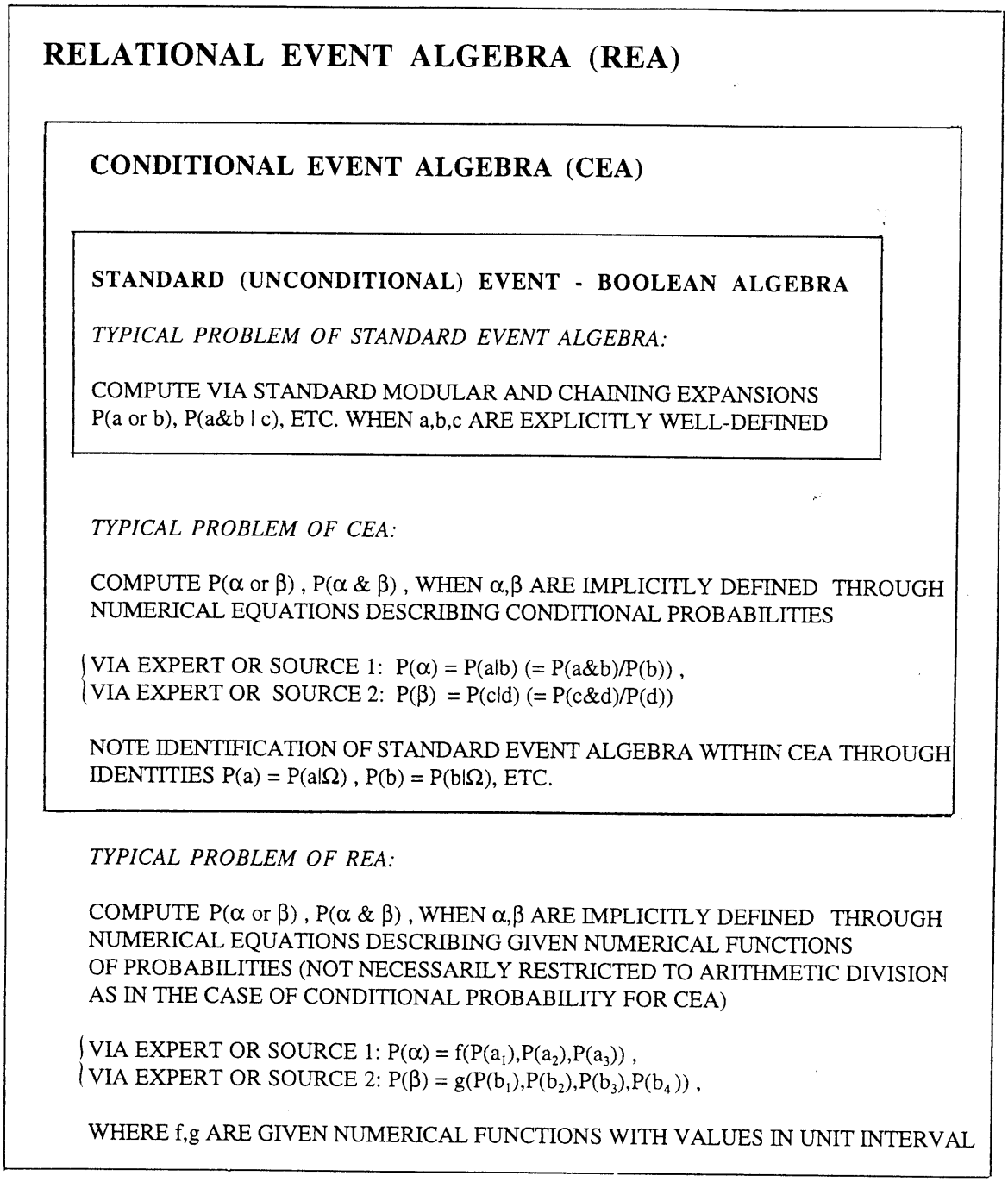

LEGEND: a,b,c,d, a_1,a_2,a_3, b_1,b_2,b_3,b_4 ARE ALL ORDINARY EVENTS, Ω IS UNIVERSAL EVENT, AND P IS A PROBABILITY MEASURE.

Figure 1. Development and applications of relational event algebra. This figure outlines the basic inclusion relations among standard event or Boolean algebra, the more general previously established conditional event algebra, and the much more general relational event algebra, the latter being the subject of this FY 95 NRaD IR project.

REFERENCES

1. Goodman, I. R., H. T. Nguyen, and E. A. Walker. 1991. *Conditional Inference and Logic for Intelligent Systems: A Theory of Measure-Free Conditioning*, Amsterdam, North Holland.

2. Goodman, I. R. December 1994. "Toward a Comprehensive Theory of Linguistic and Probabilistic Evidence: Two New Approaches to Conditional Event Algebra," *IEEE Trans. Sys. Man & Cybern*., vol. 24, no. 12, pp. 1685–1698.

3. Goodman, I. R. and H. T. Nguyen. September 1995. "Mathematical Foundations of Conditionals and Their Probabilistic Assignments," *International Journal of Uncertainty, Fuzziness & Knowledge-Based Systems*, vol. 3. no. 3, pp. 247–339.

4. Goodman, I. R.. 1995. "Use of Relational Event and Conditional Event Algebra in Addressing Modeling and Combining of Information in Expert Systems," *Proceedings of the 11th Conference on AI for Applications in Expert Systems,* IEEE Computer Society Press, Los Alamitos, CA, pp. 270–276.

5. Goodman, I. R. December 1994. "Applications of New Algebras Extending Traditional Probability to Problems of Data Fusion in Command, Control & Information Systems," *Proceedings of the First Workshop in Command, Control & Information Systems Research*, Eynsham Hall, Oxford, U.K., pp. 326–361.

6. Goodman, I. R. 1994. "Relational Event Algebra and Its Applications to the Fusion of Data," *Proceedings of the 7th Joint Service Data Fusion Symposium* (*DFS′94*), APL, Johns Hopkins University, Laurel, MD, pp. 423–437.

7. Goodman, I. R. 1995. "New Results in the Theory and Applications of Relational Event Algebra to the Combination of Evidence Problem," *Proceedings of the 1995 International Symposium on C2 Research & Technology*, National Defense University, Washington, DC, pp. 398–411.

8. Dubois, D., I. R. Goodman, and P. G. Calabrese (guest eds.). December 1994. "Special Issue on Conditional Event Algebra," *IEEE Trans. Sys. Man & Cybern.*, vol. 24, no. 12.

9. Goodman, I. R. 1995. "Conditional Events and Fuzzy Conditional Events Viewed from a Product Probability Space Perspective," in *Fuzzy Logic and Its Applications to Engineering, Information Sciences, and Intelligent Systems*, (Z. Bien & K. C. Min, eds.), Kluwer Publishers, Dordrecht, Netherlands, pp. 287–296.

10. Goodman, I.R.. 1996. "A New Approach to Conditional Fuzzy Sets," submitted to *Advances in Fuzzy Theory & Technology*, vol. IV (P. P. Wang, ed.), Duke University, with extended abstract included in the *Proceedings of the Second Annual Joint Conference on Information Sciences*, Wilmington, NC, pp. 229–232.

11. Goodman, I. R. 1995. "New Results on Conditional Fuzzy Sets and Their Applications," *Proceedings of the 6th International Fuzzy Systems Association World Congress* (*IFSA′95*), vol. I, Sao Paulo, Brazil, pp. 213–216.

12. Goodman, I. R. 1995. "Applications of Random Set Representations of Fuzzy Sets to Determining Measures of Central Tendency," *Advances in Fuzzy Theory & Technology*, vol. III (P. P. Wang, ed.), Duke University, Durham, NC, pp. 99–110.

13. Goodman, I. R. 1995. “Applications of Product Space Algebra of Conditional Events and One-Point Random Set Representations of Fuzzy Sets to the Development of Conditional Fuzzy Sets,” *Fuzzy Sets & Systems*, vol. 69, pp. 257–278.

Principal Investigator: 0601152N
I. R. Goodman NRaD ZU07

Strategy Development in Environments with Incomplete Information for Command Control

Objective(s). Develop and test an algorithm for optimal decision-making when there is incomplete and inaccurate information.

Accomplishment(s). Developed an algorithm combining Bayesian methods and Markov Random Fields to characterize and efficiently search an adversarial tree of possible decisions. This algorithm was shown to be effective in simple decision-making problems and is now being tested on more complex problems.

Typical computer programs used for command and control (C^2) problems are primarily designed to allow a human strategist to understand the large amount of information provided by increasingly more sensitive and abundant sources. Although all this information may be provided to the program, the full fidelity of this information must be reduced to present an understandable picture to a human, who then develops a strategy. Rather than attempt to further reduce and combine relevant information to the point where a human can understand and develop an effective strategy, a method for allowing the computer to use the full fidelity of the information to develop an effective strategy is needed. Computer programs that propose good strategies for solving C^2 problems are the next step in the effort to provide computational tools for solving C^2 problems.

Most of the existing algorithms for strategy development are based on the search of a game tree and are generally tested using parlor games such as chess. Such games differ substantially from most C^2 problems not only in their complexity but also in the information available to the decision-maker. In a game such as chess, the board position accurately provides the decision-maker with the complete information necessary to make the correct move. However, for most C^2 problems, the information available to the decision maker is often erroneous and incomplete. For this reason, decision-making algorithms that have proved very effective in games like chess are typically ineffective for solving C^2 problems.

This work takes a probabilistic approach for developing good strategies for solving C^2 problems. The algorithm assumes that the accuracy of all available information is probabilistically characterized, and that the information from related sources satisfies a Markov property. As before, a game tree search is performed, but now the information is considered optimally using Bayesian methods. In addition, probabilistic calculations are used to optimally select the direction of future searches.

Test results applying this algorithm to several parlor games have been very good. Tests are now underway using a C^2 problem involving scheduling jobs on networks of heterogeneous computers.

Principal Investigator: 0601152N
Mike Gherrity NRaD ZW87

COMMUNICATIONS

Performance Analysis of a Multichannel Adaptive Equalizer for Line-of-Sight (LOS) Digital Radio

Objective(s). Analyze the performance of a multichannel adaptive equalizer for conditions common to the line-of-sight (LOS) communication environment.

Accomplishment(s). Derived and analyzed the performance of the theoretically optimum Wiener solution of a multichannel equalizer operating in the presence of spatially distributed interferers. Developed a new numerical technique of calculating the probability of receiver error under conditions of intersymbol interference and applied this method to accessing the performance of the multichannel equalizer.

The Navy is currently evaluating several possible approaches to provide high-data-rate line-of-sight (LOS) communications among ships. For the LOS environment of interest to the Navy, these communications links will be required to operate in the presence of severe flat and frequency-selective fading and spatially distributed interferers resulting from other traffic, jammers, and from reflections from ship structures. The time-varying spatial and temporal nature of this environment is ideally suited for multichannel adaptive equalization (MAEQ). This technique combines the spatial processing of adaptive narrowband beamforming with the temporal processing of single-channel adaptive equalizers into a single joint spatial-temporal filter. Figure 1 shows the structure that was analyzed. Significant performance improvements have been demonstrated over narrowband beamformers and single-channel adaptive equalizers in a variety of operating environments. The MAEQ consists of M omni-directional, spatially distributed antennas, each followed by a two-sided equalizer and a decision-feedback equalizer. While this type of multichannel equalizer has received increased attention in recent years, little or no analysis has been done on the effect of the combined spatial and temporal characteristics of the MAEQ on its performance in the LOS environment.

There were three main accomplishments of this project in FY 95. First, the steady-state Wiener solution of the MAEQ was derived for simultaneous multipath fading with additive interference. The problem was formulated in a convenient matrix format, and the optimum Wiener weights and minimum mean square error (MMSE) were derived using this formulation. Second, closed-form expressions of the MAEQ Wiener weights and MMSE for the jamming interference case without fading multipath were derived. These expressions are a function of system design parameters such as signal-to-noise ratio (SNR), signal-to-interference ratio (SIR), number of equalizer taps, number of antennas, receiver impulse and frequency responses, and the spatial distribution of the antennas. Then, given design constraints on some of these, the remaining parameters can be chosen to optimize performance. The final accomplishment was the development of a numerically efficient technique for calculating the probability of error of a coherent communication receiver in the presence of intersymbol interference for arbitrary one- and two-dimensional modulation formats. The technique was applied to the MAEQ problem to access system performance.

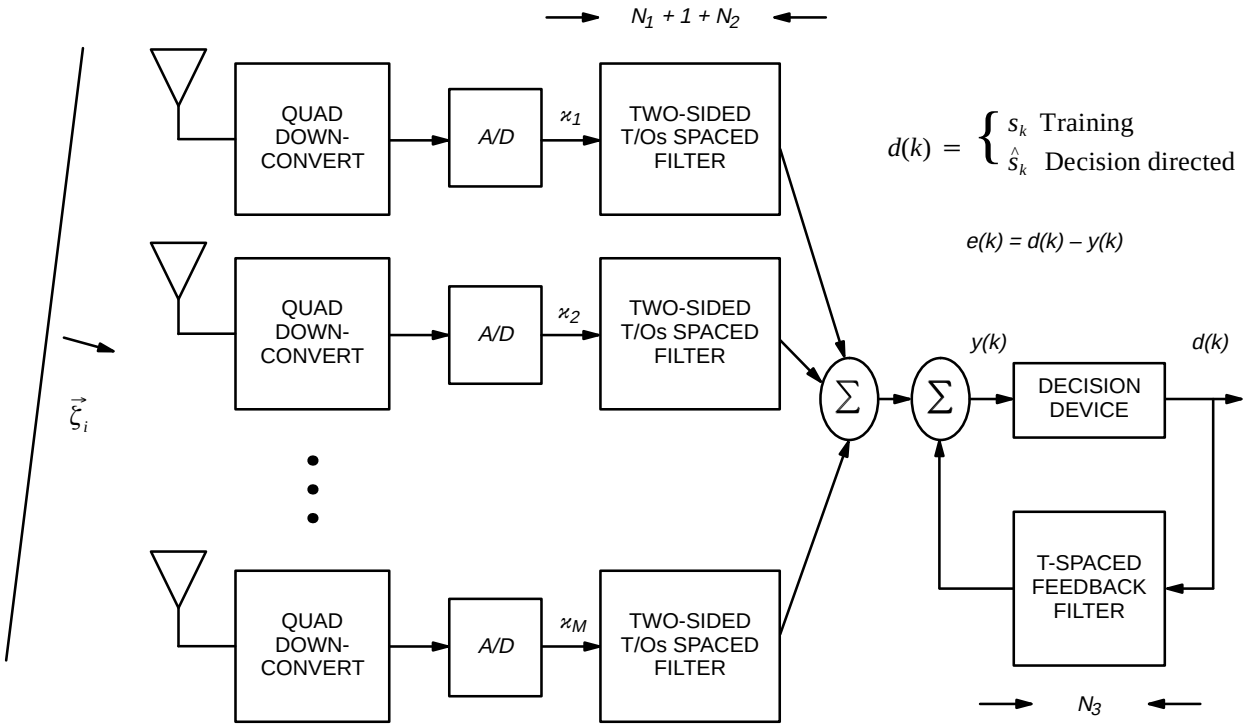

Figure 1. Multichannel adaptive equalizer.

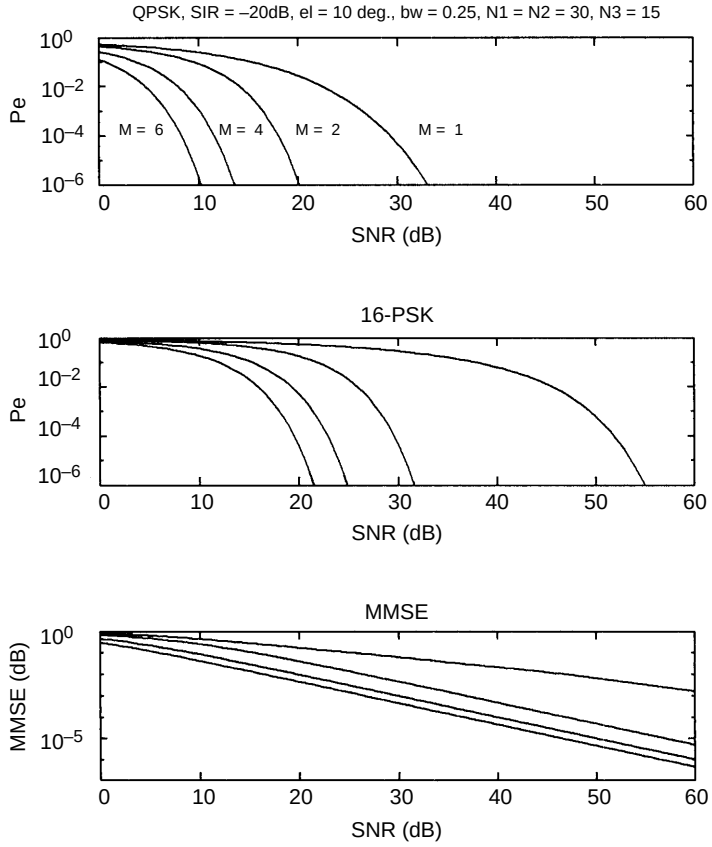

Figure 2. QPSK and 16-PSK for 1, 2, 4, and 6 antennas with an interference elevation angle of 10° and bandwidth of 0.25.

The results derived in this project are useful in relating the system parameters, modulation scheme, probability of error, and MMSE to assist in the design of multichannel receivers for Navy applications. To demonstrate, figure 2 is a plot of probability of error for quadriphase-shift-keyed (QPSK) and 16-phase-shift-keyed (PSK) modulation formats and the corresponding MMSE versus SNR for half-wavelength, equally spaced vertical line arrays with 1, 2, 4, and 6 antennas in which an interferer is arriving with an elevation angle of 10°, normalized bandwidth of 0.25, and SIR = –20 dB. The symbol rate is the same for both formats. For the single antenna case, an unrealistically high SNR is required to meet a probability of error specification of 10^{-6} for 16 PSK. However, there is a dramatic drop in the required SNR by adding just one more antenna. Conversely, there is only a modest improvement in performance between the 4- and 6-antenna arrays due to similar spatial nulling capabilities for this interference arrival angle. These plots also are useful in relating the MMSE to probability of error. For unit variance symbols, a probability of error of 10^{-6} requires an MMSE of approximately 0.040 for QPSK and 0.003 for 16 PSK for all antenna arrays. So, for a proposed modulation format, the system parameters can be chosen so that a certain probability of error design criterion is met for a given interference scenario.

Principal Investigator: 0601152N
Michael Reuter NRaD ZU12

Parameter Optimization for the Asynchronous Transfer Mode (ATM) Leaky Bucket Policing Algorithm

Objective(s). Develop and implement new bounds for the Asynchronous Transfer Mode (ATM) Leaky Bucket (LB) parameters and tabulate them in a manager's lookup table for traffic management.

Accomplishment(s). Developed an exact algorithmic solution for the discrete stationary cell-loss probability for an ON–OFF source queuing model that converges to the square of the Leaky Bucket depth and also validated the algorithm by using a commercial simulation package.

Asynchronous Transfer Mode (ATM) network is an emerging gigabit technology with a premise to transport mixed-mode variable bit-rate traffic on the same link. This is done through packet multiplexed switching that is transported in dynamic tailored permanent and switched virtual circuits. The idea is that a user negotiates a contract based on his needs, i.e., bandwidth on demand. The user will give the traffic descriptors and the network manager will check the resources to find if the link can support additional users or not. Our research should provide the smarts for the network manager during call set-up negotiations to figure the required bandwidth needed and to advise the user that his needs can be met through a certain bandwidth subject to a certain quality of service (QOS). In our context, QOS is the probability that violating cells will be discarded due to either network congestion or the user's violations. To guarantee that the user would not violate his contract by delivering more than he contracted for, there is a policing algorithm called the Leaky Bucket (LB), also known as the Generic Flow Algorithm. This algorithm is a fluid-flow-based model and resembles a credit system. The user is allowed a certain credit that is monitored by a counter. If the incoming traffic is delivered at a rate slower than the constant leak rate, bandwidth (R), the cells will go through. However, if the traffic is delivered at a rate faster than the leak rate, the cells will be stored temporarily in a bucket of a certain bucket depth, (B), subject to the remaining available credit. It is very important to recognize that B is a threshold and therefore is a measure of preemptive control to avoid network congestion. To use the network efficiently, we are faced with the difficult problem that both parameters, R and B, should be small.

The desire to have both parameters, R and B, small is unattainable because of the intricate dependencies R has to be small when B is large and vice versa. Our work illustrated the compromise between R and B subject to a required QOS by testing certain traffic profiles. We approached the problem by making several assumptions. Use an ON–OFF queuing model and identical independent geometrically distributed sources; then the cell-loss probability is a function of the mean parameters of the active and silent periods and the LB parameters R and B. We developed an iterative exact solution for the discrete stationary cell-loss probability as a function R and B and generated curves to illustrate the tradeoff between R and B. Both simulation package and iterative algorithmic model gave close results. The problem with the simulation model is that the convergence rate grows exponentially with the buffer size, B, and the algorithmic model grows to the square of B. For that reason, we are working on a closed-form theoretical equation similar to the analog form developed by Butto et al. (1991) to invert numerically rather than using the convergence methods to find optimum parameters and

bounds. The results will be tabulated that will facilitate admission control by providing an *a priori* knowledge for different traffic sources through a table-lookup.

This research is especially crucial for the Navy because our links are relatively low data rate, and our channels are noisier than the commercial links for which ATM is designed. The dynamic battlefield scenarios of the Navy have atypical traffic descriptors that deserve special attention, and *a priori* knowledge is very important in time-critical-link establishment and utilization efficiency.

REFERENCES

Butto, M., E. Cavallero, and A. Tonietti. April 1991. “Effectiveness of the ‘Leaky Bucket’ Policing Mechanism in ATM Networks,” *IEEE Journal on Selected Areas in Communication*, vol. 9, no. 3, pp. 335–342.

Principal Investigator: 0601152N
Hana A. Abusalem NRaD ZU11

Photonic Frequency Converting Feed Network for Broadband Transmit/Receive Antennas

Objective(s). Demonstrate the capability of using optical signal-mixing techniques for efficiently upconverting and downconverting microwave/millimeter wave (MMW) antenna signals.

Accomplishment(s). Demonstrated record microwave frequency conversion efficiencies using photonic link signal mixing in conjunction with a radio frequency (RF) overdriven optical modulator.

The microwave/millimeter wave (MMW) frequency converting performance of two distinct photonic link signal-mixing systems have been numerically modeled and experimentally verified. One system configuration uses the detected-beat frequency of two solid-state lasers to generate the local oscillator (LO) requirement. The other photonic mixer configuration uses a single solid-state laser and a radio frequency (RF) overdriven optical modulator to generate the LO requirement (figure 1). Each configuration uses an optical modulator with an input low-noise amplifier to introduce the microwave information signal for mixing. The beated-laser and the cascaded-modulator-mixer configurations have been evaluated and compared with the cascaded-modulator configuration and show superior performance in terms of conversion loss, dynamic range, and residual phase noise.

Numerical simulation predicts that mixer conversion losses as low as 6 dB and 4.7 dB are possible for the beated laser and the optimally DC-biased cascaded Mach–Zehnder (M–Z) modulator configurations, respectively. This is an unexpected, but at the same time, welcome result that implies that using an RF overdriven optical modulator to generate the LO can outperform the 100-percent modulation depth-beated-laser approach. Simple Fourier analysis of the resulting optical time domain signals has been used to explain this result. In the laboratory, we have demonstrated a 6-dB conversion loss for the beated-laser approach and a 4.7-dB conversion loss by using the optimally biased series M–Z modulator configuration. Both results agree with theory. By adjusting the DC bias of the M–Z modulator, a conversion loss as low as 3.5 dB has been measured, although this low optical-bias configuration does significantly compromise the overall link RF efficiency and is only useful if excess optical power is available. The only drawback of the series modulator approach is that a high-frequency optical modulator with a low half-wave voltage is required to maintain reasonable LO drive powers. A big advantage of this approach is that no optical phased-locked-loop is required for high-phase stability frequency conversion. Using the cascaded-modulator link configuration with one M–Z modulator and one electroabsorption modulator, a conversion loss of 4.7 dB has been measured along with a projected spurious free dynamic range of 128 dB-$Hz^{4/5}$. These results are impressive and imply that photonic signal mixing can be useful for remote transmit/receive applications up to 50 GHz.

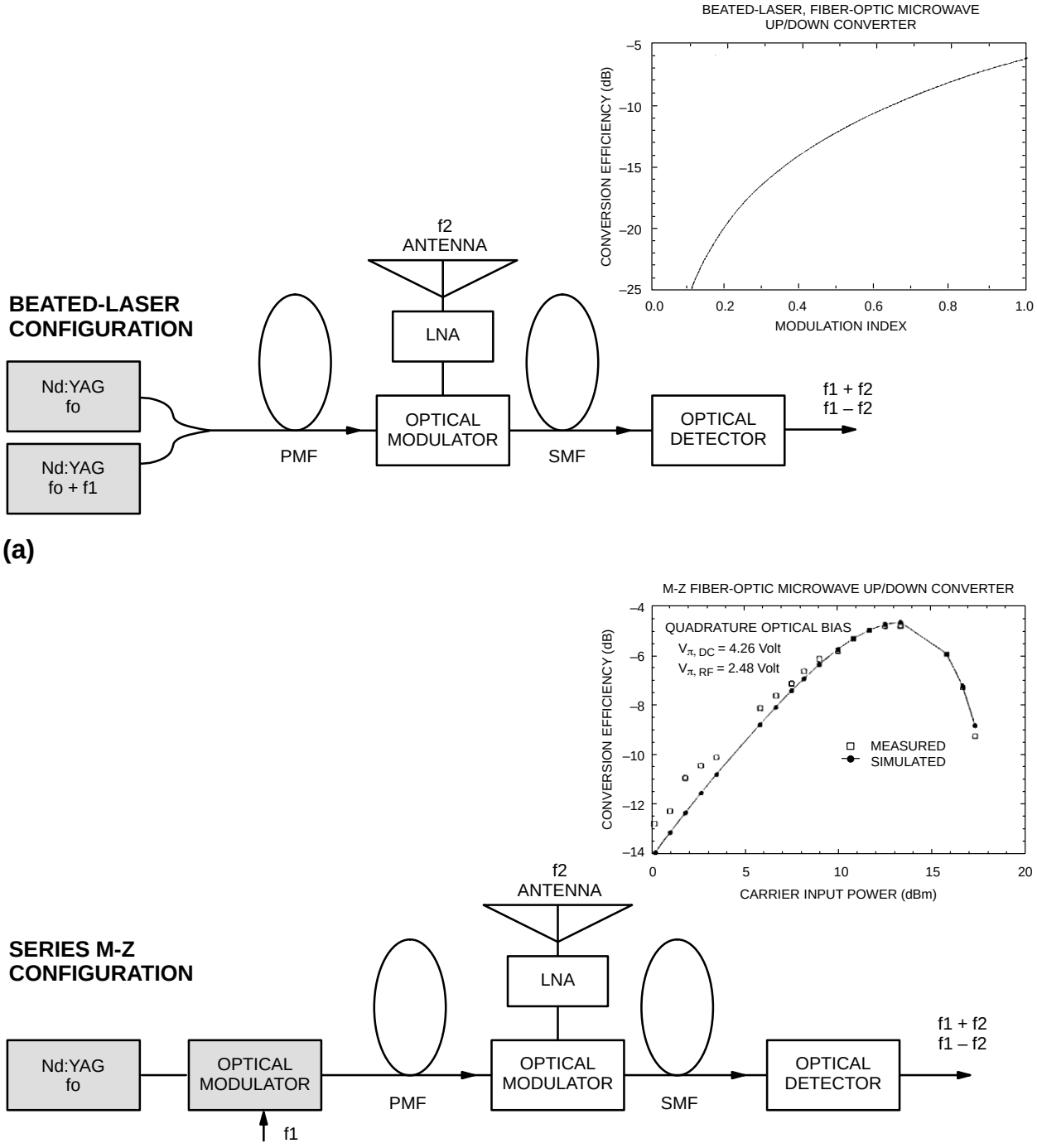

Figure 1. Photonic link signal-mixing configurations along with associated mixer conversion loss for (a) beated-laser and (b) series M–Z modulator approaches.

Principal Investigator: 0601152N
Stephen A. Pappert NRaD ZU10

Near Vertical Incidence Skywave Antenna

Objective(s). Reduce required antenna size particularly for HF communications (2 to 30 MHz) for Near Vertical Incidence Skywave (NVIS) antenna.

Accomplishment(s). Seven spiral antenna models have been fabricated on printed circuit boards; impedance, polarization, and pattern measurements have been initiated; and 10 spiral models have been evaluated using Numerical Electromagnetic Code (NEC) 4.

There is a requirement for a compact, phasable, multioctave, planer, high-efficiency, spiral-mode antenna design that can improve beyond line-of-sight (BLOS) communications in the HF band (2 to 30 MHz). In the past, such designs have experienced problems. In particular, no satisfactory antenna solution has been found to satisfy Near Vertical Incidence Skywave (NVIS) requirements, especially for small mobile platforms (ships, jeeps, etc.) in which the dimensions of the available space are only a small fraction of a wavelength. A new spiral antenna design has been developed as a disclosure to the NRaD Patent Counsel Office by the Principal Investigator for this project. There are three unique features of this design that are relevant to the NVIS problem:

1. a sinuous spiral structure that decreases the phase velocity of the wave as it travels out through the spiral,
2. provision for phasing of the spiral element so that it could be used in a phased array, and
3. reduction of the conducting surfaces of the element (which occupy 50 percent of the surface of a classical conjugate spiral antenna) to a wire outline of the surface.

As a direct result of this NRaD project, NRaD has developed an internal end-to-end capability in the design, fabrication, and testing of printed-circuit antenna models. In particular, a physical design can be specified in *Math Cad* and interfaced to *Tango* (a software program used to compile "gerber" files that are delivered to a printed circuit board fabrication shop). A matching balanced-to-unbalanced (balun) transformer and coaxial cable connector are attached to the finished board. Impedance, pattern, and polarization measurements are taken on the Code 852 pattern range. The range includes a 30-meter-high arch well-suited for the high-angle pattern measurements required for an NVIS antenna. The same physical design developed in *Math Cad* can also be input to NEC 4 for numerical evaluation.

Seven spiral models have been fabricated. Four models are 4-spiral (two have partial or complete sinuous windings, and two have smooth windings differing in the rate at which they open) and three are 8-spiral models (three of the spirals are connected together to one side of the balun, three to the other side, and the two boundary windings float). Because of instrumentation breakdowns on the pattern range with a consequently heavy backlog of scheduled measurements for a number of other sponsored projects, only very preliminary electrical measurements have been taken. These indicate that, for wideband operation, it has not been possible to achieve substantial reductions in spiral size with the sinuous windings, i.e., the outer circumference of the spiral must be somewhat more than 1 wavelength. However, over the lower frequency range where the spiral behaves as a resonant

structure, the sinuous winding does indeed lower the resonant frequencies in accordance with the reduced-phase velocity. Such behavior will be of only limited usefulness in applications where wide-band operation is desired at low frequencies.

Principal Investigator: 0601152N
Willard M. Cronyn NRaD ZU05

Ultra-Wideband Impulse Radio Propagation

Objective(s). Determine whether ultra-wideband impulse radio is feasible for non-line-of-sight communication.

Accomplishment(s). A transmitter, receiver, and antennas were built and numerous measurements taken and analyzed.

Impulse radio refers to an ultra-wideband communication technology that conveys information using pulse-position modulation of nanosecond pulses. The bandwidth is a result of the Gaussian shape of the pulses and the pseudo-random spacing. Typical bandwidths are on the order of 100 percent of center frequency. This gives impulse radio the features of conventional spread-spectrum by using a much simpler technique.

This project is designed to measure propagation characteristics of impulses over a non-line-of-sight path. The VHF band was selected to maximize diffraction while avoiding the environmental noise found in the HF band. The impulse transmitter was designed to operate with a center frequency of 100 MHz with a 100-MHz bandwidth. Impulse generation is accomplished by driving a transistor into avalanche mode. The transmitting antenna is biconical while the receiving antenna is a conical monopole. Signal reception is via a digital-sampling oscilloscope, and samples are downloaded to a computer for analysis. Trigger synchronization is accomplished using a synchronized receiver that detects the impulses and maintains phase lock.

Measurements have been conducted on the NRaD model range and at a seaside cliff area of NRaD. Results have been good for short-range tests (<100 meters) but disappointing for longer ranges. Impulse spreading or flattening due to frequency-dependent group delay did not appear to be a factor in signal degradation. Impulse integrity was maintained even when the propagation path included hills and cliffs. The signal level, however, quickly dropped far below the noise level as the range increased.

Principal Investigator: 0601152N
Jeffrey L. Coleman NRaD ZU01

OCEAN SURVEILLANCE

Matched-Field Tracking

Objective(s). Develop new method for detecting quiet submarines (i.e., diesel-electric on battery power) in shallow water.

Accomplishment(s). An algorithm has been developed that allows coherent processing over a 3- to 5-minute period of time. This provides sufficient processing gain for detection of very quiet targets.

Data are collected for an extended period (approximately 3 to 5 minutes in the underwater case), and a set of covariance matrices are calculated. A new set is generated at approximately 10-second intervals. The Matched-Field Tracking (MFT) algorithm calculates the set of tracks that best correspond to the experimental data set. The algorithm includes the effects of shallow-water, multipath propagation and the spectral content of possible targets.

Advantages of MFT include automatic target detections, low false alarms, and good connectivity. The algorithm collects data in segments and, without operator intervention, generates a list of possible targets. Because this list includes target depth, the identification of submarines is greatly simplified. The false alarm rate tends to be low because of the low output data rate. Obviously a system that produces output every 5 minutes will tend to have a lower false alarm rate than one with a 10-second output schedule. Also, connectivity is good because the low data rate simplifies the connection of the signal processor to associated data networks.

Principal Investigator: 0601152N
Homer Bucker NRaD ZW85

Signal Detection Using Stochastic Resonance

Objective(s). Examine the signal-detection performance of small networks of nonlinear dynamic elements driven by time-periodic signals embedded in Gaussian noise.

Accomplishment(s). Stochastic resonance was found to enhance the signal-detection performance of a single nonlinear dynamic detector when the internal parameters are carefully adjusted. When additional elements are coupled into the array, the performance is further enhanced.

Optimizing the output signal-to-noise ratio (SNR) in nonlinear dynamic systems via the stochastic-resonance (SR) phenomenon has received considerable attention recently. The effects of coupling bistable elements have also been studied from an SR standpoint. However, the study of SR in terms of important signal-processing measures (other than the SNR) has received limited attention. In this project, we considered the signal-detection statistics of arrays of coupled, nonlinear, dynamic elements. We showed that these statistics follow the SNR behavior: They exhibit a maximum as a function of noise (or some other suitable chosen control parameter), and coupling significantly enhances signal detection over what might be achievable with a single element.

We consider a coupled system of bistable elements as simple continuous generalizations of the well-known (discrete) Hopfield neural network elements. The response of a “reference” element to an external time-sinusoidal signal is quantified as the signal detection statistics, probability of detection and probability of false alarm. Gaussian noise (uncorrelated from site-to-site) is assumed to be present in each element. By (numerically) computing the output SNR from the power spectral density of the reference element, we can analytically compute the above statistics to a high degree of accuracy.

The probability of detection is found to exhibit a global maximum at a critical value of the applied noise strength; for these computations, the detection threshold is continuously varied so that the false alarm probability is kept fixed at a predetermined value. When the reference element is coupled into a small array (with the coupling coefficients carefully selected), the detection probability is enhanced. We also compute the Receiver Operating Characteristic (ROC) curves for a single element and a small network. In these curves, one plots the detection probability versus the false alarm probability for continuously changing detection thresholds. Once again, we find that the ROCs display the basic SR effect and that coupling enhances the detector’s performance.

Principal Investigator: 0601152N
Adi Bulsara NRaD ZU03

Acoustic Bottom Interaction Using the Parabolic Equation

Objective(s). Develop theory, algorithms, and a computer code to accurately model the propagation of acoustic energy near the liquid-solid interface, including elastic effects in the solid, using a parabolic equation (PE) framework.

Accomplishment(s). An advanced computer code was developed that can accurately model liquid and viscoelastic acoustic propagation effects with extensive coupling and scattering at interfaces and in the media.

With the U.S. Navy's new focus on shallow-water areas instead of the open ocean, and with modern Navy missions requiring rapid deployment into unpredictable, relatively unknown littoral areas, it has become critical to accurately understand how sensor fields, surveillance systems, and Navy assets should be placed for effective operation in shallow water, and how the shallow-water acoustic environment affects threats to Navy operations (including mines, unfriendly sensors, diesel submarines, and others). Because acoustic energy typically undergoes extensive bottom interaction in shallow-water environments, understanding shallow-water propagation and its impact on deployment and risk requires accurate, high-throughput modeling of acoustic bottom-interaction effects, including scattering, viscoelastic propagation, coupling effects, and others. The near-bottom zone is the most complex acoustic zone in the acoustic propagation domain, but it is critical to understand this zone because mines, sensors, and other warfare assets or threats are very likely to exist near or on the bottom.

This project developed stable finite-element in-plane (2-dimensional) viscoelastic acoustic propagation algorithms and a corresponding computer code to provide accurate modeling of the complex bottom zone. The technique builds on the pioneering work of Michael Collins (M. D. Collins, *Journal of the Acoustical Society of America*, vol. 93, p. 1736, and subsequent work) in using the parabolic equation (PE) approach. The technique includes a split-step Pade matrix approach, stepwise matching interface conditions, energy-conservation and higher order scattering approximations (with out-of-plane scatter corrections), rotated boundary-condition corrections, and recoupling corrections, along with other detailed considerations. The goal has been to produce as accurate a high-throughput model as possible.

The code is written in Fortran-77 compatible code, with some embedded graphics linked to X11-R4 (or higher) implementations. Implementation-dependent graphics or other system-dependent functions are designed with a no-compile option in an attempt to maximize portability. Environmental input is through a preprocessor that produces a high-access-speed database and attempts to compensate for inconsistencies or lack of detailed (or accurate) environmental knowledge. Significant sections of the underlying algorithms can be implemented in parallel if parallel processors are available. The native system implementation is for Solaris™ operating systems.

*Solaris is a trademark of Sun Microsystems, Inc.

Principal Investigator:
Dr. C. David Rees

0601152N
NRaD ZW94

High-Modulation-Rate Tunable Laser

Objective(s). The objective of this program is to produce a laser diode-pumped, solid-state dye laser capable of a modulation frequency of at least 700 kHz.

Accomplishment(s). Modulated pumping of the dye laser produced frequencies of up to 10 MHz, and an all solid-state, diode-pumped dye laser was demonstrated.

The success of this program relies on completing two major tasks. The first is a demonstration that the dye laser is capable of a high modulation rate. To this end, we have modified our existing laser diode-pumped, continuous wave (cw) dye laser to demonstrate amplitude-modulated output using a modulated pump source. Several frequency ranges were investigated. Low repetition rate (up to 3 kHz) pumping was demonstrated by mechanically chopping the cw pump laser. Higher modulation rates (up to 100 kHz) were demonstrated using an acousto-optic modulating crystal to produce a modulated pump beam. A directly modulated laser diode produced pulse modulation rates as high as 10 MHz. The limitation in this case was the modulation capability of the laser diode driver, not the diode itself or the dye laser.

The second major task is to obtain solid-state, dye-laser gain elements that can be used in the modulated dye laser. This task has several components. The first is to identify vendors and obtain samples for evaluation. The important parameters for evaluation are: dye-fluorescence lifetime, spectral emission and absorption bandwidths, aging (dye depletion), fluorescence efficiency, and ability of the dye/matrix pair to produce high-repetition-rate laser output. Once the appropriate dye/host/vendor are identified, an appropriate laser resonator and pump optics can be designed for demonstration. The evaluation step is underway. We have identified both novel modified plastics doped with dyes as well as novel dye-doped sol-gel hosts. A modified PMMA (methyl methacrylate) laser rod doped with rhodamine 700 has been received and is currently being evaluated. A sol-gel host doped with the same rhodamine dye is being prepared for us at the University of California at Los Angeles (UCLA).

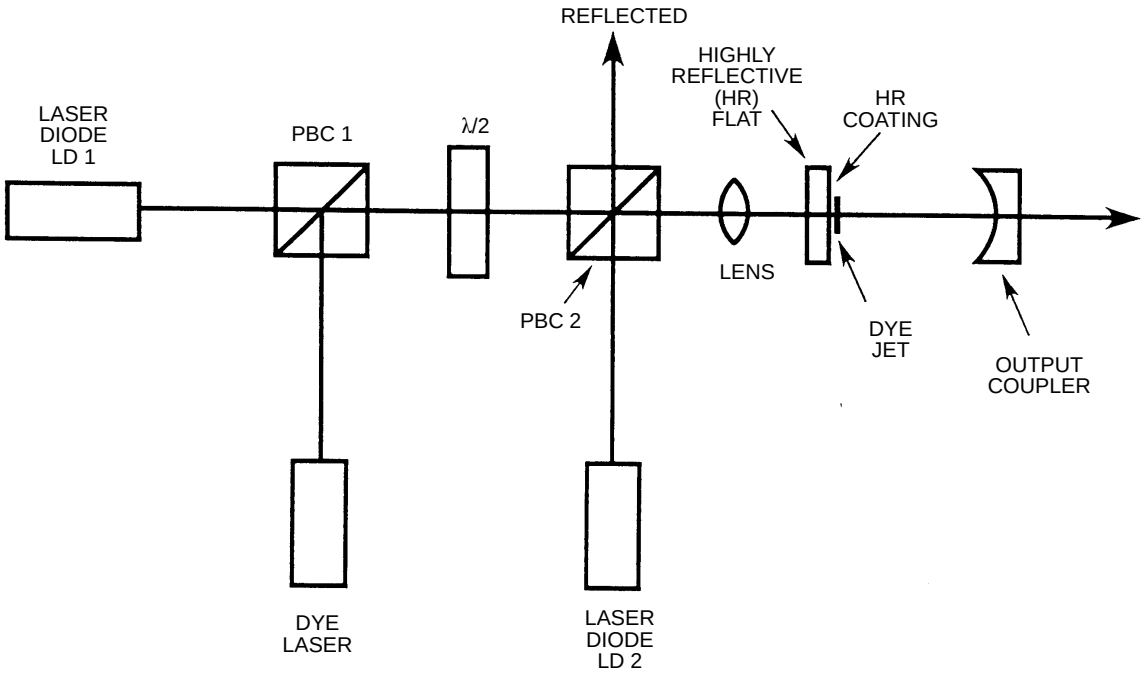

Figure 1. Pump optics and laser resonator configuration. (Polarization beam combiner cubes are labeled PBC.)

Principal Investigator: 0601152N
Richard Scheps NRaD ZU14

Correlations Between Atmospheric Turbulence-Induced Intensity Fluctuations in the Mid- and Long-IR Wavelength Bands for Over-Ocean Propagation Paths

Objective(s). Measure the correlation between the intensity fluctuations, induced by atmospheric turbulence, in the mid- and long-infrared (IR) bands for over-ocean propagation paths.

Accomplishment(s). An instrument has been developed to measure the correlation between intensity fluctuations in the mid- and long-IR bands for a 7-kilometer over-water transmission path.

The intensity of optical radiation propagating through a turbulent atmosphere fluctuates in time about a mean intensity. The objective of this project is to measure the bichromatic correlation between the atmospheric turbulence-induced intensity fluctuations in the mid- and long-IR bands. It was anticipated that the bichromatic correlation data would be useful in developing infrared search and track (IRS&T) algorithms for discriminating between targets and clutter. The program was further justified, from a scientific standpoint, because very few measurements of the bichromatic correlation at any wavelength have been conducted over water.

A dual-band instrument was developed to measure the intensity fluctuations. The transmitter (figure 1) and receiver were both Newtonian telescopes with 20-cm apertures (figure 2). A sandwiched mercury, cadmium, telluride (MCT) and indium antimonide (InSb) detector 3 mm in diameter was located in the focal plane of the telescope. The transmitter was operated over a 7-km over-water path. Bandpass filters were used to measure the crosstalk between the MCT and InSb channels. The crosstalk was minimal. The correlation coefficient between the fluctuations in the two channels was calculated from the experimental data and compared to theoretical predictions. The correlation was high but slightly less than the theoretically predicted value. This discrepancy was attributed to insufficient signal-to-noise in the MCT channel, and additional modifications to the instrument are being considered.

Figure 1. Photograph of transmitter.

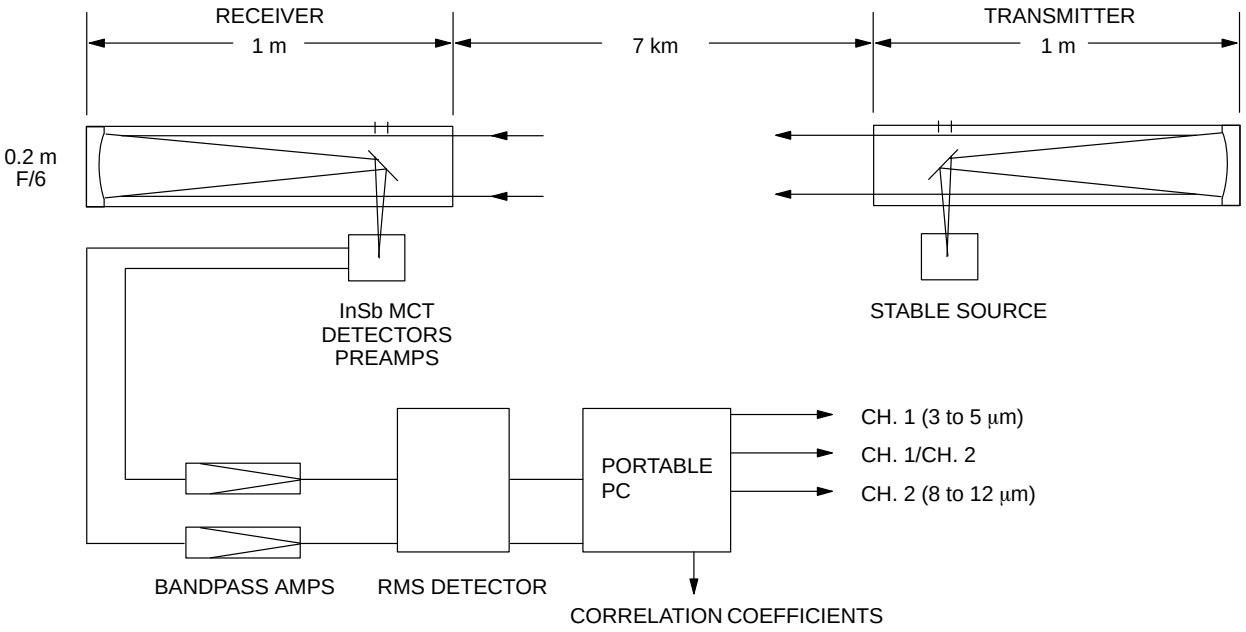

Figure 2. Block diagram of transmitter and receiver.

Principal Investigator:
C. S. (Ike) Bendall

0601152N
NRaD ZU02

The Effects of Benthic Characteristics on Water-Column Optical Properties

Objective(s). The purpose of this project is to examine and characterize benthic processes that may effect water-column optical properties and, thus, impact naval operations in near shore regions.

Accomplishment(s). The main result was to first emphasize that benthic processes do indeed have a very significant impact on the optical properties of the near-shore water column and, second, to begin to quantify what this impact may be. In addition, we suggest how one might take advantage of the knowledge of benthic characteristics to benefit naval operations.

Increased naval operations in regional conflicts have shifted research emphasis from open ocean to coastal areas. Knowledge of coastal processes is required for intelligent operation in near-shore areas. The focus of this project is on benthic or sedimentary processes and how they may impact the optical properties of the near-shore water column and the subsequent naval operations that rely on water clarity. These operations range from optical mine hunting to Navy Seal operations (diving).

Our approach was to characterize the water column and the sediment bed and relate these characteristics to local hydrodynamic and biological processes and to each other. Water-column characteristics include spectral optical properties, suspended sediment concentration and size distribution, and phytoplankton concentration. The sediment bed is characterized in terms of organic fraction, spectral optical reflectivity, density, particle-size distribution, mineralogy, and potential for erosion (critical shear). These measurements were made in conjunction with system tests, including two passive, optical, hyperspectral imagers and an underwater range-gated lidar, all looking for submerged (mine-like) targets. Using such methods, we can directly determine how the understanding of these coastal processes impacts a specific Navy goal.

Principal Investigator: 0601152N
Jon Schoonmaker NRaD ZU15

An Integrated Hybrid Neural Network and Hidden Markov Model Classifier for Sonar Signal Classification

Objective(s). Develop a new scheme for classifying sonar transient signals with strong temporal variability.

Accomplishment(s). Developed a hybrid classifier that jointly uses a neural network and a hidden Markov model for classifying sonar transient signals with strong temporal variability. Formulated a modified Viterbi algorithm to aid in segmenting the observation sequence into a fixed number of states. Demonstrated the hybrid classifier using biologic experimental data.

Classification of underwater targets using nontraditional signals, i.e., acoustic transients, has been a subject of recent interest. Underwater acoustic transients from man-made structures and biologics are very rich in structure and detail, but very diverse in temporal characteristics. The transient classification problem is difficult for the wide intraclass variations due to the large temporal variability. The most common type of classifier used for this task is the neural network (NN). The NNs have been used successfully in classifying such transients, and the success is achieved by using a large number of training exemplars to capture the temporal variations. Recently, the hidden Markov model (HMM) has also been studied for acoustic transient classification due to the inherent time-modeling structure of the HMM. The occurrence of an underwater transient is an acoustic event and is essentially a time-evolving phenomenon. The HMM can easily handle the wide range of temporal variability associated with such phenomenon. On the other hand, the NN is a very powerful classifier for static patterns, i.e., patterns with very little or no temporal variability. In other words, if there is wide temporal variability in the signal, the HMM is likely to perform better; if the signal presents itself as a static pattern, the NN is likely to perform better. In this study, a hybrid classifier is developed. The hybrid classifier incorporates the advantages of both the HMM and the NN classifiers in one single classifier, i.e., one classifier that is able to handle wide temporal variability as well as to provide strong interclass discriminative power.

In the hybrid classification scheme, the HMM, implemented by a modified Viterbi algorithm, is first used to segment the observation sequence belonging to every exemplar into a fixed number of states. After this segmentation, all the frames belonging to the same state are replaced by one average frame. Thus, every exemplar, irrespective of its time-scale variation, is transformed into a fixed number of frames, i.e., a static pattern. The NN is then used as the classifier for these time-normalized exemplars. Experimental results using biological data have demonstrated that the hybrid classifier has less demand for training data and yet is able to achieve a high recognition rate when compared to that of a stand-alone NN classifier.

Principal Investigator: 0601152N
George Chen NRaD ZU04

Environmentally Adaptive Radar Waveforms

Objective(s). Model the physics of low-altitude radio frequency (RF) electromagnetic propagation and surface clutter in range-dependent littoral environments and develop waveforms and signal processing to allow for improved sensor and combat system performance via adaptation to synoptic conditions. Adaptation would entail design of RF waveforms for use in the remote sensing of the propagation environment to allow for improved sensor and combat system performance via adaptation to synoptic conditions.

Accomplishment(s). In FY 95, computer simulations began on focused wave mode (FWM)-type waveforms in marine refractivity ducts using an electromagnetic parabolic-wave equation model. Validation of this model was accomplished by independent calculations using Sommerfeld-type wave models for mixed (Robin)-type boundary conditions, and by comparison with exact geometric and uniform theory of diffraction calculations for wedge diffraction models in collaboration with Applied Research Lab, University of Texas. Propagation simulations of low-altitude (e.g., 3 to 10 m) targets in range-dependent surface ducts characteristic of marine environments have shown substantial improvement in target illumination over conventional types of transmit waveforms. The FWM pulse involves spatial aperture shading based upon matching dominant propagation modes in ducts. This technique was based upon a hypothesized or known refractive environment. A method has been proposed with D. Boyer, Naval Surface Warfare Center, Dahlgren Division (NSWCDD), to do passive remote sensing using matched-field-type algorithms (using an existing forward propagation model based upon the parabolic equation [PE] method). The target illumination calculations were based upon a smooth-sea-surface model and did not include noise due to surface back scatter or clutter. To remedy this, development was started on a PE-based sea-surface clutter model using multiple forward-scatter, single back-scatter theory, and a realistic sea-surface, gravity-wave spectrum (Toba) for horizontally polarized signals.

Low observable targets, such as cruise missiles, flying at low altitudes are difficult to detect at long ranges, and place increasing demands on shipboard weapon and fire-control systems. The propagation and clutter environment, as sensed by shipboard radar sensors, limits system detection and tracking effectiveness and, thereby, degrades reliable weapon delivery. The propagation and clutter seen by sensors is highly variable spatially and temporally, but current sensors are optimized to operate based upon static environmental assumptions.

The problem is both one of obtaining sufficient target illumination at long range and of detecting a small radar cross-section target echo against strong surface clutter. The target detection problem is often compounded by atmospheric environmental conditions that increase anomalous propagation effects. In marine environments or over land, spatial gradients of temperature or humidity often exist near the surface. These gradients produce local extrema in the index of refraction profile, called surface ducts, that can channel or trap electromagnetic energy. Detailed measurements of near-grazing incidence propagation and clutter display large variations with respect to frequency, target and sensor altitude, target bearing, and time.

Usually, the presence of a surface duct is viewed as being deleterious to radar system performance because the resultant propagation conditions are often complex and vary dramatically with the local environmental conditions. However, instead of viewing anomalous propagation as simply a detriment to system performance, one could adopt the approach of trying to mitigate or even exploit the environmental effects to improve system performance. In fact, it may be feasible to design waveforms that can probe or remote-sense the propagation conditions surrounding a ship or transmit environmentally adaptive radar pulses that reduce surface clutter.

Principal Investigator: 0601152N
Frank J. Ryan NRaD ZU13

Robust Adaptive Locally Optimal Detection

Objective(s). Develop robust implementations of the locally optimal detection statistic based on Gaussian mixture noise densities.

Accomplishment(s). Implementations of this algorithm were developed that improve the detection performance in sea clutter by 10 or more dB.

The detection of random signals, e.g., signals for which the phase is incoherent from sample to sample or not modeled, due perhaps to the desirability of a simpler surveillance system, is often accomplished with the power detector

$$\mathcal{G}(z) = \sum_{i=1}^{n} \frac{-2}{\sigma^2} + \frac{\|(z_i)\|^2}{\sigma^4},$$

where σ^2 is an estimate of the noise variance. The power detector is the locally optimal detector of zero mean signals in Gaussian noise. In multiple target or nonhomogeneous noise backgrounds, this is implemented using a constant false alarm rate (CFAR) processor to estimate σ. To make detection decisions, the statistic, with σ varying to accommodate fluctuations in the noise power, is compared to a fixed threshold that depends upon the desired false alarm probability.

An alternate approach is to use a non-Gaussian statistical model of the clutter to derive detection algorithms. Earlier work (reference 1) shows that the locally optimal detector in exponential mixture noise offers significant performance improvement if the parameter values are known. In nonstationary environments, parameters estimated from nearby data may not be sufficiently close to the parameters of the noise-only component of the test data to achieve the potential gain of the exponential mixture detectors. In related work for the advanced periscope detection program, exponential mixture densities are shown to provide good fits to sea clutter; however, the values of the parameters are uncertain due to the spatial and temporal inhomogeneity of the noise. One approach explored here for developing a robust processor is to assume that each parameter is in a known interval and to use the exponential mixture processor that minimizes the maximum false alarm rate for noise densities having parameters within these intervals. A less computationally intensive algorithm uses percentiles of the parameters calculated from bins near the test bin.

To date, the order statistic algorithm has been compared on a limited set of data with a CFAR algorithm. Figure 1 shows the intensity of data that consists of sea clutter returns to which a synthetic target was added. The intensity peaks are too numerous and too high for the Gaussian model to accurately describe these data, and the data are not spatially uniform. Figure 2 shows the output of a CFAR processor, and figure 3 shows the output of the order statistic exponential mixture detector. The CFAR detector could not detect the signal in these data without producing an unacceptable number of false alarms. However, the order statistic mixture detector produces no false alarms with the threshold set above the level corresponding to a PFA of 10^{-4}, and the signal, initially in range bin 100, is detected at thresholds having a PFA of 10^{-8} or less.

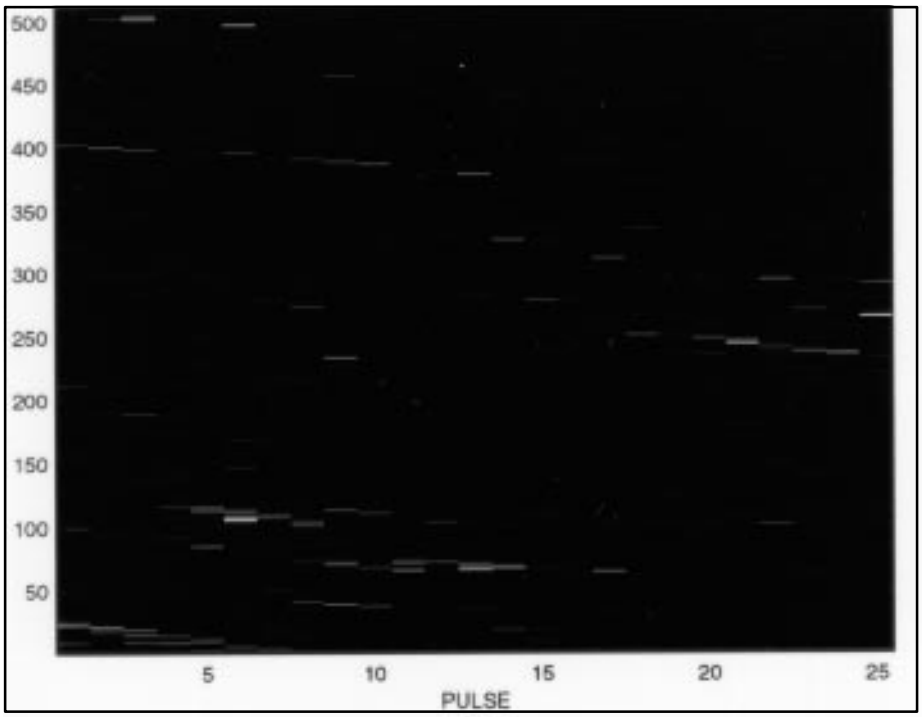

Figure 1. Intensity of the data input to the processors.

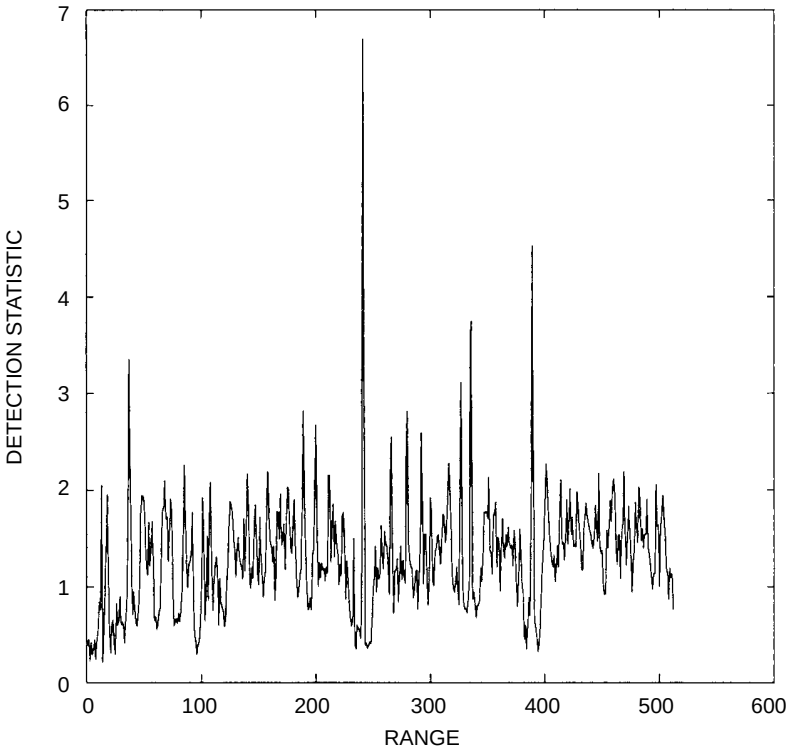

Figure 2. The output of a CFAR processor.

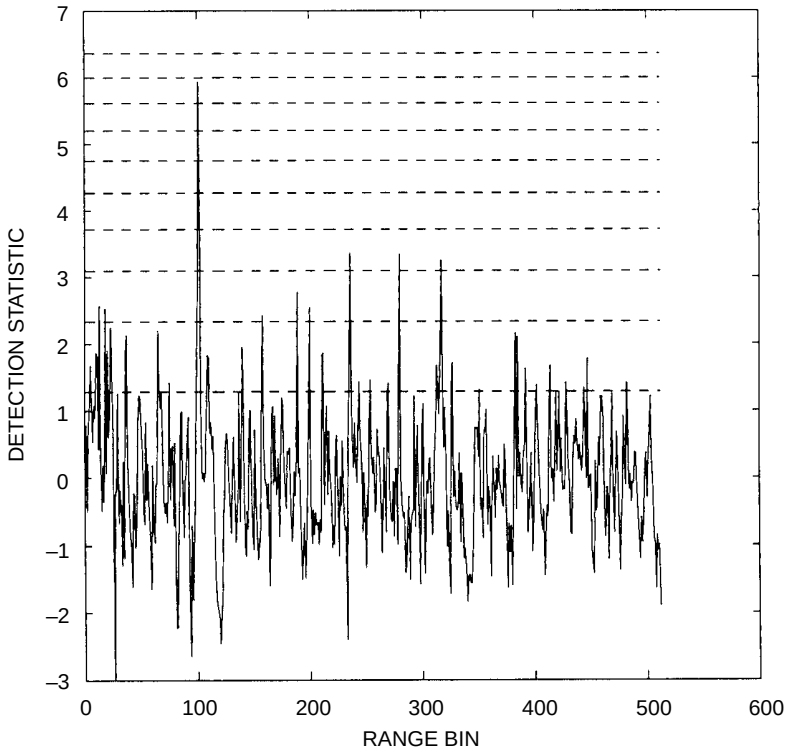

Figure 3. The output of the order statistic parameter selector mixture processor.

REFERENCE

1. D. W. J. Stein, November 1995. “Detection of Random Signals in Gaussian Mixture Noise,” *IEEE Transactions on Information Theory,* pp. 1788–1801.

Principal Investigator: 0601152N
David Stein NRaD ZW98

MULTIMISSION RESEARCH

Measurement and Prediction of Sediment Assimilation Capacity

Objective(s). Develop a model to relate chemical sorption processes to toxicity and bioaccumulation.

Accomplishment(s). A kinetic nonequilibrium model was developed to relate thermodynamic and mechanistic chemical sorption processes to bioavailability and toxicity for laboratory testing.

A theoretical kinetic nonequilibrium model was developed to relate thermodynamic and mechanistic chemical sorption processes to bioavailability and toxicity for laboratory testing. A literature review was completed to corroborate the modeling approach. The development of a sediment column test system was initiated to conduct column breakthrough studies to test and validate the modeling framework and provide samples for toxicity testing and chemical analysis.

A bioluminescent bioassay system (QwikLite) was evaluated to test the toxicity of effluent fractions generated from column breakthrough studies by measuring the amount of light reduction in the dinoflagellate (*Gonyaulax polyedra*) as a function of exposure to fluoranthene and phenanthrene. A reference toxicant, sodium dodecyl sulfate (SDS), was used to evaluate the sensitivity of the QwikLite assay to other short-term chronic toxicity tests developed for saltwater species. The light reduction in *Gonyaulax polyedra* was more sensitive to SDS than mysid shrimp (*Mysidopsis bahia*) survival; similar in sensitivity to sea urchin (*Arbacia punctulata*) fertilization and sheepshead minnow (*Cyprinodon variegatus*) larvae survival; and less sensitive than red macroalga (*Champia parvula*) sexual reproduction and silverside (*Menidia beryllina*) larvae survival. A logistic exposure-response model was fitted to describe the relationships observed between bioluminescent light reduction and fluoranthene and phenanthrene exposure. The exposure-response model can be used to characterize the potential for ecological effects from fractions eluted from the sediment column test system.

Principal Investigator: 0601152N
Bob Johnston NRaD ZU08

Bioluminescent Signatures of Underwater Bodies

Objective(s). Investigate whether the flow-induced stimulation of naturally occurring luminescent plankton can be effectively used as a method of flow visualization in both laboratory and field studies.

Accomplishment(s). The response of unialgal cultures and naturally occurring mixed assemblages (which were composed primarily of combinations of the unialgal cultures studied) of bioluminescent dinoflagellates to quantified levels of hydrodynamic shear stress have been compared through a series of pipe flow experiments. Excellent agreement has been found. The results have important ramifications towards inferring flow characteristics from bioluminescent observations.

Observations of bioluminescence, often anecdotal or indirect, have been used to infer hydrodynamic properties of the stimulating flow field. For example, it has been previously thought that turbulent flow is necessary for significant stimulation of bioluminescence. This hypothesis has been assessed in the present study by measuring the response of luminescent marine plankton to quantifiable hydrodynamic stimuli using laminar and turbulent pipe flow. The response threshold occurred in laminar flow at a wall-shear stress value of approximately 1 dyn cm^{-2}. For wall-shear stress values > 10 dyn cm^{-2}, the maximum intensity of individual bioluminescent flashes was nearly constant, regardless of whether the flow was laminar or turbulent.

These findings have important ramifications towards inferring flow characteristics from bioluminescent observations. The presence of flow-stimulated bioluminescence can no longer be used as an unambiguous indicator for turbulent flow. However, this does not necessarily preclude the use of bioluminescence as an effective tool for flow visualization. Turbulent flow may still result in increased bioluminescence by stimulating more luminescent organisms through its thicker boundary layer, increased mixing, and greater rates of entrainment. We have demonstrated in the laboratory that this occurs by using axisymmetric models towed through a tank of the bioluminescent dinoflagellate, *Gonyaulax polydra*. Furthermore, it appears that once calibrated (for example, through pipe flow experiments), luminescent plankton could be potentially effective as flow markers that could trace fluid pathlines in complicated flow geometries, and mark the boundaries of turbulence, or the area of entrainment.

Estimates of shear stress along a 6:1 ellipsoid indicate that at 2 m/s (typical dolphin cruising speed), levels were above threshold values of 1 dyn cm^{-2} along most of the body. However, anecdotal observations of flow-induced bioluminescence on swimming dolphins often note a lack of stimulated bioluminescence along the entire dolphin. As shown in figure 1, given sufficient numbers of luminescent organisms, dolphins can cause significant bioluminescent displays.

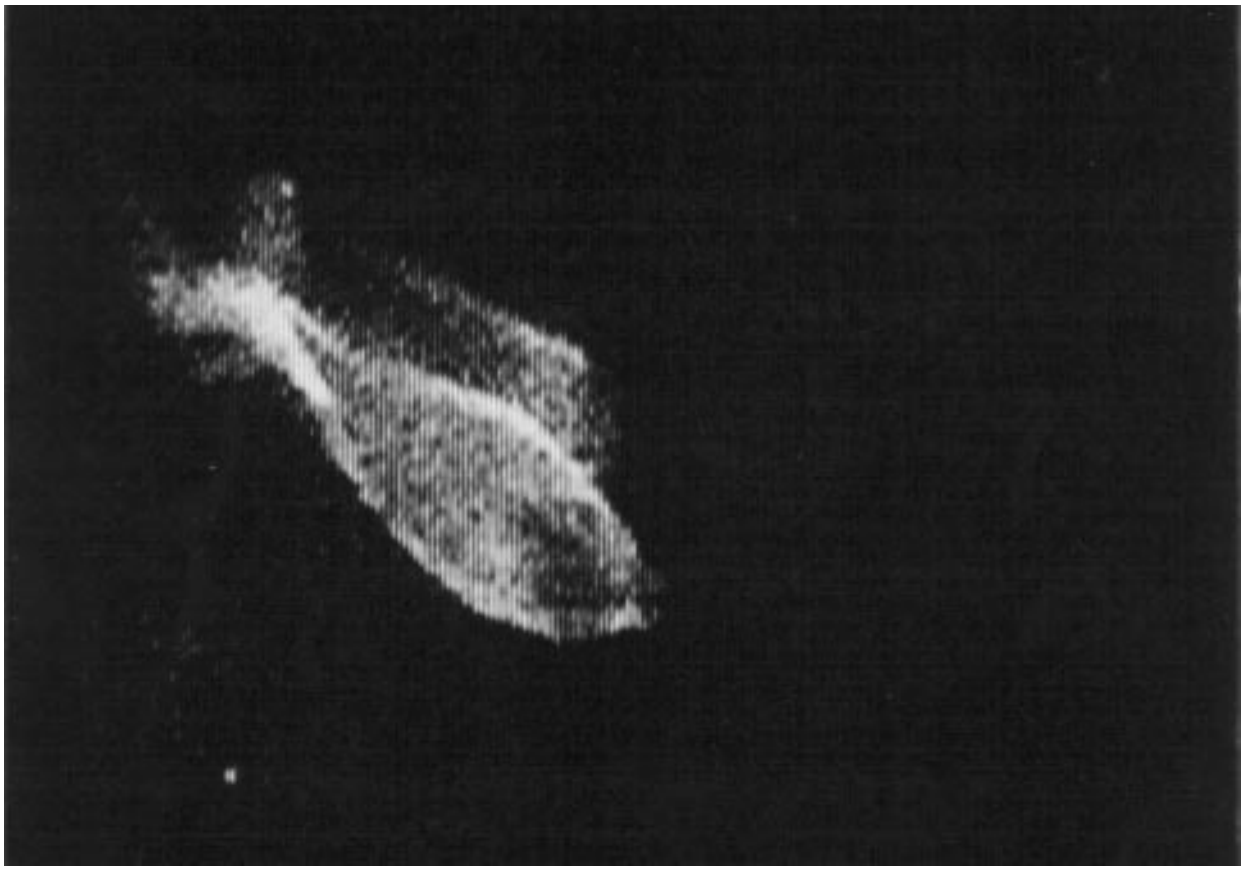

Figure 1. Dolphin (Tursiops truncatus) swimming (≈ 2 kn) along boat during red-tide conditions.

Principal Investigator: 0601152N
Jim Rohr NRaD ZW77

Tidal Dispersion Mechanisms in a Coastal Embayment

Objective(s). Identify and quantify processes that are responsible for the dispersion of natural and anthropogenic substances in a tidally influenced coastal embayment.

Accomplishment(s). Reviewed existing literature, developed one-dimensional scaling model of dispersion mechanisms, formulated experimental design for field experiments, successfully performed field experiments at five locations in San Diego Bay, performed data reduction and analysis of field data, quantified dispersion mechanisms at study sites, performed model simulations using a two-dimensional finite difference model (TRIM), compared modeling results to field results at selected stations.

The Navy must provide an uncompromised level of defense capability without undue stress on the shoreline and marine environment. This issue is especially acute in coastal estuaries and embayments such as San Diego Bay, where the impact of large numbers of Navy ships, submarines, support craft, and shoreside facilities must be balanced against a background of ecological, recreational, and aesthetic conservation. Since zero discharge is not technically possible, the question inevitably becomes at what level can wastes be assimilated by the coastal ocean, and from a scientific perspective what are the fundamental processes that determine the fate of these substances? The first step toward answering these questions lies in understanding the mechanisms, interactions, and scales of motion that control circulation and mixing in estuaries.

For a tidally driven system, it has been hypothesized that large-scale circulation and turbulence features that lead to enhanced mixing are generated primarily by mechanisms associated with the topography of the embayment. These mechanisms include shear dispersion, tidal trapping, and tidal pumping. In San Diego Bay, as in most systems, areas exist where all of these processes may be active and, thus, this system provides an accessible, representative, field-scale model on which we can test these hypotheses. The ability to perform field observations on the time and spacial scales required to resolve these mixing processes is largely due to the recent development of sophisticated current and hydrographic mapping technologies. This includes instrumentation such as the Acoustic Doppler Current Profiler (ADCP) that allows rapid, accurate, underway measurement of water velocities through the entire water column; fast-response, reliable towed conductivity, temperature and depth (CTD) systems; and high-resolution Global Positioning System (GPS) navigation and tracking devices. This unique technological capability provides the basis for significant advancement in the understanding of field-scale estuarine circulation processes.

During FY 94, we developed a simple scaling model to highlight areas where specific mixing processes might be important in San Diego Bay. The results of this scaling indicate that:

1. Shear dispersion has limited influence in most of the bay due to the long time scale for transverse mixing and short time scale of vertical mixing compared to tidal period.
2. Tidal trapping may be a significant mechanism, especially in the outer bay near Shelter Island/ Harbor Island, where velocities are high and trap volumes are significant.

3. Tidal pumping is probably the dominant mixing mechanism in much of the bay due to horizontal expansions and contractions.

Vertical residual circulation is thought to be small due to limited stratification. The results are in general agreement with recent observations of longitudinal salinity gradients.

Based on these results, field experiments were designed and carried out at five locations in San Diego Bay. During each experiment, cross-sectional and axial variations in flow, tracer concentrations, and hydrographic characteristics were measured using the instrumentation described above. The field experiments were completed during the fourth quarter of FY 94. Preliminary analysis of the field data suggested that:

1. Dispersion and transport near the mouth of the bay is dominated by the time-dependent variations associated with the tidal pumping process, with second-order effects due to vertical and lateral residual circulation.
2. Sections deeper within the bay are more strongly influenced by lateral residual circulation, and by tidal trapping effects due to side basins.

During FY 95, data analysis was completed, and numerical simulations were performed using a high-resolution, two-dimensional model of the bay. From the field measurements, variations in longitudinal dispersion, net tidal exchange, and bay residence times were resolved at the five study sections. Strongest dispersion ($\sim$260 m^2 s^{-1}) was measured at the mouth station where time-dependent variations associated with the tidal pumping process dominated the tidal exchange. The tidal exchange ratio at the mouth (percent of ocean water entering the bay on flood tide) was measured to be $\sim$40 percent, leading to an overall residual time for the bay of about 6 days (based on time required for reduction to 1/e of starting concentration). Weakest dispersion (approximately 30 to 70 m^2 s^{-1}) was found at the Shelter Island and Harbor Island sites located 5 to 7 km inside the bay. At these sections, tidal residual transport, shear dispersion, and time-dependent variations all contributed substantially to the net transport (figure 1). Tidal exchange ratios at these two sections ranged from about 10 percent at Shelter Island, to about 6 percent at Harbor Island, with corresponding residence times of 20 and 35 days for the regions of the bay beyond these sections. Dispersion levels were found to rise again at the sections near the Coronado Bridge to a range between the other study regions (approximately 60 to 160 m^2 s^{-1}). Transport in this region of topographical expansion was again dominated by time-dependent variations associated with the tidal pumping and trapping processes. Tidal exchange ratios in this region were similar for both sections at 4 to 5 percent giving estimated residence times for the inner bay of close to 40 days. Concentration differences between the start and end of the tide cycle suggested that variations with periods longer than the M2 time (12.4 hours) may also contribute significantly to the transport.

Model simulations using TRIM were performed to allow comparison to cross-sectional flow, tracer, and transport measurements from the field. The tidal flow was found to be well-represented by the model except at the mouth section where modeled flows generally exceeded measured flows by about 20 percent. This discrepancy was partially attributed to leakage across/over the rock jetty on the eastern channel boundary. Tidal variations in concentration were more poorly resolved, possibly due to difficulties in establishing similar initial distributions in the contaminant distributions between the model and the field. Tidal exchange ratios estimated from the model followed a similar trend as the

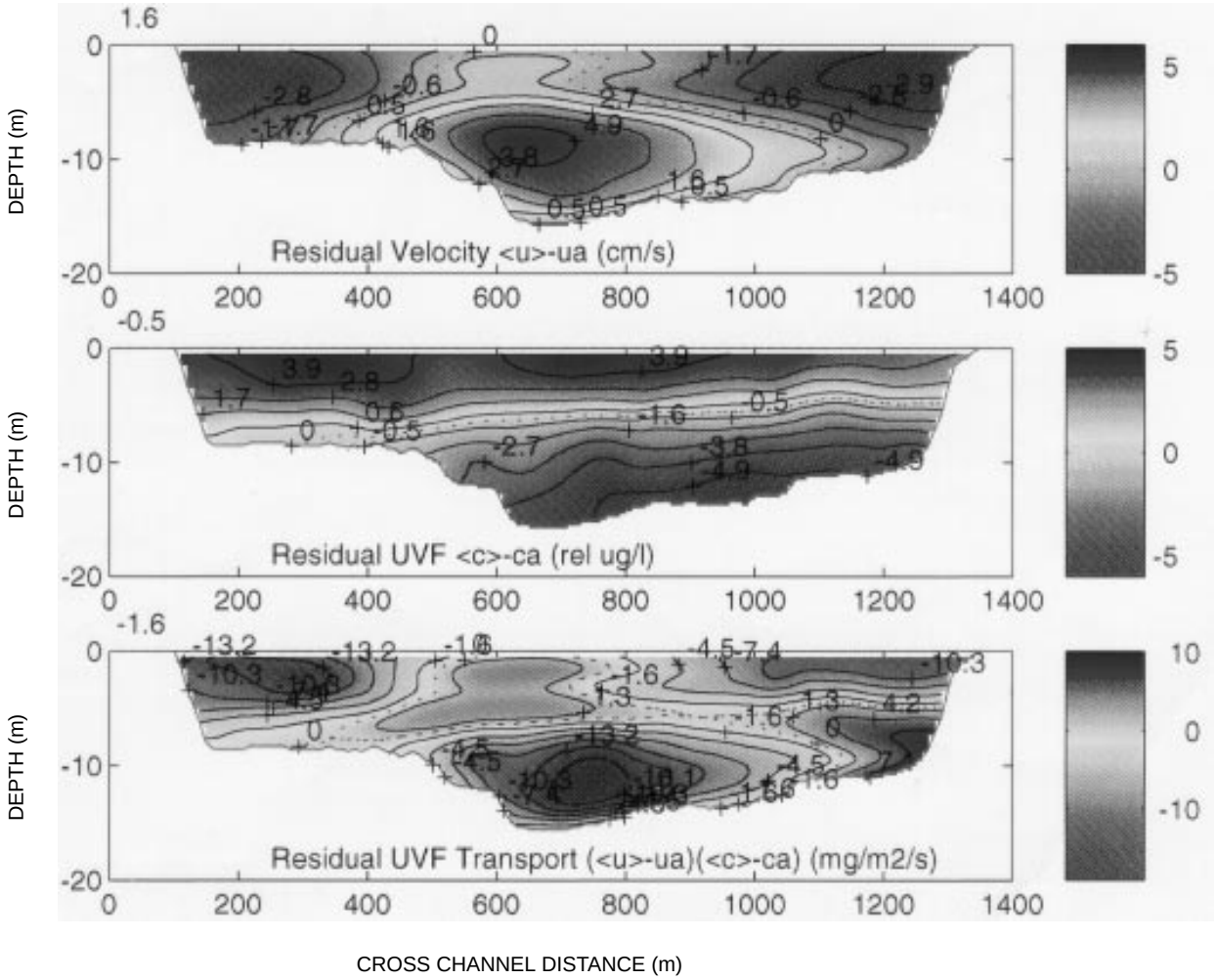

Figure 1. Cross-sectional structure of the tidally averaged residual circulation, fluorescence concentration, and transport at the Harbor Island site. The spatial correlation of the vertical variations in flow and concentration lead to a substantial contribution to the net tidal transport. Note that mean components of the flow (u_a) and concentration (c_a) have been removed.

field results with strongest exchange at the mouth (~50 percent) and weaker exchange at the inner bay stations (~12 to 18 percent). The modeled exchange was generally 5 to 10 percent higher than the exchange estimated from the field measurements. Visualization of the model results suggests that better agreement might be obtained by increasing the small-scale diffusion constant in the model and, thus, reducing the effective shear dispersion.

Overall results and conclusions from the work completed to date are summarized below.

- ADCP and UVF techniques provide a unique method for resolving transport processes.
- Good overall agreement between scaling, salt balance, and transport estimates of dispersion (30 to 260 $m^2 s^{-1}$).

- Bulk tidal exchange ratio varies from ~40 percent at the mouth to ~5 percent south of the bridge.
- Estimated residence times are long (~100 days) for the inner bay.
- Dominant mechanisms of dispersion vary with distance from mouth, topography, and stratification (table 1).

Table 1. Dominant mechanisms of dispersion that measured sections in San Diego Bay.

Region	Primary Mechanism	Secondary
Mouth	tidal pumping	vertical residual
Shelter Island	trapping/subtidal	shear/trapping
Harbor Island	vertical residual/subtidal	shear
Bridge North	pumping/subtidal	trapping/shear
Bridge South	trapping/subtidal	pumping/shear(–)

- Strong exchange at the mouth indicates the importance of bay–ocean exchange in controlling overall residence time of the bay.
- Importance of trapping in inner bay suggests that dredge and fill operations may have significant effects on contaminant transport.
- Subtidal effects may be important especially in regions where other mechanisms are absent (e.g., Shelter Island).
- TRIM model shows reasonable agreement with field measurements of flow and exchange, although exchange is generally overestimated by the model by about 5 to 10% compared to the field measurements.

Principal Investigator: 0601152N
D. Bart Chadwick NRaD ZW86

Super Composite Projectors

Objective(s). Explore the bending–extension (b–e) coupling effect of certain composite radiator materials for potentially substantial improvements (e.g., substantial reductions in fundamental frequencies) of low-frequency, wall-driven composite projectors, such as bender bar projector and split cylindrical transducer.

Accomplishment(s). Developed beam-type theories for b–e coupled composite beams and split cylinders bonded with actuator(s). Performed static and dynamic analyses on beams and split cylinders in three beam-actuator and one cylinder-actuator configurations. Discovered substantial bending deformation increases and fundamental frequency reductions for two-layered, cross-ply laminated beams and split cylinders in all four configurations.

New emphasis on joint warfare in major regional conflicts requires research to significantly improve systems of ocean surveillance, which is one of the important mission areas of NRaD. Examples of low-frequency, wall-driven acoustic projectors currently used in the systems are: bendar bar projector, split cylindrical transducer, and wall-driven oval (WALDO) ring transducer. The actuators used in these projectors are lead zirconium titanate (PZT) drivers located in the wall. The flexing radiator materials used originally were ceramics and metals, and more recently were fiber-reinforced composites due to the need for small size, low weight, low frequency, etc., for the projectors. For future projectors, a great deal of effort has been focused on seeking powerful actuator materials with higher field-induced strains than those attained by PZTs. This research explores the radiator materials to seek an additional way of improving projector performance more than merely upgrading the actuator materials. As is well-known, the basic radiation mechanism of all wall-driven transducers is the conversion of the extensional deformation of the actuator into the bending motion of the radiator. In light of this, it seems natural and beneficial to look into a radiator material with inherent b–e coupling properties, such as the b–e coupled fiber-reinforced laminated composites. Therefore, the objective of this research is to explore the potential benefit of the b–e coupling effect for developing low-frequency, wall-driven, super-performance composite projectors, which use PZT or high-energy density active materials as actuators, and fiber-reinforced composites with b–e coupling properties as radiator materials.

To achieve the research objective, four closely related studies with progressively increasing technical difficulties have been conducted: (1) pure bending (without any induced strain actuation) of a bare b–e coupled composite beam, (2) induced strain actuation of a b–e coupled composite beam bonded to both sides with actuators driven 180° out-of-phase, (3) induced strain actuation of a b–e coupled composite beam bonded to one side with an actuator, and (4) induced strain actuation of a b–e coupled composite split cylinder bonded to its concave side with an actuator. In these studies, the composite system chosen is N-layered regular (equal-thickness layers) antisymmetric cross-ply laminates, which have the desired coupling properties. For such laminates, the b–e coupling increases as the (even) number, N, of layers decreases or the ply stiffness ratio (the ratio of ply Young's moduli in the transverse and fiber directions), F, decreases. For a given F, the largest coupling occurs at $N = 2$, i.e., two-layered regular antisymmetric cross-ply laminate, whereas the coupling vanishes as $N \to \infty$, i.e., homogenized (regular) cross-ply laminate.

In conducting these studies, beam-type theories have been developed for a bare b–e coupled composite beam, a b–e coupled composite beam bonded with actuator(s), and a b–e coupled composite split cylinder bonded with an actuator. These theories properly account for the b–e coupling properties of the antisymmetric cross-ply laminates, combined with the effects of stiffnesses and densities of the (thick) actuator(s). Using these theories, static and free-vibration solutions have been obtained for the b–e coupled composite beams and split cylinders (under the studies) with appropriate boundary conditions. From these solutions, analytical formulas have been derived for relative (static) bending deformation, α_b, and relative fundamental frequency, α_f, of the composite beams and split cylinders due to the b–e coupling properties of regular antisymmetric cross-ply laminates. Here α_b and α_f, respectively, are the ratios of the middle surface bending curvature and fundamental frequency of beams and split cylinders made of N-layered antisymmetric cross-ply laminates to those of homogenized cross-ply laminates. Application of these analytical formulas to the existing laminates has favorably revealed that substantial bending deformation increases and fundamental frequency reductions of the composite beams and split cylinders can be achieved with graphite/epoxy, Kevlar-49/epoxy, s-glass/epoxy, and e-glass/epoxy two-layered cross-ply laminates. Table 1 summarizes the maximum values of α_b and α_f for the beams and split cylinders that are under the four studies and that are made of the existing two-layered regular antisymmetric cross-ply laminates. Figures 1 and 2 illustrate the variations of α_b and α_f with respect to the ratio of actuator thickness to beam thickness, H, for two-layered regular antisymmetric cross-ply laminated beams under the second and third studies, respectively.

Table 1. Maximum relative bending deformation, α_b, and relative fundamental frequency, α_f, for beams and split cylinders made of the existing two-layered regular antisymmetric cross-ply laminates.

Composite System	α_b		α_f	
	Studies 1 and 2	Studies 3 and 4	Studies 1 and 2	Studies 3 and 4
E-glass/Epoxy	1.23	1.14	0.90	0.84
S-glass/Epoxy	1.83	1.35	0.74	0.70
Kevlar 49/Epoxy	2.38	1.53	0.65	0.63
Graphite/Epoxy	2.59	1.60	0.62	0.61

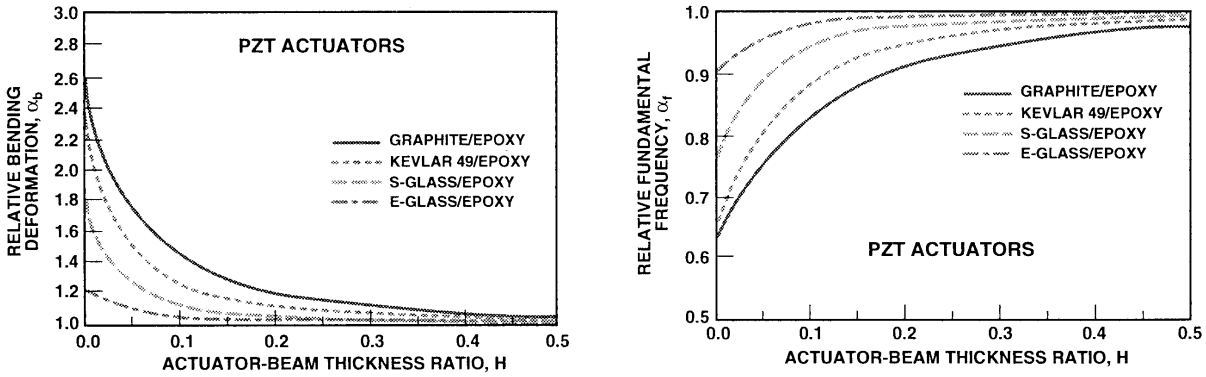

Figure 1. Bending deformation increase and fundamental frequency reduction of two-layered regular antisymmetric cross-ply laminated beams under the second study.

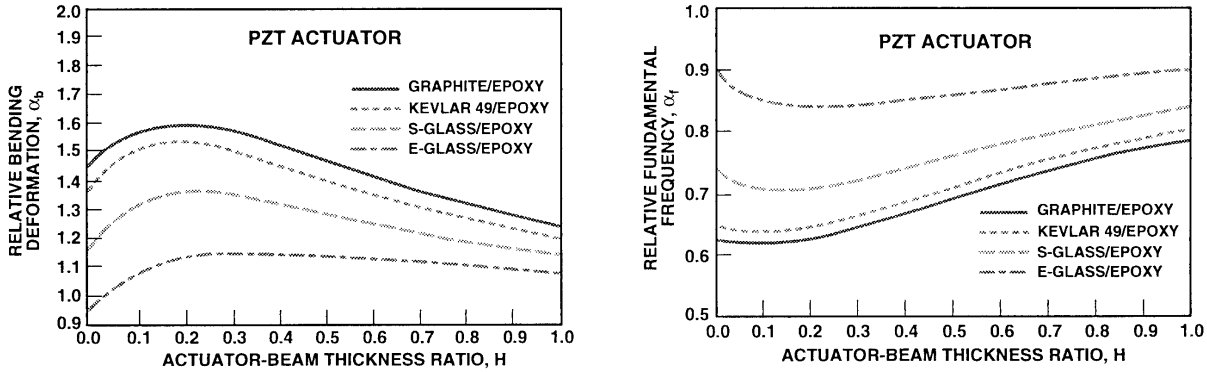

Figure 2. Bending deformation increase and fundamental frequency reduction of two-layered regular antisymmetric cross-ply laminated beams under the third study.

Principal Investigator: 0601152N
Po-Yun Tang NRaD ZU17

Elimination of the Mechanical Dither of a Ring Laser Gyroscope by the Implementation of a Quantum Well Mirror

Objective(s). Determine the feasibility of using a quantum well (QW) as an optical phase shifter (at 6328 Angstroms) for biasing the ring laser gyroscope (RLC) out of its lock-in region.

Accomplishment(s). A quantum well structure was fabricated by Bell Laboratory. The structure was analyzed for surface characteristics and its optical properties. Based on the results of the program, transition funding for FY 96 has been provided by the Office of Naval Research (ONR).

A two Ga6Al4As/AlAs quantum well (QW) surface in a 40-layer superlattice was fabricated by Bell Laboratories and delivered for investigation. The design was developed by NRaD and Temple University.

The surface characteristics were examined first to determine the optical flatness and the number of scattering centers per unit area. The surface characteristics are important because they define the lock-in region and the random wander error in the ring laser gyroscope (RLG). The optical flatness scans demonstrated that the root mean square (rms) value of the surface peaks and valleys was 3.6 Angstroms. This value is greater than the typical values of an RLG mirror, 0.5 to 1 Angstrom. The discrepancies between the two surfaces can be accounted for by the GaAs substrate. An optical scan was performed on a GaAs substrate and the value for the surface flatness was 1.5 Angstroms rms. The deposition of material onto a substrate smooths out the surface characteristic of the substrate. Based on this information, the surface flatness of the substrate used by Bell Laboratory is greater than 3.5 Angstroms rms. A substrate of a lesser quality was used for the fabrication of the superlattice.

The surface flatness for a quantum well mirror can be achieved by purchasing good-quality substrates and not by machine-polishing an optical blank to a smooth surface, as is typical for RLGs. The examination of the number of scattering centers provided a numerical value of 165. This is a composite number of the surface scans used to characterize scattering centers. The value of 165 is greater than the value 100, which is a characterization of a C-class mirror with a lock-in band of 1200 deg/hr.

An estimate of the lock-in band produced by the superlattice structure is 1600 deg/hr. The lock-in band must also be considered with respect to the drive frequency of the dither drive, be it mechanical or optical. The ratio of the lock-in region number to the drive frequency defines the random walk of the RLG. If the drive frequency of the superlattice (>100 MHz) is compared to the currently used mechanical dither (369 Hz), the superlattice structure can be used as currently fabricated to replace the mechanical dither of the RLG. The calculation of the random walk error due to the lock-in produces a reduction in this error of 516. This is based on the drive frequencies stated above.

Optical measurements were also performed to determine the optical activity at 6328 Angstroms. The substrate was etched away using a chemical jet process. After processing, the absorption was recorded on a UV-Visible Spectrophotometer. An exciton absorption peak was observed at 6400 Angstroms. This indicates that a change in the structural composition of the QW is needed to shift the

peak to 6328 Angstroms. Shifting of the exciton peak through the application of an applied voltage will be performed. The applied voltage will shift the exciton peak to shorter wavelengths.

Principal Investigator: 0601152N
Francis A. Karwacki NRaD ZW90

Photolithographically Defined Thin-Film Lithium (Li) Microbatteries

Objective(s). Develop a photolithographic thin-film lithium (Li) process from which micro high-voltage batteries can be fabricated for dark-time sensor processing.

Accomplishment(s). A demonstration device consisting of three photolithographically patterned thin-film Li cells has been fabricated. The process development looks promising. All the steps through the final liftoff have been individually demonstrated.

Environmental sensors commonly require stable low-noise, high-voltage sensor bias for optimum detection. Current technological options for bias include switching power converters or stacked button cell batteries. An alternative is the recently developed high-voltage silicon-on-insulator photovoltaic array [1]. Such arrays, however, make no provision for energy storage during periods of darkness. This project is developing a novel photolithographic thin-film lithium (Li) process from which micro high-voltage batteries can be fabricated for dark-time sensor biasing.

Rechargeable thin-film lithium battery cells with demonstrated energy storage densities of about 1 W/cm^3 have been recently developed at Oak Ridge National Laboratory [2]. These thin-film cells are capable of thousands of charge-discharge cycles and have very long shelf lives. Coupling a series-connected array of such cells to a long-duration, solid-state photocell results in high-voltage storage batteries with years of operational life. The photolithographically fabricated high-voltage thin-film battery arrays can be stacked and combined with the high-voltage photocell charging array using only conventional microelectronic fabrication and packaging techniques. Thus, inexpensive compact microminiaturized high-voltage power packs of indefinite duration are conceptually possible and practical. A demonstration device consisting of three photolithographically patterned thin-film Li cells has been fabricated. The current collectors (terminals) of the cell consist of platinum electrodes on a ceramic substrate. A $LiMn_2O_4$ cathode is then deposited, followed by a lithium phosphorous oxynitrite electrolyte. Conventional liftoff photoresist processing is employed, with polymethyl methacrylate (PMMA) used for electrolyte definition to avoid degrading the hygroscopic electrolyte.

The process development looks promising. All the steps through the final liftoff have been individually demonstrated. Remaining tasking is to integrate them on a compatible substrate. The last liftoff done on a test device worked, but the Li reacted with and discolored the glass. Currently, all the steps of the process are being integrated on a large (3-mm-square) device on some alumina substrates compatible with the Li and the anneal. Masks for the high-voltage battery have been ordered, and this device will be processed in parallel.

REFERENCES

1. Microminiature High Voltage Power Pack Module, Navy Case No. 76,070, authorized for preparation of patent application 7 August 1995.

2. J. B. Bates et al. 1993. “Rechargeable Thin-Film Lithium Microbatteries,” *Solid State Technology,* pp. 59–64.

Principal Investigator: 0601152N
Eric Lind NRaD ZU09

Integrated UHF Transceiver on Fully Depleted Silicon on Sapphire/Silicon on Insulator (SOS/SOI)

Objective(s). Integrate on a single chip the circuits required for a UHF L-band (~2 GHz) radio transceiver to be fabricated using complementary metal-oxide semiconductor (CMOS) silicon on sapphire/silicon on insulator (SOS/SOI) technology. CMOS SOS/SOI would have the advantage of producing the entire circuit in a single monolithic technology using a relatively simple and reliable process.

Accomplishment(s). Fabricated wafer lots of passive elements and T-gate transistors using a modified CMOS process to improve high-frequency performance. Extracted high-frequency model parameters from these devices to allow simulation of UHF circuit designs. Designed and simulated low-noise amplifiers, mixers, power amplifiers, and transmit-receive switches using model parameters extracted above. Designed reticle using these circuits in preparation for wafer lot processing.

There exists a general need for low-power receivers and transceivers at UHF frequencies and above. Individual transistors in fully depleted, thin-film silicon technologies have shown gain and noise performance appropriate for operation in UHF L-band and higher. Thin-film SOS/SOI has price/performance advantages over both GaAs and bulk silicon technologies. The CMOS monolithic technology available on thin-film SOS/SOI would also allow on-chip integration of additional signal-handling functions such as digital signal processing (DSP) or encryption/decryption. This approach should produce the more compact receivers desired for programs such as ARPA's Micro-Global Positioning System (GPS).

As mentioned above, individual transistors fabricated in NRaD's Integrated Circuit Research and Fabrication Branch have shown excellent high-frequency gain and noise performance. This project's objective was to incorporate these transistors in the design of UHF radio building block circuits (e.g., low-noise amplifiers, mixers, power amplifiers) for performance testing. The initial system target specifications for the UHF transceiver were determined to be:

1. UHF frequency band: 2.4000 to 2.4835 GHz (ISM band)
2. Intermediate frequency: 200 to 400 MHz range
3. Low-noise amplifier noise figure target: <3.5 dB
4. Transistor drawn gate length of 0.5 micron for T-gate transistors

The information available from the transistors mentioned above was not adequate for UHF circuit design. To acquire the additional information needed, two wafer lots were processed for passive elements (inductors, capacitors) and T-gate transistors using the equipment and the modified CMOS process, which would be used on the UHF circuit lot. Both test lots were completed and high-frequency model parameters extracted from the devices.

Design studies were conducted on the UHF circuits at the University of California at San Diego (UCSD) under the direction of Dr. Peter Asbeck. Information on GaAs designs of power amplifiers,

low-noise amplifiers, mixers, T/R switches, and voltage-controlled oscillators (VCOs) was assembled and analyzed for use on SOS/SOI. Preliminary model parameters were extracted from existing T-gate transistor lots fabricated at NRaD. Once a reasonable estimate of the range of device parameters was obtained, designs were simulated for operational performance of the circuit designs. Finalization of the designs for the UHF circuit reticle required the model parameters from the test lots described above, which included important process modifications. Circuit simulations on the final designs were completed in August 1995. The reticle set has been ordered and will be produced as soon as the completed layout data are sent to the mask maker. Processing of wafer lots can begin once the reticles are received from the mask maker.

Fabrication and testing of the UHF circuit lots will continue into FY 96 along with continued testing of the T-gate test transistor lot.

Principal Investigator: 0601152N
Michael Wood NRaD ZU18

PUBLICATIONS AND PRESENTATIONS

REFEREED JOURNALS, BOOKS/CHAPTERS, AND DISSERTATIONS (PUBLISHED/ACCEPTED)

Refereed Journals

Axford, R. A., L. B. Milstein, and J. R. Zeidler. 1996. "On the Misconvergence of the Constant Modulus Algorithm (CMA) for Blind Equalization in the Reception of PN Sequences," *IEEE Transactions on Signal Processing* (in press).

Bucker, H. P. 1996. "Active Matched-Field Tracking," *Journal of the Acoustical Society of America* (in press).

Bulsara, A. R. and L. Gammaitoni. March 1996. "Tuning in to Noise," *Physics Today*, pp. 39–45.

Goodman, I. R. September 1995. "Mathematical Foundations of Conditionals and Their Probabilistic Assignments," *International Journal of Uncertainty, Fuzziness & Knowledge-Based Systems,* vol. 3, no. 3, pp. 247–339.

Goodman, I. R. 1995. "Applications of Product Space Algebra of Conditional Events and One-Point Random Set Representations of Fuzzy Sets to the Development of Conditional Fuzzy Sets," *Fuzzy Sets & Systems*, vol. 69, pp. 257–278.

Hanson, F. and P. Poirier. July 1995. "Multiple-Wavelength Operation of a Diode-Pumped Nd:$YAlO_3$ Laser," *Journal of the Optical Society of America (B)*, vol. 12, pp. 1311–1315.

Hibbs, A. D., A. L. Singsaas, E. W. Jacobs, A. R. Bulsara, J. J. Bekkedahl, and F. Moss. March 1995. "Stochastic Resonance in a Superconducting Loop with a Josephson Junction," *Journal of Applied Physics* vol. 77**,** pp. 2582–2590.

Inchiosa, M. E. and A. R. Bulsara. 1995. "Nonlinear Dynamic Elements with Noisy Sinusoidal Forcing: Enhancing Response via Nonlinear Coupling," *Physical Review E: Statistical Physics, Plasmas, Fluids, & Related Interdisciplinary Topics,* American Physical Society through the American Institute of Physics, New York, NY, vol. 52, pp. 327+.

Inchiosa, M. E. and A. R. Bulsara. March 1996. "Signal Detection Statistics of Stochastic Resonators," *Physical Review E: Statistical Physics, Plasmas, Fluids, & Related Interdisciplinary Topics,* American Physical Society through the American Institute of Physics, New York, NY, vol. 53, pp. 2021+.

Latz, M. I., J. Rohr, and J. Hoyt. 1995. "A Novel Flow Visualization Technique Using Bioluminescent Marine Plankton. Part I: Laboratory Studies," *IEEE Journal of Oceanic Engineering*, vol. 20, no. 2, pp.144–147.

Lindner, J. F., B. K. Meadows, W. L. Ditto, M. E. Inchiosa, and A. R. Bulsara. March 1995. "Scaling Laws for Spatial Temporal Synchronization and Array Enhancement Stochastic Resonance," *Physical Review Letters: Statistical Physics, Plasmas, Fluids, & Related Interdisciplinary Topics,* American Physical Society through the American Institute of Physics, New York, NY, vol. 53, pp. 2081+.

Lindner, J. F., B. K. Meadows, W. L. Ditto, M. E. Inchiosa, and A. R. Bulsara. July 1995. "Array Enhanced Stochastic Resonance and Spatiotemporal Synchronization," *Physical Review Letters,* vol. 75, pp. 3–6.

McDonnell, J. and D. E. Waagen. 1995. "Evolving Cascade-Correlation Networks for Time-Series Forecasting," *International Journal on Artificial Intelligence Tools,* World Scientific Publishing, vol. 3, no. 3, pp. 327–338.

Poirier, P. and F. Hanson. January 1996. "Discretely Tunable Multiwavelength Diode-Pumped Nd:YAlO Laser," *Applied Optics,* Lasers and Photonics section, vol. 35, pp. 364–367.

Rohr, J., M. I. Latz, E. Hendricks, and J. C. Nauen. 1995. "A Novel Flow Visualization Technique Using Bioluminescent Marine Plankton. Part II: Field Studies," *IEEE Journal of Oceanic Engineering,* vol. 20, no. 2, pp. 147–149.

Scheps, R. January 1995. "Near-IR Dye Laser for Diode-Pumped Operation," *IEEE Journal of Quantum Electronics,* vol. 31, pp. 126–134.

Scheps, R. February 1995. "Dye Laser Pumping with Red-Emitting Diode Lasers," *Federal Lab Manufacturing Technical Briefs,* pp. 16–17.

Scheps, R. February 1995. "Photon Avalanche Upconversion in ER^{3+}:YAlO3," *IEEE Journal of Quantum Electronics,* vol. 31, pp. 309–316.

Scheps, R. December 1994. "ER^{3+}:YAlO3 Upconversion Laser," *IEEE Journal of Quantum Electronics,* vol. 30, pp. 2914–2924.

Shensa, M. J. 1996. "Discrete Inverses for Nonorthogonal Wavelet Transforms," *IEEE Transactions on Signal Processing* (in press).

Stein, D. W. J. September 1995. "Statistical Characteritics of Moving Acoustic Sources in Ocean Waveguides," *Journal of the Acoustical Society of America,* vol. 98, no. 3, pp. 1486–1495.

Stein, D. W. J. November 1995. "Detection of Random Signals in Gaussian Mixture Noise," *IEEE Transactions on Information Theory,* vol. 41, no. 6, pp. 1788–1801.

Sun, C. K., R. J. Orazi, and S. A. Pappert. January 1996. "Efficient Microwave Frequency Conversion Using Photonic Link Signal Mixing," *IEEE Photonics Technology Letters,* vol. 8, pp. 154–156.

Books/Chapters

Goodman, I. R. 1995. "Conditional Events and Fuzzy Conditional Events Viewed from a Product Probability Space Perspective," *Fuzzy Logic and Its Applications to Engineering, Information Sciences, and Intelligent Systems,* Z. Bien & K. C. Min, eds. Kluwer Publishers, Dordrecht, Netherlands, pp. 287–296.

Goodman, I. R. 1995. "Applications of Random Set Representations of Fuzzy Sets to Determining Measures of Central Tendency," *Advances in Fuzzy Theory & Technology,* vol. III, P. P. Wang, ed., Duke University, Durham, NC, pp. 99–110.

Dissertation

Axford, R. A. June 1995. “Refined Techniques for Blind Equalization of Phase Shift Keyed (PSK) and Quadrature Amplitude Modulated (QAM) Digital Communications Signals.” Dissertation submitted to the Department of Electrical and Computer Engineering, University of California at San Diego. Successfully defended.

REFEREED JOURNALS, BOOKS/CHAPTERS, AND DISSERTATIONS (SUBMITTED)

Refereed Journals

Axford, R. A., L. B. Milstein, and J. R. Zeidler. “Blind Equalizers with Reduced Misadjustment for QAM Signals—Part 1: The Multiple Modulus Algorithm (MMA),” submitted to *IEEE Transactions on Communications*.

Axford, R. A., L. B. Milstein, and J. R. Zeidler. “Blind Equalizers with Reduced Misadjustment for QAM Signals—Part 2: “The CMA-Assisted Decision Adjusted Modulus Algorithm (CADAMA),” submitted to *IEEE Transactions on Communications.*

Goodman, I. R. “A New Approach to Conditional Fuzzy Sets,” submitted to *Advances in Fuzzy Theory & Technology,* vol. IV. P. P. Wang, Ed., Duke University.

Kundu, A. and G. C. Chen. “An Integrated Hybrid Neural Network and Hidden Markov Model Classifier for Sonar Signal Classification,” submitted to *IEEE Transactions on Signal Processing.*

McGinnis, W. C., T. E. Jones, C. T. Blue, and J. S. Briggs. “Effects of Low Oxygen Pressure and Reflected Sputter Gas Bombardment on YBa2Cu3O7 Thin Films Deposited by Ion Beam Sputtering,” submitted to *Physica C*.

Rees, D. “An Adaptive Visoelastic Parabolic Equation Propagation Method,” submitted to the *Journal of the Acoustical Society of America*.

Scheps, R. “Upconversion Laser Processes,” submitted to *Progress in Quantum Electronics.*

Shensa, M. J. “Discrete Inverses for Nonorthogonal Wavelet Transforms,” submitted to *Journal for Visual Languages and Computing*.

Shum, A. “Analysis of a Finite-Buffer ATM Multiplexer Subject to Heterogeneous Groups of On-Off Sources,” submitted to *IEEE Transactions on Communications*.

NRaD PUBLICATIONS

Russell, S. D., W. B. Dubbleday, R. L Shimbukuro, P. R. de la Houssaye. 1995. "Photonic Silicon Device Physics." NRaD TD 2825 (Jul). Naval Command, Control and Ocean Surveillance Center RDT&E Division, San Diego, CA.

Shum, A. 1995. "Discrete-Time Analysis of an ATM Multiplexer." NRaD TR 1704 (Sep). Naval Command, Control and Ocean Surveillance Center RDT&E Division, San Diego, CA.

Sprague, R. A. 1994. "Measurements of Ionospheric Variability." NRaD TD 2730 (Oct). Naval Command, Control and Ocean Surveillance Center RDT&E Division, San Diego, CA.

PRESENTATIONS TO PROFESSIONAL MEETINGS

Invited Papers and Lectures

Axford, R. A. 1995. "Blind Equalizers Based on Godard-Style Cost Functions Tailored for Quadrature Amplitude Modulated (QAM) Signals," presented at École National Supérieure de L'Électronique et de ses Applications (ENSEA), 28 June, Cergy-Pontoise, France, and at the Institut de Recherche et d'Énseignement Supérieur aux Techniques de L'Électronique (IRESTE), Université de Nantes, 29 June, Nantes, France.

Axford, R. A., L. B. Milstein, and J. R. Zeidler. 1995. "The Transversal and Lattice Multiple Modulus Algorithms for Blind Equalization of QAM Signals," *Proceedings of the IEEE Military Communications Conference (MILCOM),* 5 to 8 November, San Diego, CA, pp. 586–591.

Fogel, D. B. and J. R. McDonnell. 1994. "On-Line Learning and Control Using Evolutionary Programming," *Proceedings of the 5th International Symposium on Robotics and Manufacturing (ISRAM '94),* Intelligent Automation and Soft Computing: Trends in Research, Development and Applications, TSI Press, Albuquerque, NM, vol. 1, pp. 473–479.

Freund, R. F. April 1995. "SmartNet Scheduling for Heterogeneous HPC," banquet speech, International Parallel Processing Symposium, Santa Barbara, CA.

Goodman, I. R. 1995. "Use of Relational Event and Conditional Event Algebra in Addressing Modeling and Combining of Information in Expert Systems," *Proceedings of the 11th Conference on Artificial Intelligence for Applications in Expert Systems,* IEEE Computer Society Press, Los Alamitos, CA, pp. 270–276.

Goodman, I. R. December 1994. "Applications of New Algebras Extending Traditional Probability to Problems of Data Fusion in Command, Control & Information Systems," *Proceedings of the First Workshop in Command, Control & Information Systems Research,* 3 to 5 May, Oxford, U. K., pp. 326–361.

Goodman, I. R. 1995. "New Results on Conditional Fuzzy Sets and Their Applications," *Proceedings of the 6th International Fuzzy Systems Association (IFSA '95) World Congress,* 21 to 28 July, Sao Paulo, Brazil, vol. 1, pp. 213–216.

Goodman, I. R. 1995. "A New Approach to Conditional Fuzzy Sets," *Proceedings of the Second Annual Joint Conference on Information Sciences*, 28 September to 1 October, Wilmington, NC, pp. 229+.

Goodman, I. R. 1995. "Conditional and Relational Event Algebra: Foundations and Applications to Natural Language, Expert Systems & Deductive Logic," miniseminar presented at the University of Amsterdam, Department of Mathematics and Computer Science, 2 to 4 May 1995, Amsterdam, Netherlands.

Goodman, I. R. 1995. "New Results on the Foundation of Conditional Events and Relational Event Algebra," lecture to both LAFORIA, Computer Science Department, University of Paris V and to the French Ministry of Defense, 10, 12 May, Paris, France.

Goodman, I. R. 1995. “Overview of Conditional Event Algebra and Relational Event Algebra,” Department of Electrical and Computer Engineering, University of Massachusetts at Amherst, 23 June, Amherst, MA.

Goodman, I. R. 1995. “Application of Conditional and Relational Event Algebra to Data Fusion,” 49th Automatic Target Recognizer Government/Industry Working Group, 26 October, Hughes Aircraft Co., El Sequendo, CA.

Hanson, F. and P. Poirier. 1995. “Diode-Pumped Solid-State Laser Work at NRaD,” Diode Laser Technology Conference, 25 to 28 April, Fort Walton Beach, FL.

Inchiosa, M. E., A. R. Bulsara, J. F. Lindner, B. K. Meadows, and W. L. Ditto. 1995. ”Array Enhanced Stochastic Resonance: Implications for Signal Processing,” *Proceedings of the Third Technical Conference on Nonlinear Dynamics (Chaos) and Full Spectrum Processing* (in press).

Johnston, R. K. 1994. “An Approach to Relate Sediment-Chemical Sorption Processes to Assess Potential Toxicity and Bioaccumulation,” presentation for the Natural Resources Department of the University of Rhode Island, 15 November, Kingston, RI.

McDonnell, J. R. and D. E. Waagen. 1995. “An Empirical Study of Recombination in Evolutionary Search,” *Evolutionary Programming IV: Proceedings of the Fourth Annual Conference on Evolutionary Programming*, J. R. McDonnell, R. G. Reynolds, and D. B. Fogel, eds., MIT Press, Cambridge, MA, pp. 465–478.

McDonnell, J. R. and D. E. Waagen. 1995. “A Combined Stochastic and Deterministic Approach for Classification Using Generalized Mixture Densities,” *Evolutionary Programming I: Proceedings of the Fourth Annual Conference on Evolutionary Programming*, McDonnell, R. G. Reynolds, and D. B. Fogel, eds., MIT Press, Cambridge, MA, pp. 159–174.

Pappert, S. A., C. K. Sun, and R. J. Orazi. March 1996. “Microwave Frequency Conversion Using Photonic Link Signal Mixing for Antenna Applications,” Sixth Annual ARPA Symposium on Photonic Systems for Antenna Applications (PSAA–VI), Monterey, CA.

Reuter, M., R. North, and J. Zeidler. 1995. “Performance Analysis of a Multichannel Adaptive Equalizer for Line-of-Sight Digital Radio,” *Proceedings of IEEE MILCOM–95*, 5 to 8 November, San Diego, CA, pp. 597–601.

Rohr, J. 1995. “Experimental Observation of Dolphin Induced Bioluminescence,” ONR/ARPA Review Meeting on Bio-Locomotion and Rotational Flow over Compliant Surfaces, 20 to 22 March, Johns Hopkins University, Baltimore, MD.

Rohr, J. 1995. “The Use of Marine Bioluminescence as a Flow Diagnostic: Laboratory and Field Studies,” Aquatic and Aerial Propulsion in Nature and Technology, AquaProp ’95, 27 to 30 November, St. Petersburg, Russia.

Scheps, R. 1995. “Dye Lasers Pumped by Laser Diodes,” *Proceedings of the International Conference on Lasers ’94*, vol. 17, 158–170.

Shum, A. 1995. “Cell Loss Evaluation of and ATM Statistical Multiplexer,” Navy’s Annual Modeling and Simulation Working Group Meeting, 23 to 24 May, Harris Corporation, Melbourne, FL.

Stein, D. W. J. 1994. “Detection of Random Signals in Gaussian Mixture Noise,” *Proceedings of the 28th Asilomar Conference on Signals, Systems, and Computers*, 31 October to 2 November, Pacific Grove, CA, pp. 791–795.

Stein, D. W. J. 1995. “Robust Detection of Random Signals in Exponential Mixture Noise,” *Proceedings of the 29th Asilomar Conference on Signals, Systems, and Computers*, 30 October to 1 November, Pacific Grove, CA.

Tang, P. Y. 1994. “Modeling for Super Composite Projectors of Simple Shapes,” 2nd ONR Accelerated Research Initiative (ARI), Adaptive Quiet Structures with Active Materials Workshop, 19 October, University of Maryland, College Park, MD.

Waagen, D. E., J. D. Argast, and J. R. McDonnell. 1994. “Stochastic Determination of Optimal Wavelet Compression Strategies,” *Proceedings of SPIE Visual Communication Image Processing (VCIP)*, SPIE vol. 308, pp. 1711–1721.

Contributed Papers and Lectures

Ambrosius, S., R. Freund, S. Scott, and H. Siegel. April 1996. "Work-Based Performance Measurement and Analysis of Virtual Heterogeneous Machines," Fifth Heterogeneous Processing Workshop of the International Parallel Processing Symposium, Honolulu, HI.

Anderson, G. W., J. J. Rohr, and J. W. Hoyt. July 1996. "An Experimental Investigation of Polymer Drag-Reduction Scale Up," Symposium on Turbulence Modification and Drag Reduction, La Jolla, CA.

Axford, R. A., L. B. Milstein, and J. R. Zeidler. 1995. "A Dual-Mode Algorithm for Blind Equalization of QAM Signals: CADAMA," 29th Asilomar Conference on Signals, Systems, and Computers, 29 October to 1 November, Pacific Grove, CA.

Bamber, D. E. 1995. "A Nonmonotonic Logic of Imperfect Generalizations," colloquium presentation to the Artificial Intelligence Research Group, University of California at San Diego, 13 February, San Diego, CA.

Boyer, D. F. and F. J. Ryan. 1995. "Estimating Tropospheric Refractivity Fields Using a Nonlinear Gauss-Markov Procedure and the PE Model," *Annual Review, Progress Applied Computational Electromagnetics,* pp. 824–829.

Bull, H. T., S. C. Chen, K. N. Rubaye, C. Bendall, B. D. Nener, and G. Burfield. July 1995. "Near Sea Surface Infra-Red Transmission Experiments," SPIE International Symposium on Optical Science, San Diego, CA.

Dubbelday, W., S. Russell, and K. Kavanagh. 1995. "The Dependence of Porous Silicon Photoluminescence Intensity on Starting Silicon Crystal Structure," *Proceedings of the Materials Research Society,* vol. 358, pp. 351–356.

Freund, R. F., S. Natarajan, and V. Prasanna. April 1995. "Experiences in Using Heterogeneous Computing for Image Understanding," *Proceedings of the Fourth Heterogeneous Processing Workshop of the International Parallel Processing Symposium*, Santa Barbara, CA, pp. 53–61.

Goodman, I. R. 1994. "Relational Event Algebra and Its Applications to the Fusion of Data," *Proceedings of the 7th Joint Service Data Fusion Symposium (DFS '94),* 25 to 28 October, Applied Physics Laboratory, Johns Hopkins University, Laurel, MD, pp. 423–437.

Goodman, I. R. 1995. "New Results in the Theory and Applications of Relational Event Algebra to the Combination of Evidence Problem," *Proceedings of the 1995 International Symposium on C2 Research and Technology,* 19 to 23 June, National Defense University, Washington, DC, pp. 398–411.

Goodman, I. R. December 1994. "New Results for the Product Space Approach to Conditional Event Algebra and the Extension to Relational Event Algebra with Applications to Data Fusion," *Proceedings of the 1994 Symposium on Command and Control Research,* Naval Postgraduate School, Monterey, CA, pp. 602–622.

Goodman, I. R. 1995. "A New Formulation of the Relational Event Problem and Some Consequences," 33rd Annual Bayesian Research Conference, 16 to 17 February, University of Soutern California, Los Angeles, CA.

Goodman, I. R. 1996. “Application of Relational Event Algebra to Information Distance or Similarity Measures for Implicitly Described Events,” 34th Annual Bayesian Research Conference, 15 to 16 February, University of Southern California, Los Angeles, CA.

Hensgen, D., L. Moore, T. Kidd, R. Freund, E. Keith, M. Kussow, J. Lima, and M. Campbell. April 1995. “Adding Rescheduling to and Integrating Condor with SmartNet,” *Proceedings of the Fourth Heterogeneous Processing Workshop of the International Parallel Processing Symposium*, Santa Barbara, CA, pp. 4–12.

Hyman, M., J. Rohr, J. Schoonmaker, T. Ratcliff, B. Chadwick, K. Richter, S. Jenkins, and J. Wasyl. 1995. “Mixing in the Wake of an Aircraft Carrier,” *Oceans Proceedings*, p. 325.

Johnston, R. K. 1995. “The Use of Bioluminescent Light Reduction in the Dinoflagellate (*Gonyaulax polyedra*) to Characterize Ecological Risk,” seminar in Oceanography, 18 September, University of Rhode Island Graduate School of Oceanography, Kingston, RI.

Kundu, A. and G. C. Chen. May 1995. “An Integrated Hybrid Neural Network and Hidden Markov Model Classifier for Sonar Signal Classification,” *Proceedings of International Conference on Acoustics, Speech and Signal Processing*, Detroit, MI, vol. 5, pp. 3587–3590.

Latz, M. I., J. Rohr, and J. F. Case. 1995. “Description of a Novel Flow Visualization Technique Using Bioluminescent Marine Plankton,” *Flow Visualization VII, Proceedings of the 7th International Symposium on Flow Visualization*, J. Crowder, ed., Begell House, Inc. New York, NY, pp. 28–33.

Rees, D. June 1994. “Advances in Visoelastic PE Propagation,” Acoustical Society of America Meeting, Boston, MA.

Rees, D. June 1995. “An Improved Technique for Visoelastic Propagation,” poster presentation, 129th Acoustical Society of America Meeting, Washington, D.C.

Reuter, M., R. North, and J. Zeidler. 1995. “The Performance of Multichannel Adaptive Equalization for LOS Digital Communications Corrupted by Interference,” *Proceedings of the 1995 International Conference on Acoustics, Speech, and Signal Processing*, 1 May, Detroit, MI, vol. 3, pp.1856–1859.

Rohr, J., M. I. Latz, E. Hendricks, and J. C. Nauen. 1995. “A Novel Flow Visualization Technique Using Bioluminescent Marine Plankton,” *Flow Visualization, VII Proceedings of the 7th International Symposium on Flow Visualization*, J. Crowder, ed., Begell House, Inc., New York, NY, pp. 34–39.

Russell, S. 1996. “Evidence of Competing Etches in Stain-Etched Porous Silicon,” Abstracts, Materials Research Society, Spring Meeting, 8 to 12 April, San Francisco, CA.

Ryan, F. J. 1995. “VTRPE: A Variable Terrain Electromagnetic Parabolic Equation Model,” *Annual Review, Progress Applied Computational Electromagnetics*, pp. 816–823.

Scheps, R. 1995. “Diode-Pumped Dye Laser,” *Technical Digest*, Conference on Lasers and Electro-optics, vol. 15, p. 284.

Scheps, R. 1995. “Laser Diode-Pumped Laser,” *SPIE (OE) Proceedings*, vol. 2380, pp. 274–284.

Sprague, R. A. and A. K. Paul. 1995. “Variability Indices for the Mid-Latitude F-Region,” 1995 Radio Science Meeting, 3 January, Boulder, CO.

Sun, C. K., S. A. Pappert, and R. J. Orazi. 1996. “Millimeter Wave Frequency Conversion Using Photonic Link Signal Mixing and Harmonic Carrier Generation,” 1996 DoD Photonics Conference, 26 March, Washington, DC.

Tang, P. Y. 1995. “Bending Deformation Increase of Bending-Extension Coupled Composite Beams Bonded with Actuator(s),” *Proceedings of the Second International Conference on Composite Engineering (ICCE/2)*, 21 August, New Orleans, LA, pp. 743–744.

Tang, P. Y. 1995. “Fundamental Frequency Reduction of Bending-Extension Coupled Composite Beams Bonded with Actuator(s),” *Proceedings of the Society of Engineering Science, 32nd Annual Technical Meeting*, 29 October, New Orleans, LA, pp. 609–610.

Tang, P. Y. 1996. “Induced Strain Actuation of Bending-Extension Coupled Composite Split Cylinders,” International Society of Optical Engineering (SPIE), S, 1996 Symposium on Smart Materials, 26 to 29 February, San Diego, CA.

Wellington, R., T. Kidd, R. Freund, and M. Gherrity. April 1996. “Throughput Models for Scheduling Network Traffic,” Fifth Heterogeneous Processing Workshop of the International Parallel Processing Symposium, Honolulu, HI.

Wood, M. 1994. “Integrated UHF Transceiver,” poster presentation, Research Review and Industrial Advisory Board for NSF Industry/University Cooperative Research Center on Ultra-High Speed Integrated Circuits and Systems (ICAS), 7 November, La Jolla, CA.

HONORS AND AWARDS

Honors and Awards

The 1995 NRaD Lauritsen–Bennett Award for Science was presented to **Dr. Richard Freund.** The Lauritsen–Bennett Award annually recognizes employees who have made significant contributions in science, engineering, and staff support. The contributions may be for developing imaginative applications of new technology or scientific principles, doctrine, or concepts that open the way for further scientific study or applications.

As chief scientist for the Heterogeneous Computing Team, Dr. Freund directed development of the SmartNet network scheduling and planning software. SmartNet is an innovative approach to scheduling and planning that extends far beyond the traditional scheduling approaches by efficiently teaming networks and clusters of diverse parallel computers. Funding from the IR program has resulted in techniques for enhancing SmartNet's basic estimation and scheduling behavior. SmartNet provides global and intelligent orchestration of distributable tasks to match the available resources, taking into account both computer characteristics and network contention. In addition to a number of C 4 I sites, SmartNet has been installed at the National Institute of Health to support large protein folding studies and at the National Center for Atmospheric Research to support Weather and Climate Modeling. SmartNet has also been integrated into IBM's resource management system (RMS) Load Leveler and Cray's RMS, called Network Queuing Environment. At "Supercomputing 94," SmartNet simultaneously scheduled and managed 41 high-performance computers and workstation clusters all over the United States. SmartNet also orchestrated 17 programs from six major areas: protein folding, quantum chromodynamics, weather modeling, DNA sequence comparison, environmental modeling, and standard benchmarks. A dramatic demonstration occurred when SmartNet, after the heard "drop" of one machine, gracefully rescheduled the entire set of resources and continued execution.

Dr. Freund is recognized by the scientific community as an expert in distributed and high-performance computing. The Heterogeneous Computing Team won first place in the heterogeneous computing challenge at the annual international conference on high-performance computing, "Supercomputing 94." The team was awarded two of the four prizes in heterogeneous computing offered at "Supercomputing 93."

He has been a leader in four major research areas: high-performance computing (HPC), distributed heterogeneous computing (DHC), applications of HPC and DHC to command and control problems, and cryptologic mathematics.

Dr. Freund is the author of a number of scientific journal papers. He has coedited special issues of several professional journals on heterogeneous computing and is the subject area editor for the *Journal of Parallel and Distributed Computing* in the area of heterogeneous processing.

Dr. Freund is founder of the Heterogeneous Computing Workshop, held every year since 1991, in association with the International Parallel Processing Symposium.

Dr. Donald Bamber is serving as a member of the Board of Editors of the *Journal of Mathematical Psychology.* Dr. Bamber is also a member of the Executive Board of the Society for Mathematical Psychology.

Dr. Adi Bulsara received an NRaD Publication Award of Excellence for an open literature article he coauthored with **Dr. Dave Rees** titled, "Cooperative Behavior in the Periodically Modulated Wiener Process; Noise-Induced Complexity in a Model Neutron," and published in *Physical Review E: Statistical Physics, Plasmas, Fluids, & Related Interdisciplinary Topics*, vol. 49, no. 6, June 1994.

Bart Chadwick received an NRaD Publication Award of Excellence in Technical Documents for his coauthored NRaD TD 2435, "Benthic Flux Sampling Device Prototype Design, Development, and Evaluation."

Dr. George Chen received an NRaD Publication Award of Excellence for an open literature article he coauthored titled, "Transient Sonar Signal Classification Using Hidden Markov Models and Neural Nets," *IEEE Journal of Ocean Engineering*, vol. 19, January 1994.

Dr. I. R. Goodman has fulfilled requests for professional reviews of papers for the following journals: *International Journal of Uncertainty, Fuzziness, and Knowledge-Based Systems*; *International Journal of Intelligent Systems*; *IEEE Transactions on Fuzzy Systems*; and *Information Sciences*. On 28 July 1995, Dr. Goodman served as Chair of the session on "Knowledge Representation Using Fuzzy Logic: I, II." The session was part of the Sixth International Systems Association (IFSA '95) World Congress, Sao Paulo, Brazil. On 29 September 1995, Dr. Goodman was Chair of the "Fuzzy Set Theory" session of the Second Annual Joint Conference on Information Sciences in Wilmington, NC. Dr. Goodman was also an elected member of the Evaluation Committee for selecting the "Lofti A. Zadeh Best Paper Award" for this conference.

John McDonnell received NRaD's Publication of the Year Award for Articles in Conference Proceedings. His coauthored paper, "Evolutionary Optimization of Cascaded Networks," appeared in *SPIE*, vol. 2304, July 1994. Mr. McDonnell also received an NRaD Publication Award of Excellence for an open literature article he coauthored titled, "Evolving Recurrent Perceptrons for Time-Series Modeling," published in *IEEE Transactions on Neural Networks*, vol. 5, no. 1, January 1994.

Dr. Stephen Pappert chaired a conference session on optoelectronics at the Fifth Annual ARPA Symposium on Photonics Systems for Antenna Applications (PSAA–V) in January 1995. Dr. Pappert has also been selected to serve on the Tri-Service Photonics Coordinating Committee as chairman of the Photonic Systems Working Group. Dr. Pappert also received an NRaD Publication Award of Excellence in Technical Reports as coauthor of NRaD TR 1625, "Sea-Floor Survivability and Hazard Susceptibility of Small-Diameter Fiber-Optic Tethers Sea Test Results."

Michael Reuter, Dr. Rich North, and Dr. Jim Zeidler received the MILCOM-95 Award for Best Unclassified Paper: "Performance Analyses of a Multichannel Adaptive Equalizer for Line-of-Sight Digital Radio," *Proceedings of IEEE MILCOM-95*.

Dr. Stephen Russell received an NRaD Distinguished Publication Award as coauthor for a Conference Proceedings article titled, "Ultra-Thin Silicon on Sapphire for High-Density AMLCO Drivers," *SPIE*, vol. 2174, February 1994.

Dr. Richard Scheps was Conference Chair for the SPIE Solid-State Lasers Meeting that was held in San Jose, CA, in January/February 1996. He was also Conference Chair for the SPIE Visible and UV Lasers Meeting held in San Jose, CA, in January 1995. Dr. Scheps served as Program Chair for Laser Source Engineering at OE Laser '96. At the 1996 Conference on Lasers and Electro-optics (CLEO), Dr. Scheps served on the Program Committee for Gas and Dye Lasers. He is also the Associate Editor for *IEEE Photonics Technology Letters*.

Lydia Shen was selected to serve on the Issue Panel for the Software Acquisition Best Practices Initiative for the Department of Defense (DoD) in February 1995.

Dr. David Stein is Chair of the KTP-3 study group on non-Gaussian Signal Processing. The KTP study group is the Radar Technical Panel for Signal Processing of The Technical Cooperation Program (TTCP) (U.S., U.K., Canada, and Australia). Dr. Stein also received an NRaD Distinguished Publication Award as coauthor of NRaD TR 1666 titled, "Adaptive Locally Optimum Processing for Interference Suppression from Communication and Undersea Surveillance Signals."

Dr. Po-Yun Tang served on the Composites Committee of the Material Division of the American Society of Mechanical Engineers (ASME). Dr. Tang was the co-organizer and co-chairperson of the symposium on Multifunctional Composites: Micromechanics at the 1994 International Congress and Exposition of ASME. He also co-chaired the session on "Smart Composites: Application I" at the 2nd International Conference on Composite Engineering. Dr. Tang was also invited to participate at the 3rd ONR Accelerated Research Initiative (ARI) Workshop on Adaptive Quiet Structures with Active Materials.

Dr. Jim Zeidler, an FY 95 associate investigator, was awarded the rank of Fellow in the IEEE for contributions in adaptive signal processing. Dr. Zeidler has been principal investigator or associate principal investigator on a number of IR projects in the areas of signal processing and semiconductor materials.

PATENT ACTIVITY

INDEPENDENT RESEARCH
Patents Issued

Richard Scheps

"Intracavity Sum Frequency Generation Using a Tunable Laser Containing an Active Mirror"

Intracavity sum frequency generation to 459 nm is obtained with a Ti:sapphire laser operating at two simultaneous wavelengths of 809 nm and 1.06 microns. The 1.06-micron wavelength operation is enhanced by use of a double resonant laser cavity and a Nd:YAG gain element in place of the usual HR mirror (active mirror). Furthermore, the difference in intensity output of the Ti:sapphire laser at 809 nm relative to 1.06 microns is compensated for by using part of the 809-nm output to pump the Nd:YAG active mirror.

Patent 5,408,481 Navy case 74,751 (Serial 08/183212) filed 14 January 1994; issued 18 April 1995.

Richard Scheps

"A Compact, Rapidly Modulatable Diode-Pumped Blue Visible Laser"

A visible laser diode is used to pump a Cr,Nd:GSGG or other suitable laser operating at 1.3 microns. The residual pump light is mixed intracavity with the 1.3-micron radiation to produce blue light at approximately 440 nm.

Patent 5,412,674 Navy case 74,752 (Serial 08/225845) filed 7 April 1994; issued 2 May 1995.

Stephen D. Russell
Wadad B. Dubbelday
Randy L. Shimabukuro
Diane M. Szarflarski

"Method of Controlling Photoemission from Porous Silicon Using Ion Implementation"

This invention describes a method of controlling light emission from porous silicon and porous silicon devices using ion implantation. The emitted light intensity can be either selectively increased or decreased by suitable processing of the silicon prior to the fabrication of the porous layer. Amorphizing the silicon prior to the fabrication of the porous layer quenches the light emission. Ion implantation with doses below the amorphization level enhances the intensity of the emitted light of the subsequently fabricated porous layer.

Patent 5,420,044 Navy case 75,726 (Serial 08/118,901) filed 9 September 1993; issued 30 May 1995.

Thomas E. Jones
Wayne C. McGinnis
J. Scott Briggs

"Ceramic Superconducting Magnet Using Stacked Modules"

This invention describes a method of building a superconducting magnet by using high-temperature superconducting materials without using wire forms of these materials. This design, which uses thin films of a melt-processable, high-temperature superconductor, should enable the generation of magnetic fields, at least in the range of several Tesla.

Patent 5,426,408 Navy case 75,143 (Serial 08/060,762) filed 7 May 1993; issued 20 June 1995.

INDEPENDENT RESEARCH
Statutory Invention Registration (SIR) Issued

Carl R. Zeisse
James R. Zeidler
Charles A. Hewett
Richard Nguyen

"An Ion Implanted Diamond Metal-Insulator-Semiconductor Transistor"

A method for making a diamond transistor. In this method, a conducting layer is fabricated by ion implantation into an insulating substrate of natural diamond; source and drain ohmic contacts are provided for the conducting layer with properly annealed gold-molybdenum metallization; an insulating layer of silicon dioxide is deposited; and a gold-titanium metal layer covering the silicon dioxide forms a gate electrode.

Navy case 74,157 (Serial 07/901,615) filed 16 June 1992; SIR #1287 published 1 February 1994.

INDEPENDENT RESEARCH
Claims Allowed; Notice of Allowance/Allowability

Monti E. Aklufi — **"Chemical Sputter Deposition of Dielectric Films with Microwave Induced Plasmas"**

Chemical vapor deposition is caused through "chemical" sputtering of an inner chamber. The inner chamber serves as a source material that reacts with a process plasma to form volatile compounds, which, in turn, form desired film composition. The inner chamber may be made of a variety of materials depending upon what "source" material one desires the chamber to provide.

Navy case 72,776 (Serial 07/897,173) filed 11 June 1992; pending. Notice of Allowance 26 October 1995.

Richard Scheps
Joseph F. Myers — **"Laser With Multiple Gain Elements Pumped by a Single Excitation Source"**

A laser produces laser emission at two or more wavelengths simultaneously. The laser includes at least two gain elements, and each gain element generates a different wavelength. A single optical pumping source is used for optically exciting all laser gain elements contained within the laser resonant cavity. A wavelength dispersing element such as a prism is disposed in the laser resonator cavity for dispersing the wavelengths operating simultaneously within the laser resonator cavity and to create separate regions for each laser gain element. Laser gain elements may be tunable laser gain elements or discretely emitting laser gain elements. Arbitrarily large wavelength separations between the wavelengths operating simultaneously may be achieved in this manner to produce stable cw or pulsed output, which may be Q-switched or line narrowed. Intracavity sum frequency generation can be produced efficiently by using a non-linear sum frequency generating crystal disposed at a laser resonator cavity waist. The multiple gain elements may be of different materials or the same material.

Navy case 76,226 (Serial 08/339,993) filed 31 October 1994; pending. Notice of Allowance 5 June 1995.

INDEPENDENT RESEARCH
Patent Applications Filed

Stanislaw J. Szpak
Pamela A. Boss

"Electrode and Method for Preparation of Electrode for Electrochemical Compression of Deuterium into a Metal Lattice"

This invention provides an electrode and method for preparing the electrode that may be employed to electrochemically compress deuterium into a metal lattice of the electrode. An electrochemical cell is constructed that includes an electrolyte solution comprising a metallic salt and a supporting electrolyte. The metallic salt, when in a reduced state, absorbs deuterium. Both the electrolytic solution and supporting electrolyte are dissolved in heavy water. An anode and cathode are immersed and stable within the electrolytic solution. The anode is stable when polarized. A voltage is applied across the anode and cathode while a constant potential is maintained at the cathode. The constant potential is measured with respect to a reference electrode immersed within the electrolytic solution so that deposition of metallic ions occur in the presence of evolving deuterium during electrolysis of the electrolytic solution. By this method, the cathode is transformed into the electrode.

Navy case 73,311 (Serial 07/632,896) filed 24 December 1990; pending.

Richard Scheps
Joseph F. Myers

"Laser With Multiple Gain Elements of Different Materials"

Two or more separate "arms" of a laser resonator contain gain elements that are end-pumped. Each arm operates at a different wavelength. Each gain element can be made of a different material. The two or more wavelengths are combined in another part of the cavity into a single multiwavelength beam by using a prism. A second waist is established in the cavity for nonlinear processes.

Navy case 75,129 (Serial 08/155,034) filed 19 November 1993; pending.

Michael R. Brininstool
David M. Bullat
Po-Yun Tang

"Fiber Optic Self-Multiplexing Amplified Ring Transducer and Force Transfer Sensor with Pressure Compensation"

This invention provides a system of multiplexed array of fiber-optic sensors with force transfer transducers for detecting the presence of an environmental field condition, such as underwater acoustic pressure perturbations. The invention can be deployed in a single multiplexed array system with incoherent light and at various depths or altitudes with a hydrostatic-pressure equalizer enabling the isolation of dynamic external perturbations from other pressure variations.

Navy case 75,649 (Serial 08/434,366) filed 2 May 1995; pending.

Richard Scheps **"A Low Threshold Diode-Pumped Tunable Dye Laser"**

A method and apparatus for producing stimulated emission from a laser gain element containing an organic dye are described in which optical pumping is produced by visible laser diodes.

Navy case 75,686 (Serial 08/299,865) filed 1 September 1994; pending.

Richard Scheps **"Er:YALO Upconversion Laser"**

A novel technique for upconversion pumping is described that uses intracavity absorption to get 100% conversion efficiency.

Navy case 76,005 (Serial 08/565,075) filed 30 November 1995; pending.

Stephen D. Russell
Robert C. Dynes
Paul R. de la Houssaye
Wadad B. Dubbelday
Andrew Katz
Randy L. Shimabukuro

"Silicon Nanostructures in Silicon on Insulator"

This invention discloses a variety of electrical, optical, mechanical, and quantum-effect devices on an insulating substrate and their method of fabrication for advanced electronic, optoelectronic, optical computing, and flat panel display applications.

Navy case 76,969 (Serial 08/528,386) filed 13 September 1995; pending.

INDEPENDENT RESEARCH
Invention Disclosures Authorized

Eric J. Lind
Gary F. Mastny

"Microminiature High-Voltage Power-Pack Module"

A high-voltage array of p–n junctions is coupled to a high-voltage array of stacked rechargeable Li storage cells. Periodic illumination of the array via fiber-optic cable results in a microminiature low-noise source of high-voltage bias for sensing elements such as used in radiation monitoring equipment.

Navy case 76,070; authorized for preparation of patent application 7 August 1995.

Steven D. Russell
Shannon Kasa
Howard W. Walker

"Chemical Sensor Using Ring Oscillator Thermometry"

This invention describes a novel structure using ring oscillator thermometry for use as a chemical or biological sensor. Combustible gas sensors based on thermal sensors have been demonstrated in the prior art. These sensors, called pellistors, depend on a rise in temperature at a catalytic surface due to catalytic oxidation of the combustible gas. The pellistor measures this rise in temperature with a thermistor. The novel gas sensor incorporates a catalytic platinum layer deposited on top of a ring oscillator. Combustible gases will be catalytically oxidized at the platinum surface. The heat released by the reaction will cause local heating of the RO, and thus affect its frequency.

Navy case 76,462; authorized for preparation of patent application 11 July 1995.

Paul G. Kennedy
Willard Stevenson

"Fiberoptic Cable Junction"

A fiber-optic cable junction for joining the ends of two fiber-optic cables comprises the steps of inserting a tube fastener over each cable end and inserting a protective sleeve and a splint fastener over either cable end. The cable ends are then spliced together. The protective sleeve is positioned over the splice and is supported by fastening an inner splint rod to the cable buffer with the tube fasteners. The cable buffer is supported by an outer split rod fastened to the tube fasteners by the splint fastener.

Navy case 76,880; authorized for preparation of patent application 18 October 1995.

Richard Scheps — **"Laser Diode Wavelength and and Beam Homogenizer"**

A laser-diode power combiner comprises a dye laser operably coupled to an array of laser diodes for combining optical power from the laser diodes into a single, coherent laser beam.

Navy case 77,221; authorized for preparation of patent application 14 December 1995.

Wadad B. Dubbelday
Randy L. Shimabukuro
Stephen D. Russell — **"Electroluminescent Devices in Porous Silicon on Sapphire"**

This invention describes an electroluminescent shottky or pn diode device on silicon on sapphire and a method of manufacturing this device.

Navy case 77,291; authorized for preparation of patent application 19 November 1992.

INDEPENDENT RESEARCH
Invention Disclosures Submitted

Willard M. Cronyn — **"Compact, Phasable, Multioctave, Planar, High Efficiency Spiral Mode Antenna"**

The antenna consists of eight planar windings, each one of which is an exponential spiral. The windings are connected in groups of three to a balanced transmission line, with a "floating" winding between each of the two groups. For the purpose of phasing elements together for directional beam control, the particular grouping of windings can be changed. A sinuous variation is imposed on the spiral windings to increase the path length for each winding rotation so that the circumference through which the phase increases by 360 degrees is correspondingly decreased. This element integrates a planar structure, wideband compact design, and phasability into a single physical structure.

Navy case 76,188; disclosure submitted 15 February 1994.

Stephen M. Hart **"Optoelectronically Controlled Frequency Selective Surface"**

A PVFET is used to control the impedance, scattering frequency, and scattering cross-section of the scattering elements on a Frequency Selective Surface. The PVFETs are implanted in the arms of either wire or slot scatterers in order to make their scattering properties adjustable. The resulting OCFSS becomes a programmable electromagnetic shield or pattern control device.

Navy case 76,915; disclosure submitted 15 September 1994.

Stephen M. Hart **"Optoelectronically Controlled Waveguide"**

An OCW is composed of a metallic waveguide, a finline, and a PVFET. The finline is inserted into the waveguide making electrical contact and the PVFET is affixed to the finline in a shunt configuration. The resulting device is capable of attenuating the energy propagating in the waveguide to any desired degree. In this fashion the OCW can function as an attenuator or a switch. A PVFET is a Field Effect Transistor with a gate controlled by a PhotoVoltaic Cell.

Navy case 76,916; disclosure submitted 15 September 1994.

Stephen D. Russell **"Energy-Converting Porous Silicon Optical Element"**

This invention describes an optical element made of porous silicon on a transparent substrate for converting light of an incident energy to that of a lower emitted energy. This invention may be used for the efficient detection of normally invisible and undetectable wavelengths.

Navy case 76,947; disclosure submitted 19 October 1994.

Richard Scheps **"Underwater Imaging Technique for the Detection of Shallow Submerged Objects"**

This high-resolution underwater imaging and ranging device scans an area underwater with a pulsed laser and records the reflected signal from the illuminated area with a gated photomultipler.

Navy case 77,222; disclosure submitted 16 June 1995.

Allen Shum — **"Asynchronous Transfer Mode Cell Loss Estimation Algorithms"**

A software program for estimating traffic loss of an asynchronous transfer mode (ATM) statistical multiplexer comprises a communication channel having traffic sources and a buffer. Traffic is generated by the traffic sources and removed by the communication channel. When total traffic exceeds the capacity of the communication channel, excess traffic is stored in the buffer. When the buffer is full, excess traffic is lost. Estimating the amount of traffic that will be lost by an ATM statistical multiplexer therefore has application in the design of ATM networks.

Navy case 77,443; disclosure submitted 17 October 1995.

David Stein — **"Exponential Mixture Amplitude Disclosure"**

A method for detecting weak targets in nonstationary non-Gaussian radar clutter by using the intensity of the radar returns.

Navy case 77,579; disclosure submitted 16 January 1996.

INDEPENDENT RESEARCH
Patent Applications Abandoned

Douglas A. Sexton
Stephen D. Russell
Donald J. Albares — **"Laser-Textured Surface Absorber and Emitter"**

A method for fabricating a laser-textured surface absorber and/or emitter is devised, thereby increasing the surface area for applications, inhibiting reflected light, or increasing the emissive power of a body.

Navy case 74,124 (Serial 07/970,558) filed 23 October 1992; abandoned 13 July 1994.

Richard Scheps — **"Differential Imaging for Sensitive Pattern Recognition"**

A technique is described that uses a scanning frequency agile laser to illuminate a scene. As the laser color changes, certain objects will stand out, making them potentially easier to recognize.

Navy case 73,489 (Serial 07/958,191) filed 7 October 1992; abandoned 8 June 1994.

INDEPENDENT EXPLORATORY DEVELOPMENT

Patents Issued

Everett W. Jacobs
Roger D. Boss
Yuval Fisher

"Iterated Transform Algorithm for the Compression of Images"

This invention provides a method for compressing a digital image comprising the following steps: partitioning the image into squares of a predetermined size (the ranges); searching for a set of "suitable" transformation-domain pairs that map onto the ranges (a domain beting the area upon which a transformation acts); and minimizing the error between the transformed domains and their corresponding ranges.

Patent 5,416,856 Navy case 73,320 (Serial 07/860,648) filed 30 March 1992; issued 16 May 1995.

Carol A. Dooley
Elek Lindner

"Organotin Biocides Containing Mixed Saturated/Unsaturated Carbon Chains"

Triorganotin toxicants are disclosed that are made of mixed saturated and unsaturated four-carbon chains with double bonds at C–1 and C–3. Incorporation of these compounds into random 50:50 copolymers of methacrylic acid and methylmethacrylate produces copolymer compositions that may be used as antifouling coatings for ship hulls. Methods for manufacturing the triorganotin toxicants and the copolymer compositions are also disclosed.

Patent 5,451,618 Navy case 74,762 (Serial 08/175,890) filed 30 December 1993; issued 19 September 1995.

INDEPENDENT EXPLORATORY DEVELOPMENT
Patent Applications Filed

Everett W. Jacobs
Roger D. Boss
Yuval Fisher

"Method of Encoding a Digital Image by Using Adaptive Partitioning in an Iterated Transformation System"

This invention is a new adaptive method for partitioning an image, resulting in efficient encoding by using the iterated transformation image compression technique.

Navy case 74,198 (Serial 07/859,782) filed 30 March 1992; pending.

Terence R. Albert
Adi R. Bulsara
Gabor Schmera

"Nonlinear Dynamic Signal Processor, Based on Enhancement of Stochastic Resonance Effect in Coupled Oscillator Arrays"

Globally coupled nonlinear oscillators are subject to the weak deterministic signal of interest. The background noise enhances the signal-to-noise ratio at the output via the stochastic resonance effect. The enhancement is far greater than would be realized by a single oscillator.

Navy case 75,209 (Serial 08/249,111) filed 25 May 1994; pending.

Stephen D. Russell
Wadad B. Dubbelday
Randy L. Shimabukuro
Paul de la Houssaye
Diane M. Szarflarski

"Photonic Silicon on a Transparent Substrate"

This invention describes light-emitting (photonic) silicon on a transparent substrate and its method of fabrication.

Navy case 75,292 (Serial 08/118,900) filed 9 September 1993; pending.

Michael R. Brininstool
David M. Bullat
Po-Yun Tang

"Force Transfer Column (Longitudinal to Radial) with High-Frequency Filter Isolator for Use in Fiber-Optic Sonar Transducers"

The purpose of this proposed concept is to facilitate the use of fiber-optic cables to measure in-water acoustic perturbations.

Navy case 75,649 (Serial 08/434,366) filed 2 May 1995; pending.

INDEPENDENT EXPLORATORY DEVELOPMENT
Invention Disclosures Authorized

Wadad B. Dubbelday
Randy L. Shimabukuro
Stephen D. Russell

“Electroluminescent Devices in Porous Silicon on Sapphire”

An electroluminescent device is integrated on a sapphire substrate that is transparent to light generated by electroluminescence. Crystalline silicon is formed on the sapphire substrate and patterned into an island. A titanium silicide electrode is formed in the silicon around the island by a titanium silicide reaction and covered by an electrically insulating layer. The island is etched to expose the silicon, and a porous silicon layer is formed on the crystalline silicon. An aluminum electrode is formed on the porous silicon layer. An outer insulating layer may be formed on the aluminum electrode and the titanium silicide electrode. Additional electrodes may be formed on and through the outer insulating layer to make electrical contact with the titanium silicide and aluminum electrodes, respectively. A voltage source may be connected to the electrodes to cause light to be emitted from the porous silicon through the sapphire substrate.

Navy case 75,291; authorized for preparation of patent application 19 November 1993.

IR PROJECT TABLES

Multisponsored IR Projects for FY 95

IR Project					Other Funding				
NRaD	DTIC	Title	Funding	Amount ($K)	NRaD	DTIC	Title	Funding	Amount ($K)
ZU10	305 313	Photonic Frequency Converting Feed Network for Broadband Transmit/Receive Antennas	0601152N	122.7	CH99	305 458	Photonics for Antennas Program	0602232	50
ZW77	303 010	Bioluminescent Signatures of Underwater Bodies	0601152N	74.7	HM38	1761319	An Experimental-Numerical Study of Small-Scale Flow Intersection with Bioluminescent Plankton	0601153	20.8
ZU07	305 301	Development and Applications of Relational Event Algebra	0601152N	90.6	CD32	488 828	Joint Program of Research in Command, Control, and Communications	0305108	40
ZW98	304 008	Robust Adaptive Locally Optimum Detection	0601152N	71.7	SUBR	304 023	Advanced Periscope Detection Program	0602314	72
ZU06	305 322	Task Profiling for Heterogeneous Computing	0601152N	51.5	CA53	304 035	Joint Task Force Technology Demonstration	0603226	750
same as above					CA60	IC000083	Fleet Planning Center and the Naval Simulation System	OMN	1154.5
same as above					CD40	488 858	Technology Transition at PACOM	0602702	437.525

GLOSSARY

GLOSSARY

ABE	Autonomous Buoyed Environmental
ADCP	Acoustic Doppler Current Profiler
ATM	Asynchronous Transfer Mode
ATW	Advanced Tactical Workstation
C^4I	Command, Control, Communications, Computers, and Intelligence
CADAMA	CMA-Assisted, Decision-Adjusted Modulus Algorithm
CAOTA	Common All Optical Towed Array
CEA	Conditional Event Algebra
CFAR	Constant False Alarm Rate
CMA	Constant Modulus Algorithm
CRAD	Chief of Research and Development
DAMA	Decision-Adjusted Modulus Algorithm
DHC	Distributed Heterogeneous Computing
DoN	Department of the Navy
EDRD	Esquimalt Defence Research Detachment
ELINT	Electronic Intelligence
ERF ’95	Estuarine Research Federation Conference
FWM	Focused Wave Mode
GCCS	Global Command Control System
GPS	Global Positioning System
HMM	Hidden Markov Model
HPC	High-Performance Computing
IED	Independent Exploratory Development
InSb	indium antimonide
IR	Independent Research
IR	infrared
ISI	Intersymbol Interference
ISRC	Intentionally Short-Range Communication
JMCIS	Joint Maritime Command Information System
LB	Leaky Bucket
LCMA	Lattice Implementation of the Constant Modulus Algorithm
LMS	Least Mean Square
LO	Local Oscillator
LOS	Line-of-Sight
MAEQ	Multichannel Adaptive Equalization
MCT	mercury, cadmium, telluride
MFT	Matched-Field Tracking
MMA	Multiple Modulus Algorithm
MMSE	Minimum Mean Square Error
MMW	Microwave/Millimeter Wave
MSE	Mean-Square Error

NAVELEX	Naval Electronics Systems Command
NN	Neural Network
NOSC	Naval Ocean System Center
NSWCDD	Naval Surface Warfare Center, Dahlgren Division
NTCS–A	Naval Tactical Command System–Afloat
OBU	OSIS Baseline Upgrade
OED	OSIS Evolutionary Development
ONR	Office of Naval Research
OSIS	Ocean Surveillance Information System
OSP	Ocean Surveillance Product
OSTC	Ocean Surveillance Tracker Correlator
PAM	Pulse Amplitude Modulation
PARCOR	Partial Correlation
PE	Parabolic Equation
PECS	Physics of Estuaries and Coastal Seas
PN	Pseudo-Noise
PSK	Phase-Shift Keyed
PZT	lead zirconium titanate
QAM	Quadrature-Amplitude-Modulation
QOS	Quality of Service
QW	Quantum Well
QwikLite	a bioluminescent bioassay system
RDE	Radius Directed Equalization
REA	Relational Event Algebra
RF	Radio Frequency
RLC	Ring Laser Gyroscope
RMS	Resource Management System
ROC	Receiver Operating Characteristic
SART	Structured Analysis with Real-Time Extension
SDS	sodium dodecyl sulfate
SGL	Stochastic Gradient Lattice
SIR	Signal-to-Interference Ratio
SIR	Statutory Invention Registration
SNR	Signal-to-Noise Ratio
SOA	Software Object Abstraction
SPAWAR	Space and Naval Warfare Systems Command
SR	Stochastic Resonance
TCMA	Transversal Implementation of the Constant Modulus Algorithm
TDM	Time Division Multiplexing
TER	Tidal Exchange Ratios
TERESA	Target Recognition by Extraction of Statistical Attributes
UCLA	University of California at Los Angeles
UV	Ultraviolet
WALDO	Wall-Driven Oval
WDM	Wavelength Division Multiplexers

REPORT DOCUMENTATION PAGE

Form Approved
OMB No. 0704-0188

1. AGENCY USE ONLY *(Leave blank)*	2. REPORT DATE	3. REPORT TYPE AND DATES COVERED
	October 1995	Final: October 1994 through September 1995

4. TITLE AND SUBTITLE
IR 1995 ANNUAL REPORT

5. FUNDING NUMBERS
In-house

6. AUTHOR(S)

7. PERFORMING ORGANIZATION NAME(S) AND ADDRESS(ES)
Naval Command, Control and Ocean Surveillance Center (NCCOSC)
RDT&E Division (NRaD)
San Diego, CA 92152−5001

8. PERFORMING ORGANIZATION REPORT NUMBER

9. SPONSORING/MONITORING AGENCY NAME(S) AND ADDRESS(ES)
Office of Naval Research
800 North Quincy Street
Arlington, VA 22217−5000

10. SPONSORING/MONITORING AGENCY REPORT NUMBER
TD 2868

11. SUPPLEMENTARY NOTES

12a. DISTRIBUTION/AVAILABILITY STATEMENT
Approved for public release; distribution is unlimited.

12b. DISTRIBUTION CODE

13. ABSTRACT *(Maximum 200 words)*

This report presents brief summaries of the Independent Research (IR) projects. Three projects are described in detail: Blind Equalizers for High-Data-Rate Digital Communications; A Discretely Tunable Ultraviolet Laser for Multichannel Covert Communications; and Cell Loss Evaluation of Asynchronous Transfer Mode (ATM) Statistical Multiplexing.

14. SUBJECT TERMS AND MISSION AREAS
command and control communications; ocean surveillance multimission research; independent research (IR)

15. NUMBER OF PAGES

16. PRICE CODE

17. SECURITY CLASSIFICATION OF REPORT	18. SECURITY CLASSIFICATION OF THIS PAGE	19. SECURITY CLASSIFICATION OF ABSTRACT	20. LIMITATION OF ABSTRACT
UNCLASSIFIED	UNCLASSIFIED	UNCLASSIFIED	SAME AS REPORT